PW & GS File N° 9F007-4-6028/01-ST
"Diffusion in Liquid" – QUELD
Project 4-0028

Results of Microgravity Experiments
Final Report

PRINCIPAL INVESTIGATOR
Professor Reginald W. Smith
Nicol Hall
Queen's University
Kingston, Ont., K7L 3N6
Tel.: (613)533-2753
Fax: (613)533-6610
email: smithrw@post.queensu.ca

Pb-Au system (fig.2.2)

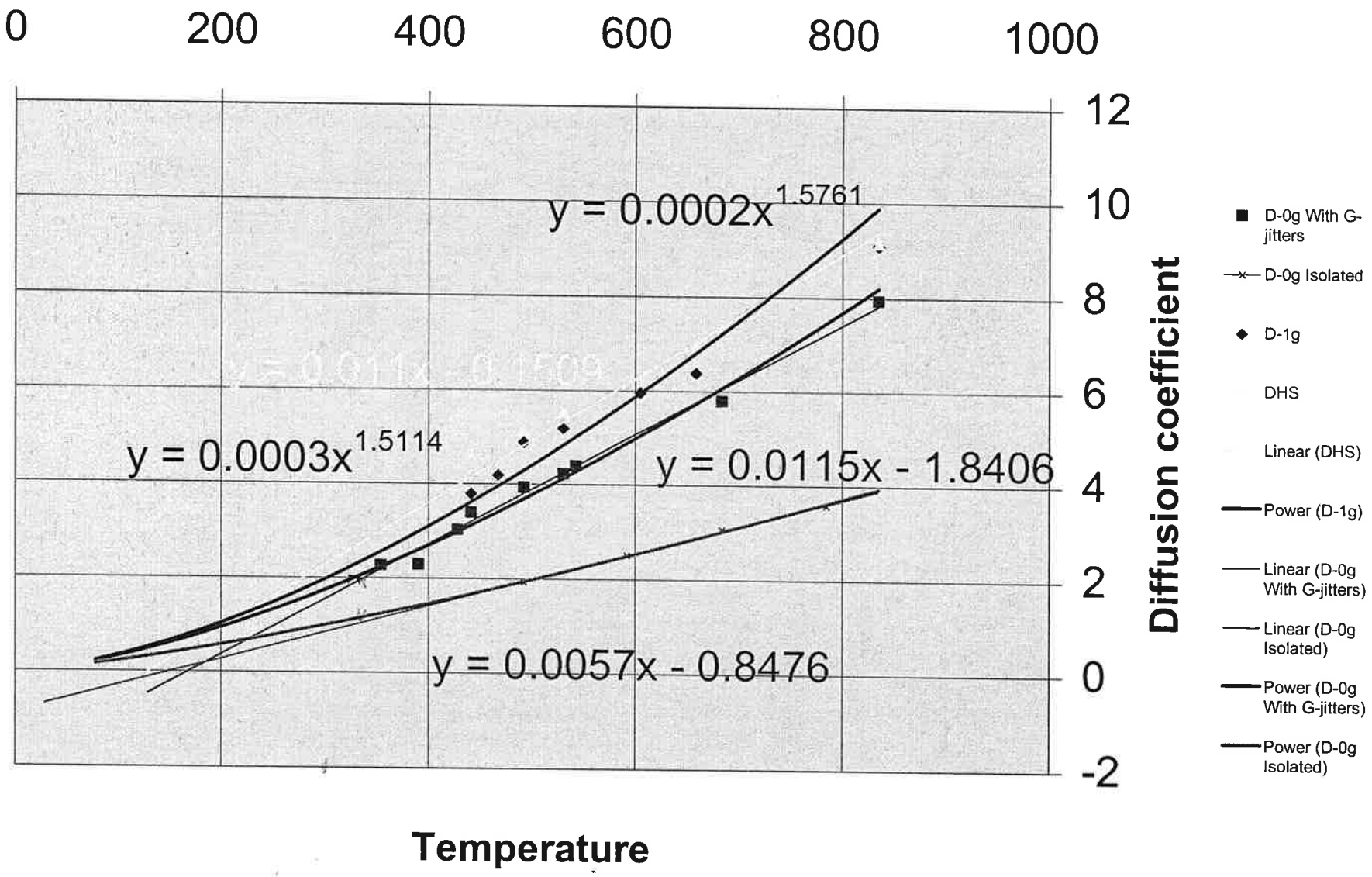

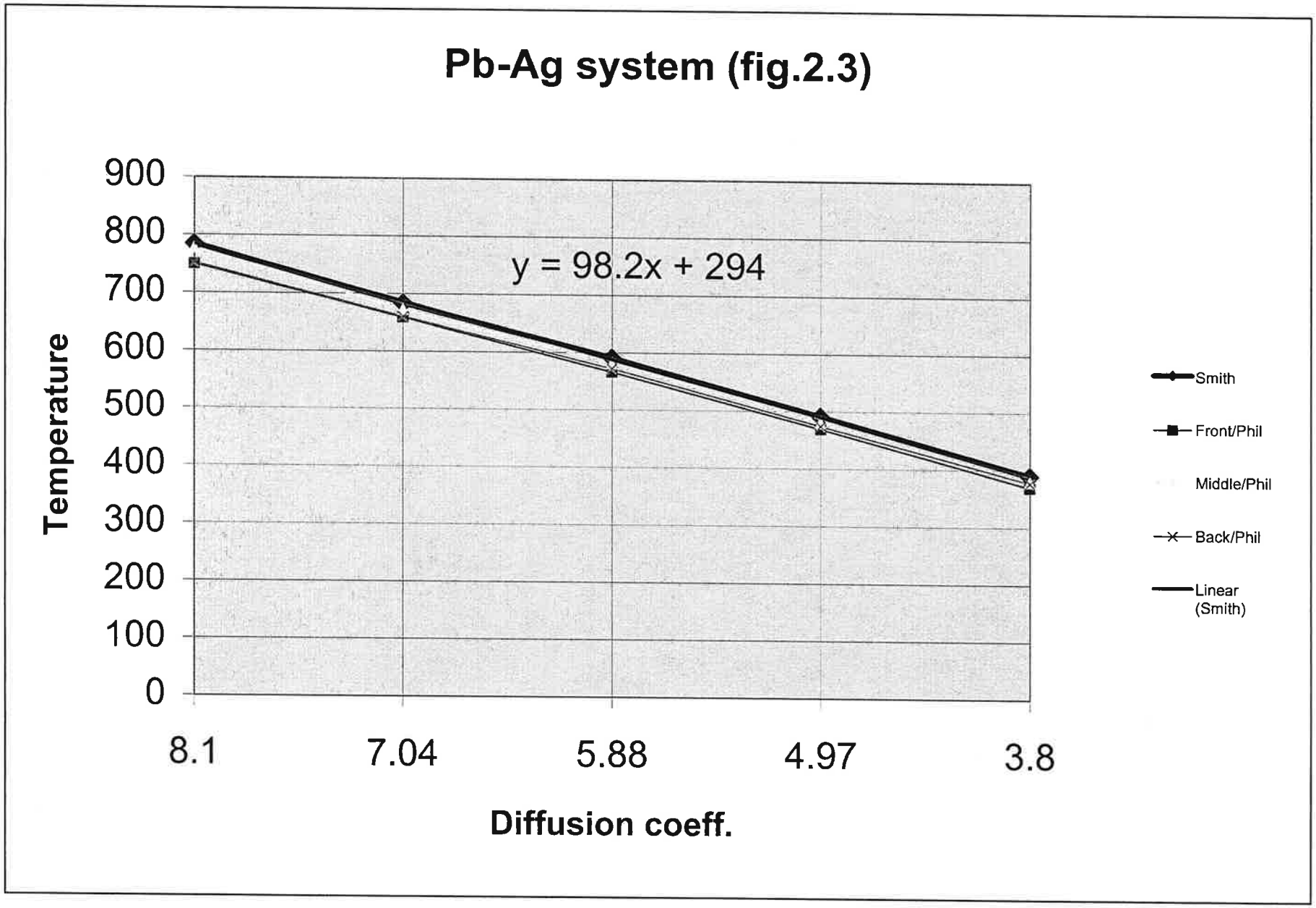
Pb-Ag system (fig.2.3)
y = 98.2x + 294
Temperature
900
800
700
600
500
400
300
200
100
0
8.1
7.04
5.88
4.97
3.8
Diffusion coeff.
Smith
Front/Phil
Middle/Phil
Back/Phil
Linear (Smith)

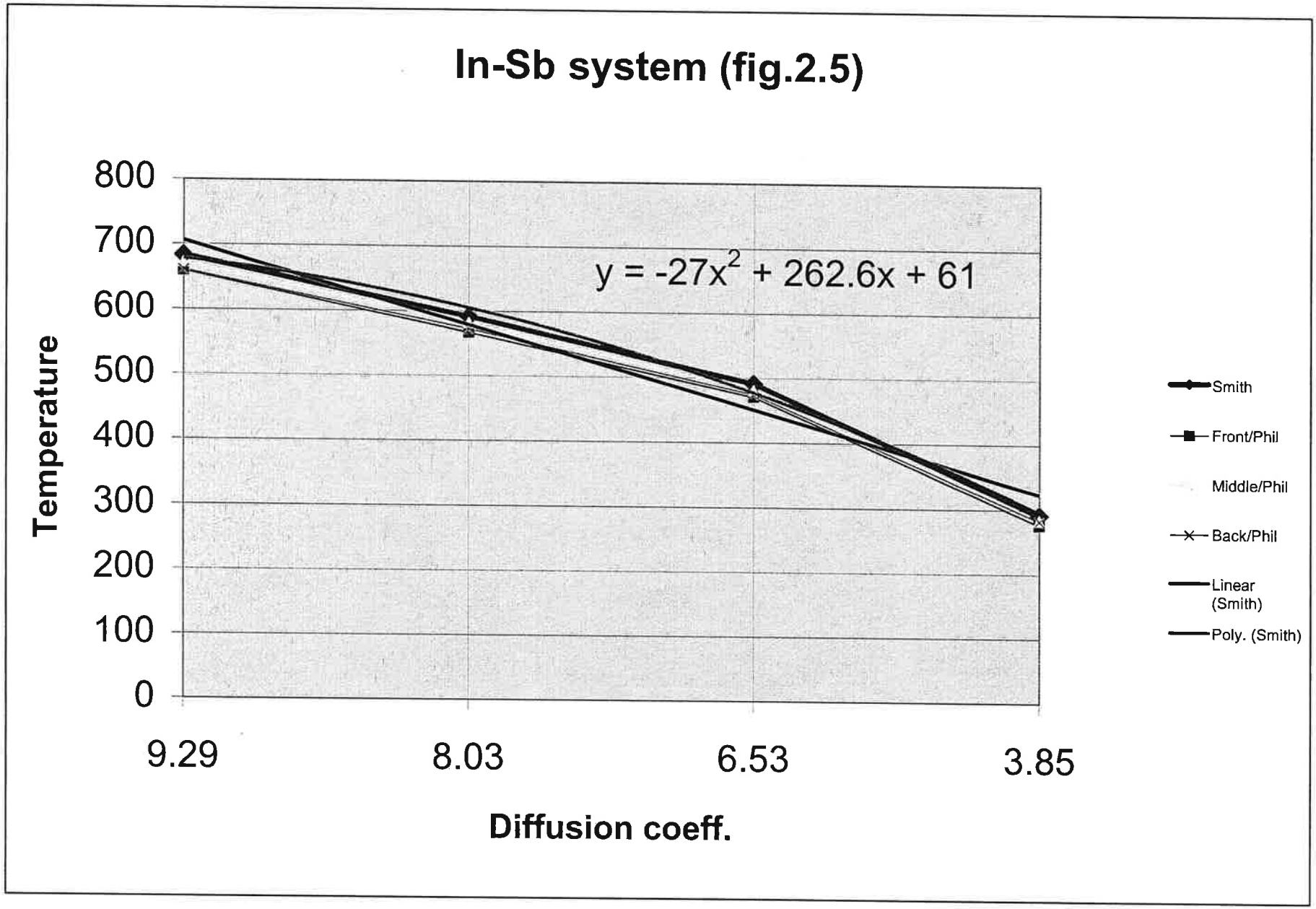
In-Sb system (fig.2.5)
800
700
600
500
400
300
200
100
0
Temperature
y = -27x2 + 262.6x + 61
9.29
8.03
6.53
3.85
Diffusion coeff.
Smith
Front/Phil
Middle/Phil
Back/Phil
Linear (Smith)
Poly. (Smith)

PW & GS File N° 9F007-4-6028/01-ST
"Diffusion in Liquid" – QUELD
Project 4-0028

Results of Microgravity Experiments
Final Report

PRINCIPAL INVESTIGATOR
Professor Reginald W. Smith
Nicol Hall
Queen's University
Kingston, Ont., K7L 3N6
Tel.: (613)533-2753
Fax: (613)533-6610
email: smithrw@post.queensu.ca

Summary

This document reports the work carried-out to-date by Queen's University in support of the MIR/MIM/QUELD II research programme of the Canadian Space Agency. In this connection, it should be noted that Queen's University has been the main contractor in the following contracts concerned with this research programme, namely:

1- Contract N° 9F007-4-6022/01-ST: "DESIGN, DEVELOP, FABRICATE AND TEST AN UPGRADED VERSION OF THE QUELD FURNACE (QUELD II)";
2- Contract N° 9F007-5-6329/01-ST: "PREPARATION AND CERTIFICATION OF SAMPLES FOR THE QUELD II FURNACE TO FLY ON MIR SPACE STATION MISSION"; and
3- Contract N° 9F007-4-6028/01-ST: "DIFFUSION IN LIQUIDS – QUELD II".

Whilst Contracts 1 and 2 have been completed and fully reported, this document is the FINAL REPORT on the scientific work done by Queen's University in support of the MIR/MIM/QUELD II research programme.

Two series of experiments were proposed by Professor Reginald W. Smith, namely:

(i) the measurement of solute diffusion coefficients in molten metals and metalloids; and
(ii) analysis of how gravity affects the interaction of particles suspended in a metallic melt with an advancing solidification front.

The results of these experiments are presented and some theoretical interpretations of significance in future materials processing in space, as part of the research programme of the International Space Station, or in materials processing in a terrestrial facility, are given.

Table of Contents

1 Introduction

The Canadian Space Agency (CSA) has spent much effort over the last ten or so years to develop the Microgravity Isolation Mount (MIM), see Appendix I. This facility is designed to form the services platform for materials science experiments which are to be conducted in Low Earth Orbit (LEO).

Contrary to popular belief, the gravitational environment in "space", i.e., in a manned laboratory in LEO, is not "g"=0. In fact, the gravitational field is best described as having "d.c." and "a.c." components (to use an electricity analogy). The d.c. component arises in the main from friction with the very thin atmosphere of the LEO, giving typically $g=5x10^{-6}g_o$ (where g_o is the gravitational level at the earth's surface). The a.c. component is superimposed on the d.c. level and is made up of a multitude of transient accelerations whose frequencies, amplitudes and planes of excitation vary with time. This a.c. component is commonly referred to as "g-jitter" and arises primarily from the momentum changes occurring on the space-craft due to the normal functioning of control systems and astronaut activity. As a result of the g-jitter, experiments done on space-crafts tend never to experience the (beneficial) effects of the d.c. component alone since the a.c. component may well involve short-period excitation of (say) $10^{-3}g_o$.

In order to explore critically the influence of gravity on physical processes, the CSA developed MIM and invited the Canadian Microgravity Community to propose experiments to be done on the Russian Space Station MIR, using the MIM as the service platform. The Principal Investigator (PI), Professor Reginald W. Smith (R.W.S), proposed two research areas in which his group already possessed much experience from terrestrial studies and earlier LEO flights. These were:

a) liquid diffusion; and
b) the interaction of particles with an advancing solid/liquid interface, as in crystal growth.

Both topics have strong associations with materials processing routes on earth as well as being of considerable theoretical interest. For example, in order to optimize the continuous casting of any given alloy, it is necessary to be able to model the solidification processes involved. This in turn requires good thermophysical data input in-order to get realistic predictions of casting factors, such as local solute segregation levels. On the theoretical side, if such thermophysical data could be predicted "ab-initio", then the need for much experimental activity to determine (say) the variation of solute diffusion coefficients (D) with temperature (T) would be removed. Likewise, the manner in which an advancing crystal surface interacts with any inclusions suspended in the medium from which the crystal is growing is of great practical interest in the growth of highly perfect crystals for electronic or opto-electronic applications or the preparation of particle-reinforced metal matrix composites, i.e., materials which have much greater engineering stiffness than the matrix alloys alone and so have many industrial applications. Of theoretical interest is the ability to predict the processing conditions necessary in order to have the uniform distribution of particles (inclusions) necessary to give the most

desirable mechanical properties or, conversely, how all inclusions might be rejected at an advancing crystal surface so that a higher crystal perfection might be obtained. The local crystal interface velocity below which all particles are rejected, i.e., pushed, and above which all particles are overgrown is known as the critical velocity (V_c).

These two projects were proposed by R.W.S. to form the basis of QUELD Science for Queen's University since each would offer considerable scope to test-out the capabilities of the MIM in both "isolating mode" (g-jitter attenuated strongly so that the sample being processed experiences only the d.c. component of the gravitational field) and in "forcing mode" (where a forced oscillation is imposed on the isolating state and which induces a predictable behaviour in the sample). In principle, by measuring the effect of some particular forcing mode and comparing the observed result with that predicted from fluid mechanical considerations, would provide the opportunity to verify and, if necessary, to massage the theoretical fluid mechanics tools used.

The details of the experiments and theoretical analyses carried-out to-date and the results obtained are given in sections 2, 3 and 4 of this Report. From these sections, a number of important results will be apparent:

(i) Liquid Diffusion: D varies directly as T for all alloy systems examined.
(ii) Particle Pushing: V_c is approximately 1μm/sec and appears to be independent of particle type and shape for the experimental conditions used; V_c increases with MIM in forcing mode.

2 Solute Diffusion in Dilute Liquid Metals and Metalloids

a) Background

In order to achieve optimum control of casting processes on earth, it is necessary to develop a numerical control model. For this, accurate diffusion data are required. The currently available data, where it exists, is often widely inaccurate, the published values for any particular liquid metal diffusion coefficient differing by 50-100%. This is primarily due to the influence of buoyancy-driven convection on the experimental system used to obtain the coefficient[1,2]. Most of these experiments have used the long capillary diffusion couple and, in order to reduce convective transport, the diameters of the capillaries have been progressively decreased. However, it has been reported that if the diffusion capillary is less than about 1mm diameter, then the rate of diffusion is reduced, the so-called "wall effect". Thus it is conventional to write:

$$D_{effective} = D_{intrinsic} + D_{buoyancy} + D_{wall\ effect} + D_{thermal\ (Sorêt\ Effect)} \qquad (2.1)$$

It has been supposed that if a diffusion couple is isothermally processed in microgravity, then $D_{buoyancy}$ and $D_{thermal}$ will be absent and so only $D_{intrinsic}$ and $D_{wall\ effect}$ should be present. Then, by choosing capillaries of different diameters, an estimate of $D_{wall\ effect}$ might be made and hence an accurate value of $D_{intrinsic}$ would be obtained. Further, if the diffusion couples are

processed at a number of temperatures, then the temperature dependence of the transport process taking place could be determined. This can provide clues to the mechanism(s) by which diffusion occurs.

Unfortunately, this proposition takes no account of the influence on $D_{effective}$ of the ever-present g-jitter on a space platform. Recently, the Canadian Space Agency has developed a Microgravity Isolation Mount (MIM) for use on space platforms in low earth obit (Appendix I). This facility may be used in three modes:

(1) "Latched" in which the so-called "flotor" (platform to which the experiment is strapped) is rigidly attached to the "stator" containing the magnetic levitation devices and control computer;
(2) "Isolating" in which g-jitter is attenuated; and
(3) "Forcing" in which a selected forced oscillation is superimposed upon the isolating condition.

The use of the MIM in the isolating mode reduces the effect of g-jitter on the measured value of D. The use of MIM in forcing mode permits the correlation of fluid dynamics predictions with the physical consequences of the actual g-jitter experienced by the sample and hence can be used to refine the theory. This is of crucial importance at the current time in view of the need to fine-tune the calculations used in examining the effects of design variants of the International Space Station (ISS) on potential g-jitter.

b) Objectives

The objectives of the experiments concluded to-date were to:

i) Measure the D values for selected molten metals and semiconductors at various temperatures.
ii) Derive (i) for a) MIM in latched mode (raw g-jitter); b) MIM in isolating mode (minimised g-jitter); and c) MIM in forcing mode (to induce predictable fluid transport).
iii) To use the data from i) and ii) to (a) refine the theory of the structure of liquids; (b) predict D values for liquid systems of scientific and commercial interest in normal and reduced gravity fused media processing.

c) Development of This Project

In 1983, R.W.S. completed successfully in a National Research Council of Canada competition to design an experiment worthy of support as a Get-Away-Special project (GAS-can). From this, Queen's University Experiments in Science and Technology in Space (QUESTS I) was born. However, the NASA STS Challenger disaster forced an extended delay and, as a result, QUESTS I finally flew with 12 diffusion experiments in 1992 and again

(QUESTS II) in 1994. This was followed by Queen's University Experiments in Liquid Diffusion (QUELD I), an STS Mid-deck experiment conceived in 1984 and designed as part of the 2nd Canadian Space Experiments (CANEX 2) associated with the flight of Dr. Steve MacLean on STS 52. During the flight Steve MacLean and his associates on Columbia processed 36 diffusion samples by manually feeding samples into two compact isothermal furnaces with attached quenching devices.

With the development of MIM, the Canadian Space Agency selected a number of materials processing systems to be mounted on MIM for a projected MIR/MIM extended mission. QUELD II was one of these and subsequently it operated on MIR for more than two years and processed a total of 200 samples of various types. Of these, there were 137 samples for Queen's University, including 121 diffusion samples (89 impurity diffusion samples, 6 interdiffusion samples and 26 ternary-impurity diffusion samples) and 16 particle pushing samples.

QUELD II is the semi-automated version of QUELD I, the operator still being required to manually load the furnaces. For its two processing channels, QUELD II uses a variant of the space-proven three-zone furnaces (see Appendix II), and quench system designed for QUESTS and QUELD I (see Appendix III). QUELD II is designed to operate with MIM as its physical and services support platform. The astronaut/cosmonaut time involved in the loading and reloading of samples is minimal (2-3 minutes) since the processing variables are introduced via a multi-sample ROM data card inserted into QUELD II when starting a new batch of samples

d) Experimental Method

The long-capillary method[3,4] was selected for use with QUELD II samples, the design of which is shown in Appendix III. Typically, a 1.5-3.0mm diameter x 40mm length specimen is maintained at a fixed temperature for a given time to permit the solute in the 2mm solute slug attached to one end of the solvent rod to diffuse into the body of the specimen. The diffusion anneal period is selected to ensure that the semi-infinite diffusion condition is not violated, i.e., no solute gets to the far end of solvent charge. The specimen is then quenched and chemically analysed using regular atomic absorption spectrophotometry techniques (AAS) in order to determine the solute distribution along the specimen. This solute distribution is then used to calculate the D value for that particular alloy, anneal temperature and MIM condition used. In addition to the "semi-infinite" specimens described above, some 20mm/20mm interdiffusion samples were also prepared and processed.

Three aspects of the experimental techniques used to obtain high quality processed diffusion couples should be stressed, namely:

(i) diffusion couple manufacture;
(ii) the quenching process used to capture the solute distribution in the specimen following the isothermal anneal; and
(iii) the preheating of the furnace before sample insertion.

(i) It has long been realised by anyone engaged in liquid diffusion studies that it is of paramount importance that the solid/solid interface between the alloy slug and the solvent capillary be planar and complete before melting, i.e., no cavities or inclusions present. The Queen's group worked with many methods before selecting one in which solvent rods are first produced (usually by casting followed by swaging) cut to length and then placed in a chill mold such that their ends project into a horizontal gallery. Then the dilute alloy, typically solvent plus 1-2wt% solute, is poured into the mold. Following casting, the finished specimen is cut from the alloy gallery by electro-die-machining (EDM). The careful selection of liquid alloy superheat and mold temperature permits a clean planar interface to be obtained between the solvent rods and the solidified alloy. (For further details, see Reference 4, a copy of which has been supplied to the CSA.)

(ii) The method of quenching used here was evaluated earlier for QUESTS and QUELD I and is described in detail in Appendix III. In this, following the diffusion anneal, spring-loaded aluminum quench blocks are brought into contact with the sample causing the liquid specimen to freeze in a controlled manner.

(iii) If a cold sample is inserted into a furnace held at the test temperature, the temperature of the furnace is quenched and gradually climbs back to its design temperature. This results in a slow heating-up of the sample. It was found in the earlier QUESTS and QUELD I projects that this situation could be largely overcome by having the furnace at an earlier determined "superheat" temperature so that, when inserted, the sample would assume the test temperature in a few seconds and the thermal mass of the cold sample would quench the furnace to the design temperature. In other words, immediately upon sample insertion, the furnace temperature is reduced to the design temperature.

e) Results

A detailed listing of the samples prepared for the MIR/MIM/QUELD programme is shown in Appendix V, of these 121 diffusion couple samples were prepared by Queen's University for its part of the liquid metal diffusion studies of the MIR/MIM/QUELD II mission. These samples were designed for liquid diffusion studies in 23 alloy systems of varying solvent-type, solute addition, sample size (1.5, 2.0, and 3.0 mm in diameter) and experimental conditions, e.g. temperature of exposure, and MIM condition (isolating, latched, or forcing).

However, of the samples prepared and shipped to MIR, only 63 provided data of sufficient quality to permit the derivation of accurate diffusion coefficients. Also, 11 more samples from Increment 2 were analyzed and the diffusion coefficients calculated but the results were found to be unsatisfactory due to only partial insertion of the sample. The others were deficient due to inadequate processing and/or specimen flaws. A major lost of samples occurred for those processed as part of Increment 2 of the MIR programme. Unfortunately, one of the sample mounting arms became bent so that only 11 of the 37 samples were fully inserted into the furnace and so could be processed as desired. In order to determine which samples had been

processed correctly, it was necessary to perform a detailed analysis. The details of this were supplied to the CSA and are attached here as Appendix VI.

LEAD-GOLD SYSTEM

Figure 2.1 depicts the results obtained earlier with the STS flights 47 and 52 respectively, of QUESTS I and QUELD I and the equivalent 1g values. These were obtained for long capillary (semi-infinite) 1mm diameter samples in which a 2mm section of Pb-1wt%Au alloy was attached to a 38mm pure lead filament. The Pb and Au were of at least 99.999wt% purity. It is seen that the microgravity results lie below those corresponding to terrestrial measurements[3]. For comparison, the variation of D with temperature for Pb-Au, calculated using the hard sphere model (HS) of liquid metals[5], is also given. It is seen that the latter quite closely represents the 1g behaviour but is significantly higher than the microgravity-derived data.

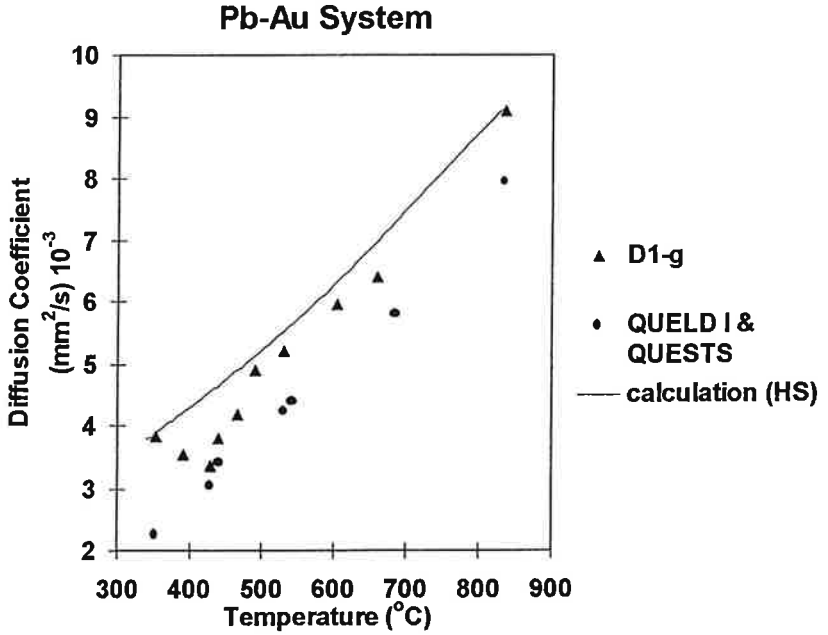

Figure 2.1: Diffusion Coefficients of Gold in Lead Space and Ground-based Experimental Results

Figure 2.2 shows some of the early data obtained from the MIR/MIM/QUELD mission. Here the earlier QUESTS I/QUELD I data of Figure 2.1 are represented by the solid line of Figure 2.2. Significantly below this lie the data points obtained with MIM in isolating mode but using specimens of 1.5mm diameter. The actual numerical values are shown in Table 2-1.

Table 2-1 Diffusion Coefficients of Gold in Lead (mm^2/s) 10^{-3}
Space and Ground-based Experimental Results

$T°C$	D_{1-g}	D_{0-g}	D_{HS}
341			3.78
354	3.81	2.27	
390	3.53		
428	3.35	3.03	
441	3.79	3.40	4.67
467	4.19		
492	4.89		5.14
530	5.19	4.23	5.53
542		4.40	
605	5.96		
659	6.39		6.96
684		5.80	7.31
835	9.10	7.95	9.16

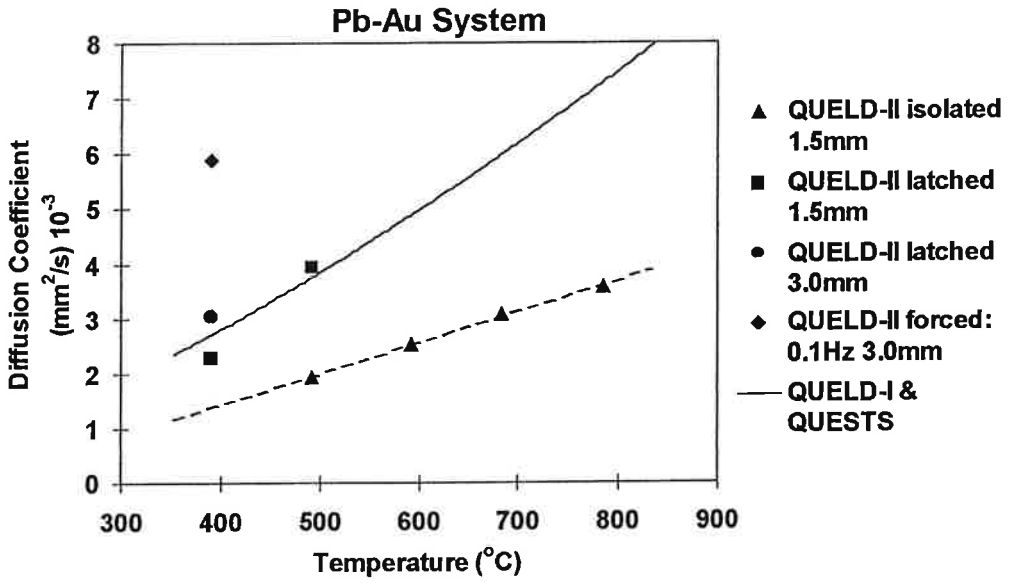

Figure 2.2 Diffusion Coefficients of Gold in Lead (3 MIM Modes)

The results from g-jitter isolation experiments are very interesting. The diffusion coefficients obtained are lower than those from latched experiments, as expected. However, the difference is significant, since, in comparison with QUESTS I/QUELD I results, the diffusion coefficients from QUELD-II g-jitter isolation experiments are about 50% lower. Of particular note is the fact that while the curves for QUELD I and QUESTS I data are concave upwards, that for g-jitter isolation is essentially a straight line, i.e., $D \propto T$ over the range of temperature studied.

It is noted that the D values produced with MIM in latched mode correspond closely with the equivalent values derived from earlier QUESTS I/QUELD I experiments on the Shuttle. This suggests that, as far as gathering high-fidelity liquid diffusion data using small diameter specimens is concerned, the reduced gravity environment of the MIR is no "worse" than that of the Shuttle. Also, it is seen that the diffusion coefficient obtained with a larger specimen diameter (3mm), and with MIM in latched mode, is somewhat larger than that of the equivalent specimen of smaller diameter (1mm) used earlier with QUESTS I/QUELD I. This is to be expected since g-jitter is likely to be able to create more convective transport in larger diameter diffusion couples.

Also shown in Figure 2.2 is the effect of using the MIM in forcing mode to superimpose a forced oscillation of 0.1 Hz upon the MIM isolating condition for a 3mm sample. The forced oscillation resulted in a mean flotor acceleration of 4 milli-g at 45° to the long axis of the diffusion couple. The resulting D value is twice as large as that of a 1.5mm diameter MIM-latched sample, a reflection of the increased mass transport induced by the forced oscillation. The actual numerical values are shown in Table 2-2.

Table 2-2 Diffusion Coefficients of Gold in Lead (3 MIM Modes) (mm^2/s) 10^{-3}

T°C	ISOLATING	LATCHED	3 mm	QUELD-I & QUESTS	0.1 Hz (1998)
354				2.27	
390		2.30			5.89
390			3.04		
428				3.03	
441				3.40	
492	1.93	3.94			
530				4.23	
542				4.40	
592	2.51				
684	3.07			5.80	
715					
785	3.58				
835				7.95	

LEAD-SILVER SYSTEM

As with the Pb-Au system described above, here a 2mm section of Pb-1wt% Ag alloy was attached to a 38mm pure lead filament. Again, metals of 99.999% purity were used. The diffusion coefficient data obtained with the Pb-Ag diffusion couples are shown in Figure 2.3. The data was obtained with the MIM in the isolating mode. It is seen that these data points may be fitted closely to a $D \propto T$ (linear) relationship. For comparison, the full curve shown in Figure 2.3 is that for $D \propto T^2$, based on the D value for 400°C. The actual numerical values are shown in Table 2-3.

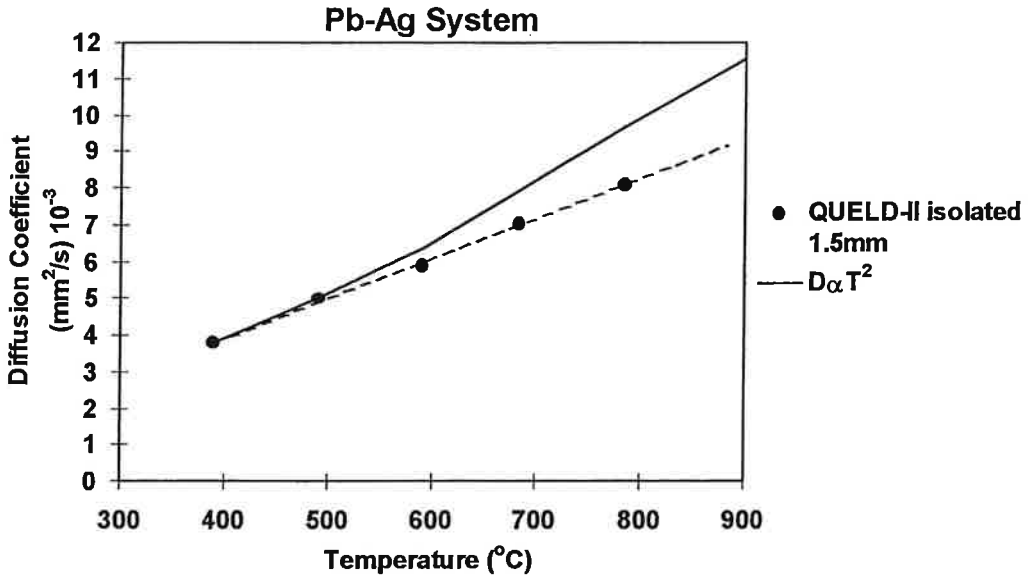

Figure 2.3 Diffusion Coefficients of Silver in Lead

Table 2-3 Diffusion Coefficients of Silver in Lead (mm^2/s) 10^{-3}

Temperature °C	Holding Time hrs	MIM Mode Isolating
390	1.10	3.80
492	1.02	4.97
592	0.93	5.88
684	0.85	7.04
785	0.67	8.10

ANTIMONY-INDIUM SYSTEM

Using Sb/Sb-1wt% In diffusion couples prepared as for Pb-Au diffusion couples, limited data for the diffusion of indium in liquid antimony, measured with MIM in isolating mode, were obtained and are shown in Figure 2.4. A near-linear relationship of D with T is suggested. The actual numerical values are shown in Table 2-4.

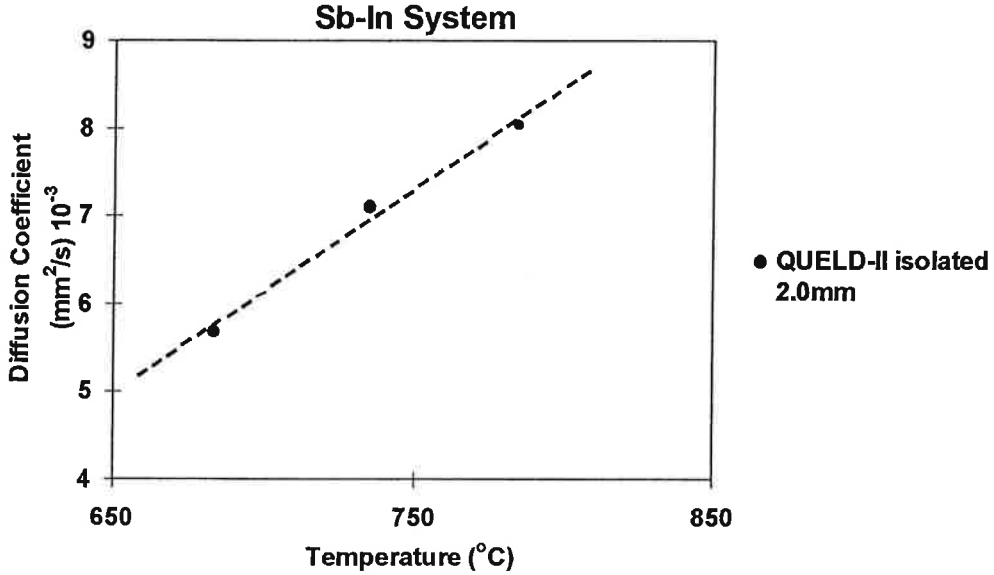

Figure 2.4 Diffusion Coefficients of Indium in Antimony

Table 2-4 Diffusion Coefficients of Indium in Antimony (mm^2/s) 10^{-3}

Temperature °C	Holding Time hrs	MIM Mode Isolating
684	1.75	5.67
735	1.46	7.10
785	1.17	8.02

INDIUM-ANTIMONY SYSTEM

Similar data to that of Sb-In is shown for the diffusion of antimony in liquid indium Figure 2.5, again using a 1wt% alloy diffusion couple and MIM in isolating mode. A near-linear relationship of D with T is suggested. The actual numerical values are shown in Table 2-5.

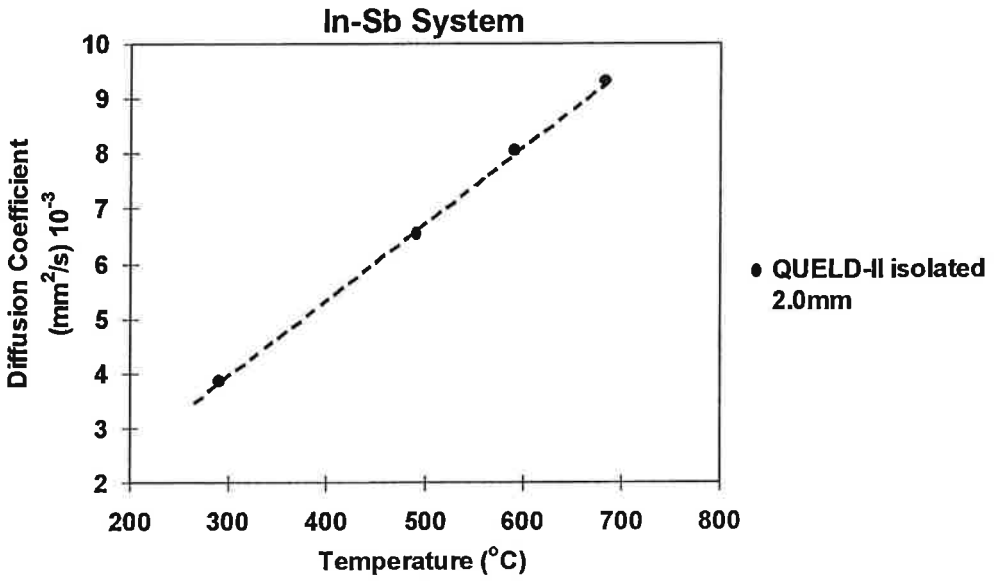

Figure 2.5 Diffusion Coefficients of Antimony in Indium

Table 2-5 Diffusion Coefficients of Antimony in Indium (mm^2/s) 10^{-3}

Temperature °C	Holding Time hrs	MIM Mode Isolating
292	1.88	3.85
492	1.52	6.53
592	1.33	8.03
684	1.15	9.29

LEAD-ANTIMONY SYSTEM

Again, similar data to In-Sb were observed. The diffusion couples were prepared as per the Pb-Au diffusion couples using a 1 wt% alloy and also measured with MIM in the isolating mode. A near-linear relationship of D with T is once more suggested in Figure 2.6 and the actual numerical values are shown in Table 2-6.

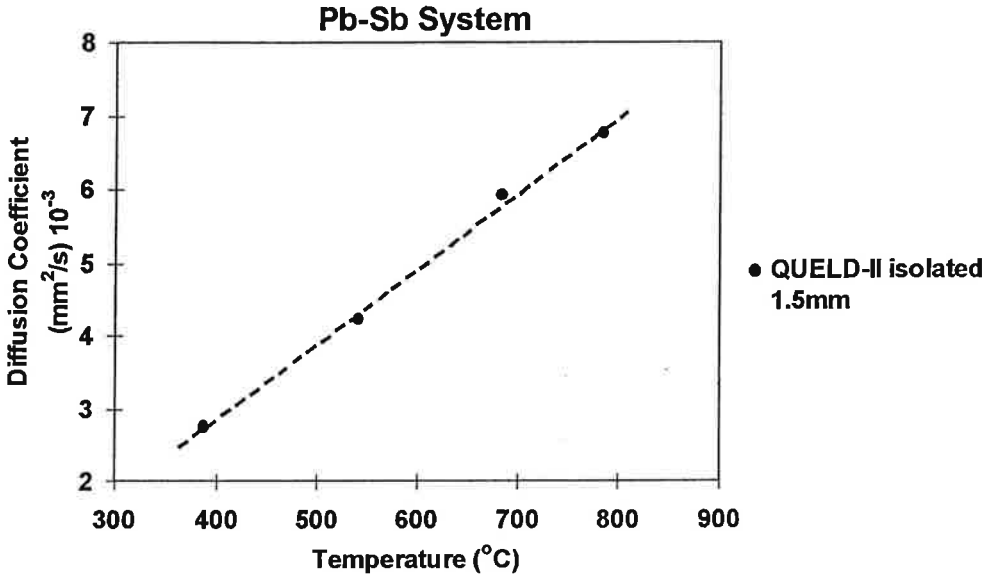

Figure 2.6 Diffusion Coefficients of Antimony in Lead

Table 2-6 Diffusion Coefficients of Antimony in Lead (mm^2/s) 10^{-3}

Temperature °C	Holding Time hrs	MIM Mode Isolating
390	1.70	2.74
542	1.52	4.21
684	1.15	5.91
785	0.97	6.75

TIN-GOLD SYSTEM

Again, similar data to In-Sb were observed. The diffusion couples were prepared as per the Pb-Au diffusion couples using a 1 wt% alloy and also measured with MIM in the isolating mode. A near-linear relationship of D with T is once more suggested in Figure 2.7 and the actual numerical values are shown in Table 2-7.

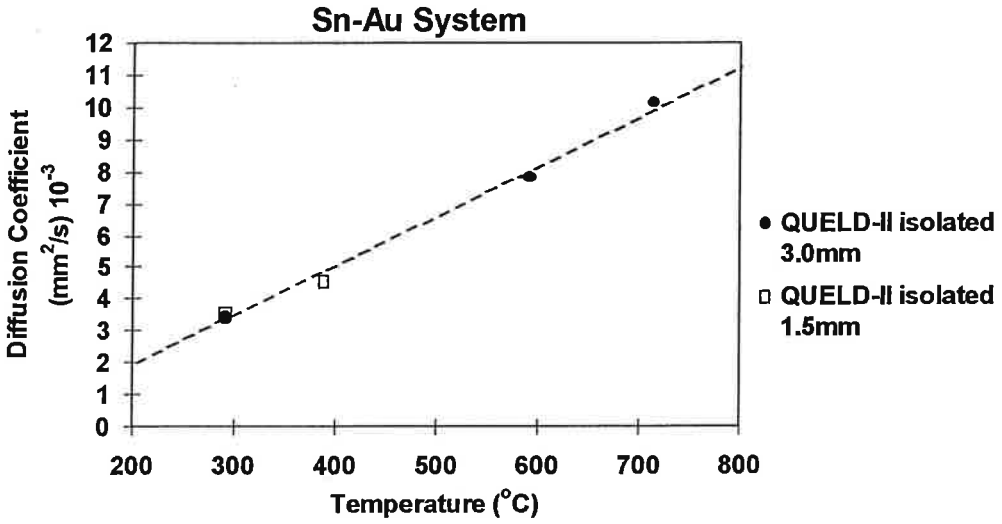

Figure 2.7 Diffusion Coefficients of Gold in Tin

Table 2-7 Diffusion Coefficients of Gold in Tin (mm^2/s) 10^{-3}

Temperature °C	Holding Time hrs	MIM Mode Isolating(3.0mm)	MIM Mode Isolating(1.5mm)
292	1.08/1.30	3.42	3.51
390	1.10		4.54
592	1.13	7.78	
715	0.57	10.07	

TIN-ANTIMONY SYSTEM

Once more, similar data to In-Sb were observed. The diffusion couples were prepared as per the Pb-Au diffusion couples using a 1 wt% alloy and also measured with MIM in the isolating mode. A near-linear relationship of D with T is once more suggested in Figure 2.8 and the actual numerical values are shown in Table 2-8.

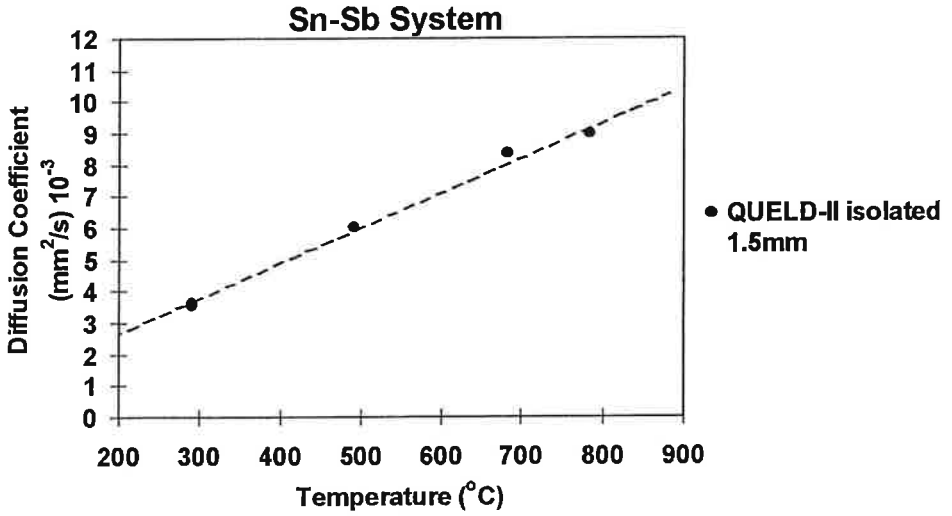

Figure 2.8 Diffusion Coefficients of Antimony in Tin

Table 2-8 Diffusion Coefficients of Antimony in Tin (mm^2/s) 10^{-3}

Temperature °C	Holding Time hrs	MIM Mode Isolating
292	1.76	3.62
492	1.29	5.98
684	0.81	8.32
785	0.67	8.94

ANTIMONY-GALLIUM SYSTEM

Once again, a near-linear relationship of D with T is suggested in Figure 2.9 and the actual numerical values are shown in Table 2-9.

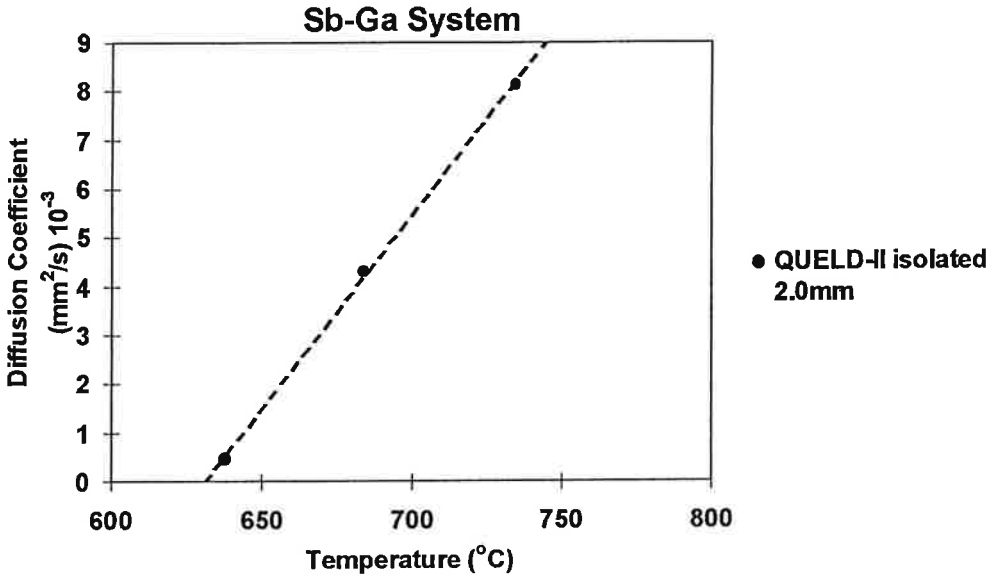

Figure 2.9 Diffusion Coefficients of Gallium in Antimony

Table 2-9 Diffusion Coefficients of Gallium in Antimony (mm^2/s) 10^{-3}

Temperature °C	Holding Time hrs	MIM Mode Isolating
638	2.14	0.45
684	1.75	4.27
735	1.46	8.12

BISMUTH-ANTIMONY SYSTEM

Once again, a near-linear relationship of D with T is suggested in Figure 2.10 and the actual numerical values are shown in Table 2-10.

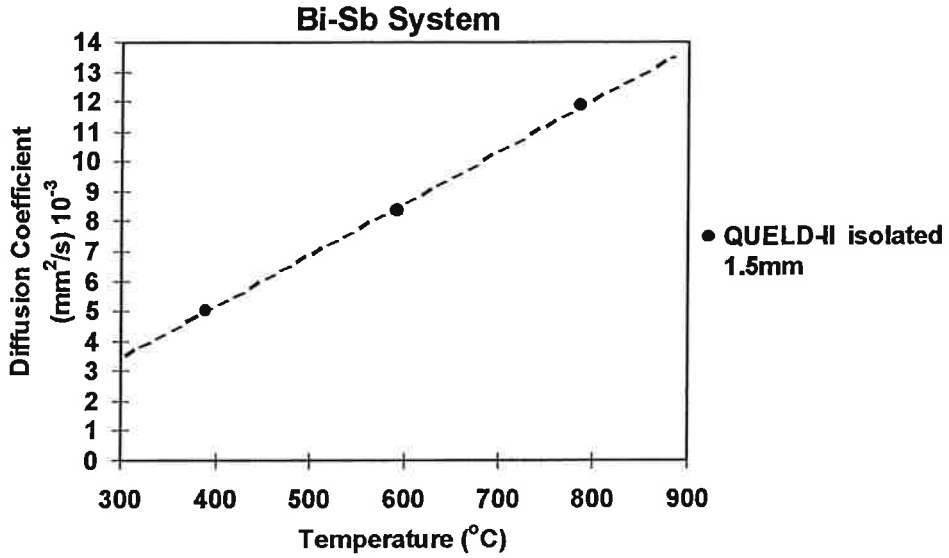

Figure 2.10 Diffusion Coefficients of Antimony in Bismuth

Table 2-10 Diffusion Coefficients of Antimony in Bismuth (mm^2/s) 10^{-3}

Temperature °C	Holding Time hrs	MIM Mode Isolating
390	1.00	5.00
592	0.71	8.36
785	0.52	11.82

BISMUTH-SILVER SYSTEM

Similarly, diffusion coefficients as a function of temperature are shown in Figure 2.11 and the actual numerical values are shown in Table 2-11.

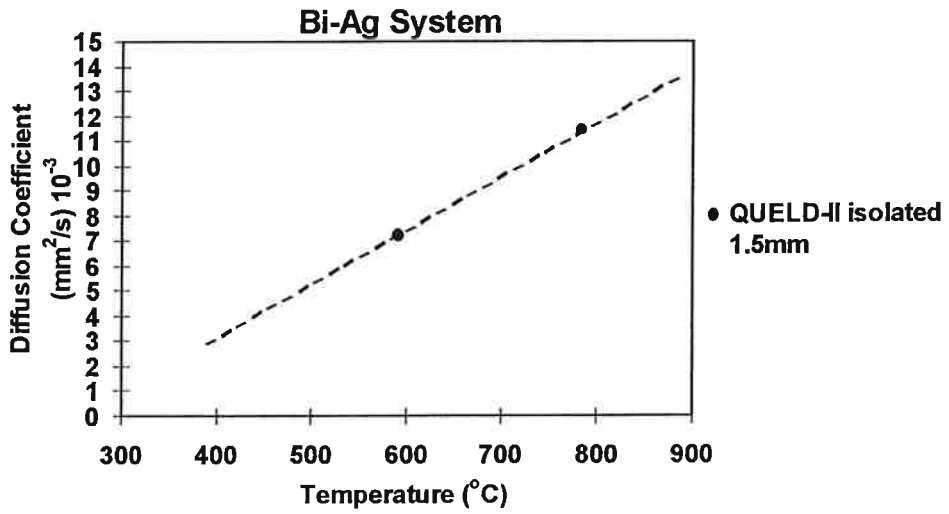

Figure 2.11 Diffusion Coefficients of Silver in Bismuth

Table 2-11 Diffusion Coefficients of Silver in Bismuth (mm^2/s) 10^{-3}

Temperature °C	Holding Time hrs	MIM Mode Isolating
592	0.63	7.20
785	0.50	11.38

BISMUTH-GOLD SYSTEM

Similarly, diffusion coefficients as a function of temperature are shown in Figure 2.12 and the actual numerical values are shown in Table 2-12.

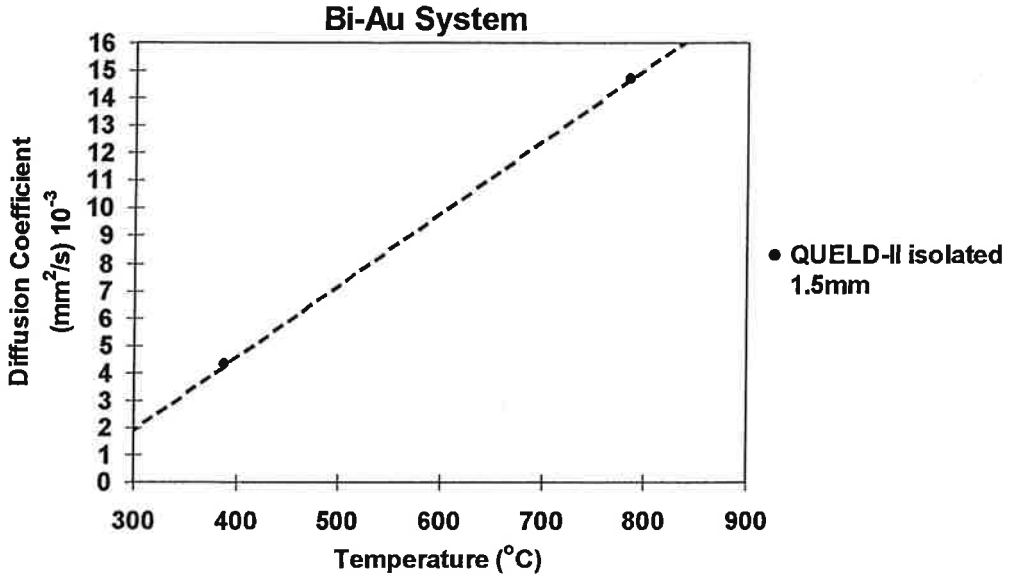

Figure 2.12 Diffusion Coefficients of Gold in Bismuth

Table 2-12 Diffusion Coefficients of Gold in Bismuth (mm^2/s) 10^{-3}

Temperature °C	Holding Time hrs	MIM Mode Isolating
390	1.10	4.27
785	0.57	14.68

ALUMINUM-NICKEL SYSTEM

Similarly, diffusion coefficients as a function of temperature are shown in Figure 2.13 and the actual numerical values are shown in Table 2-13.

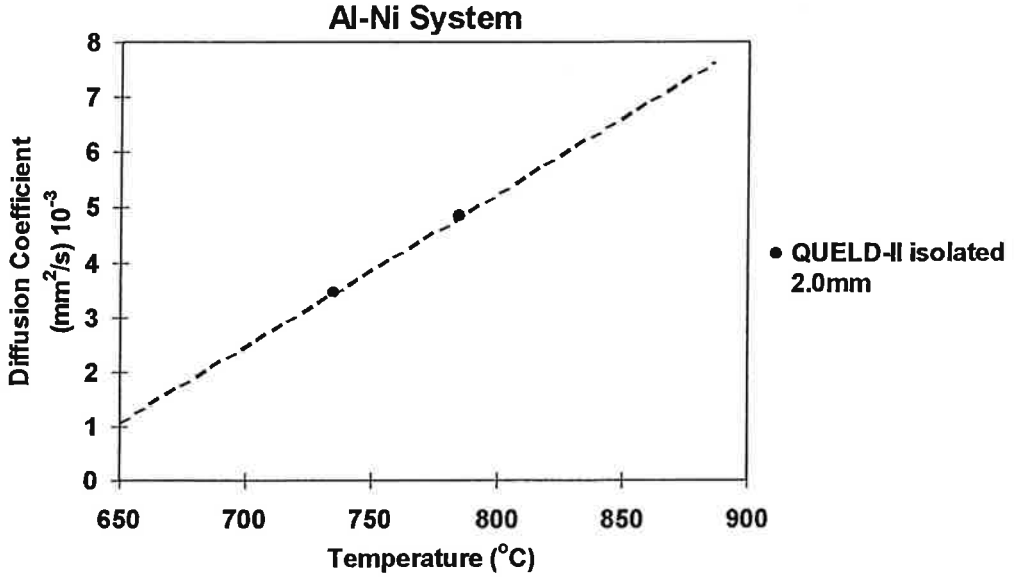

Figure 2.13 Diffusion Coefficients of Nickel in Aluminum

Table 2-13 Diffusion Coefficients of Nickel in Aluminum (mm^2/s) 10^{-3}

Temperature °C	Holding Time hrs	MIM Mode Isolating
735	1.12	3.43
785	1.08	4.83

ALUMINUM-IRON SYSTEM

Similarly, diffusion coefficients as a function of temperature are shown in Figure 2.14 and the actual numerical values are shown in Table 2-14.

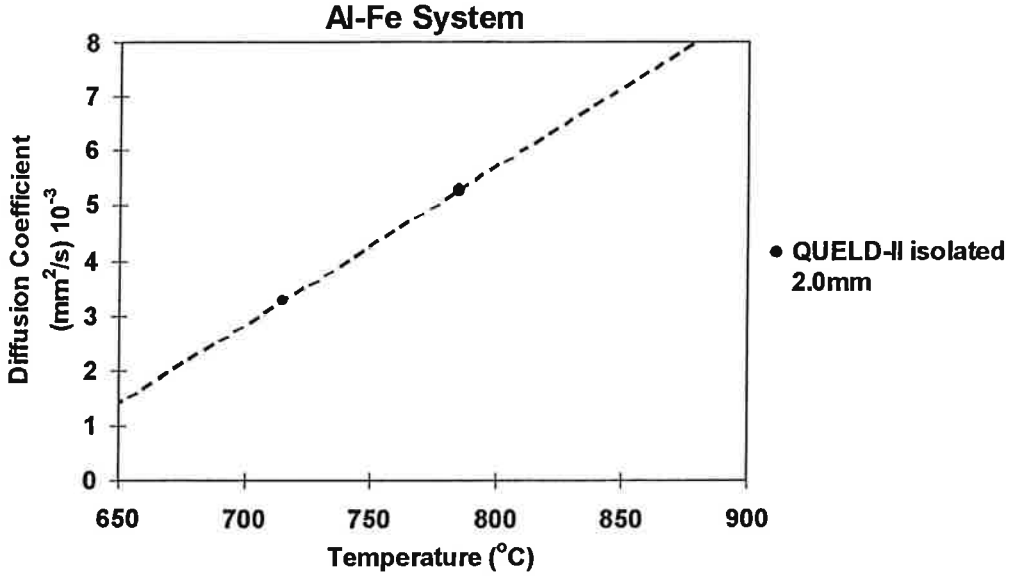

Figure 2.14 Diffusion Coefficients of Iron in Aluminum

Table 2-14 Diffusion Coefficients of Iron in Aluminum (mm^2/s) 10^{-3}

Temperature °C	Holding Time hrs	MIM Mode Isolating
715	1.02	3.26
785	0.86	5.28

f) Discussion

There have been a number of models proposed for the structure(s) of liquid metals and the manner in which this controls the rate of solute diffusion. Each predicts a particular relationship of D with T. These are summarised in Table 2-15. However, in order to comment on the validity of any one model it is necessary to have high quality data for selected alloy systems. As noted earlier, stray convection has confounded terrestrial experiments and so degraded the quality of the data obtained. The use of microgravity research facilities has permitted an increased data quality to be obtained in liquid diffusion experiments.

Figure 2.1 shows that the effects of convection in terrestrial experiments on Pb-Au alloys is significant, D falling markedly when similar experiments are performed on space-craft. However, the experimental examination of the physical effects of the time-dependent variations in the gravity level aboard a space-craft has only been possible with the relatively recent development of the MIM-type disturbance isolating system. While the experimental procedures adopted and reported here may not reveal the truly intrinsic value of D for a particular alloy system, they give values which are much closer to this ideal value and so should more easily permit a detailed correlation of experiment with theory. This is now in progress.

Table 2-15 Theories/Models of Diffusion in Liquids

Diffusion Coefficient – Temperature relationship	Theory
$D = D_o \exp\left(-\frac{Q}{RT}\right)$ where Q is the activation energy, R is the gas constant, and D_o is a system constant	Conventional Description of Data[6]
$D = \frac{kT}{6\pi R\eta}$ where R is the particle radius and η is the viscosity of the medium	Stokes Einstein Theory[7]
$D = A\sqrt{T}\exp\left(\frac{-bV^*}{V_f}\right)$ where V* is the critical volume associated with diffusing atom, V_f is the free volume of the liquid, and B and b are constants	Model of Critical Volume[8]
$D = AT^2$ where A is a system constant	Fluctuation Theory – Swalin 1959[9]
$D = -a + bT$ where a and b are system constants	Fluctuation Theory – Reynik 1969[10]
$D = \alpha\sqrt{T}\left(\frac{9.385T_m}{T}\right)^{-1}$ where T_m is the melting point and α is a system constant	Hardsphere Models[11]
$D = A^1T^m$ where m = 1.7 – 2.3 and A^1 is a system constant	Molecular Dynamics[12]

The influence of low frequency (0.1 Hz) oscillation at 45° to the specimen axis was found to produce an observable increase in the measured value of D for the Pb-Au alloy, as had been anticipated. Since a detailed analysis of the effects of forced vibration on liquid diffusion couples of the dimensions used in this series of experiments was not available when planning the experiments, a forced oscillation of 0.1 Hz, but with a square wave form, was requested for the processing of some of the diffusion samples. This would provide a fundamental oscillation mode of maximum amplitude 4 mg and at 0.1 Hz, plus a range of harmonics at various frequencies and amplitudes. This was done on the basis that, since there was no clear description of the atomic movements involved in liquid diffusion, a variety of forcing modes might all contribute to the solute redistribution process, in addition to the bulk convective transport induced in the sample by the low frequency components of the forcing oscillation. As is seen in Figure 2.2, the value of D was about doubled for Pb-Au.

The most successful and systematic study of self and inter-diffusion in liquid metals in the 1980's is Frohberg's work in the Sn system. One conclusion obtained by Professor Frohberg was that the temperature dependence of the diffusion coefficient appeared to obey the predictions of the fluctuation theory ($D \propto T^2$) more closely than an Arrhenius-type relationship for both self diffusion in Sn and inter-diffusion in liquid Sn-In alloys.

When considering the marked reduction in diffusion coefficient in the absence of significant g-jitter and the fact that it was found that $D \propto T$ for all the alloy systems examined, attention is directed to Figure 2.15.

More recently, Frohberg *et al.*[13] have demonstrated how the diffusion coefficient varies with temperature for various types of experimental environments. In the 1g case, with considerable buoyancy-driven solute transport at higher temperatures, the variation was found to be a power law relationship, which may be approximated by an exponential, while in the case of microgravity experimental results with buoyancy convection much reduced but with g-jitter present, it was best represented by a $D \propto T^2$ relationship.

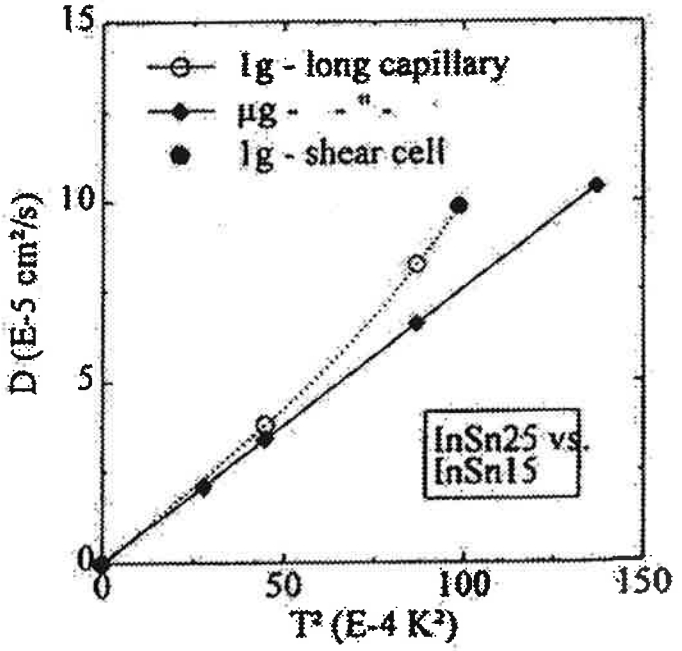

Figure 2.15 Diffusion Coefficients in the In-Sn System[13]

However, as the contribution to mass transport by g-jitter is reduced still further by using the MIM in the isolating mode, the diffusion coefficient and temperature relationship becomes linear, as shown in detail in the results section of this report.

As it can be seen in Figure 2.15, due to Frohberg[13], experiments with the long capillary technique were made in microgravity and on the ground, 1g, while the shear cell technique was

used for the experiments on the ground only. It becomes apparent that the measured diffusion coefficient is independent of the measurement technique used.

Returning to the $D \propto T$ behaviour reported here, it should be noted that while Frohberg *et al.*[13] have reported a $D \propto T^2$ relationship for experiments conducted without benefit of a MIM, $D \propto T$ is commonly observed to describe both fluidity (≡ reciprocal viscosity) and diffusion in non-electrolyte liquids if care is taken to suppress buoyancy-driven liquid flows. This view has been championed by a number of researchers, particularly Hildebrand[14]. This is shown, for example, in Figure 2.16. The measured diffusion rates for various species in CCl_4 and C_6H_6 was found to be closely linear with temperature over the temperature range tested. The corruption of data by buoyancy effects was rendered insignificant by measuring the diffusion coefficient using the experimental conditions governed by Fick's First Law, i.e., the flow of the chosen species through a membrane. This is given by

$$\text{Flux} = D\frac{\partial C}{\partial x} \qquad (2.2)$$

where C is the concentration and x is the distance.

In these experiments, the membrane between the species source and the large solvent-vessel beneath it consisted of a 9 mm thick slab of 2962 lengths of fine bore stainless steel hypodermic tubing in a parallel array and imbedded in solder. The small diameter of the hypodermic tubing effectively dampened-out any buoyancy contributions to the observed value of the diffusion coefficient.

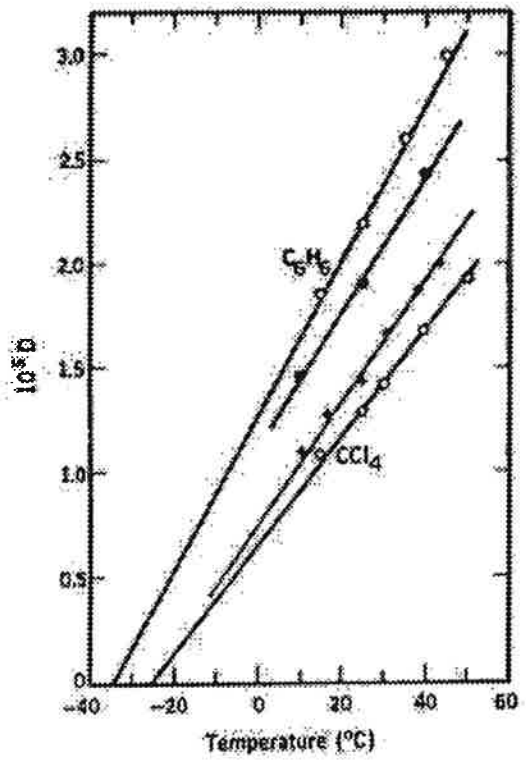

Figure 2.16 Diffusion Coefficient of C_6H_6 and CCl_4[14]

In Figure 2.16, the diffusion coefficients are expressed in cm^2/sec where the symbol "o" represents the self-diffusion coefficients of C_6H_6 and CCl_4, as shown near their corresponding lines. The symbol "•" represents the diffusion coefficient of CCl_4 in C_6H_6 while "+" represents the diffusion coefficient of I_2 in C_6H_6.

We are now seeking funding to conduct molecular dynamics simulations of liquid diffusion, the first phase of which will be to develop suitable semi-empirical potentials for the alloys of interest using the "embedded atom method"[15].

g) Conclusions

While fully definitive statements must await further experimental and theoretical analysis, it appears that the results obtained to date support the following conclusions, namely:

1) The D values with the "raw" g-jitter of MIR (corresponding to MIM latched) are similar to those obtained in similar alloy diffusion couples in 1992 on STS 47 and 52. Thus as far as liquid diffusion in narrow capillaries is concerned, both space vehicles provide similar reduced gravity environments.
2) The D value may be reduced markedly by reducing the gravity field from 1 g to that of the STS or MIR in low earth orbit.

3) The reduction of g-jitter afforded by MIM, reduces the measured value of D even further, perhaps by another factor of 2 for the Pb-Au alloy.

4) The experimental data obtained thus-far in the present study points to a linear relationship between D and T when g-jitter is suppressed.

5) The use of a MIM on any manned space platform operating in low earth orbit (LEO) is essential when attempting to obtain accurate experimental values for liquid diffusion coefficients, even taking note that MIM is ineffective in isolating the experimental facility from disturbances induced by 'jitter' of less than 0.01 Hz. These more accurate D values should permit a detailed examination of our current understanding of the structure(s) of liquid metals and semiconductors. Such an understanding should eventually permit the accurate prediction of D values for all alloy systems, a feat only possible as a result of the judicious use of LEO processing.

6) Low frequency, small amplitude (<4 milli-g) single axis forced g-jitter does appear to induce appreciably increased liquid transport in narrow long capillary liquid diffusion specimens of Pb-Au.

3 The Influence of Gravity on Particle Pushing during the Freezing of Reinforced Aluminum Alloys

a) Background

Over the past 35 years there has been extensive research examining the interaction between solid particles and a solid/liquid interface. While the earlier work was primarily concerned with reducing the inclusion content of steels, more recently attention has turned to the study of the distribution of particles in Particle Reinforced Metal Matrix Composites (PRMMC). When a particle interacts with the solid/liquid interface of the matrix as the matrix freezes, the particle can either be rejected at the interface i.e. "pushed", or it will become incorporated into the solid. For incorporation into the solid, two conditions can apply. The particle may become engulfed, which is to be incorporated into a planar interface, or it will become entrapped. An entrapped particle is one that has been pushed by the advancing local solid/liquid interface, but then becomes trapped between cells or dendrite arms, finally to be incorporated into the solid. Whether the contributing particles are simply pushed or entrapped, particle clustering tends to take place in PRMMCs.

For the industrial use of MMCs it is highly desirable to manufacture the material with an uniform distribution of particles. It has been shown that a high degree of clustering in a PRMMC leads to low ductility due to a high constraint on matrix deformation and consequently a higher risk of damage initiation, even cracking.[16] It is therefore important to understand the causes of particle pushing and entrapment and also to characterize clustering. It has been demonstrated that there is a critical velocity (V_C) of the solid/liquid interface in a PRMMC as it is frozen that will lead to particles being incorporated into the solid with no pushing or entrapment. If the velocity of the interface is greater than V_C then the particles will be engulfed, otherwise if the velocity is less than V_C, then the particles will be rejected locally from the interface, resulting in particle pushing and/or particle entrapment[17].

The original experimental materials used were often water or an organic liquid matrix[17,18,19,20,21,22]. More recent experimentation has employed the use of a metal matrix and ceramic particles to give insight into PRMMC processing. Two main theoretical approaches have been used to study particle behavior at the solid/liquid interface. These may be described as the "thermodynamic" and "kinetic" approaches. Most of the original research made the assumption that there was a planar solid/liquid interface interacting with single particles; buoyancy forces were usually neglected. This is the basis of the thermodynamic approach, which examines the net change in free energy for engulfment, and is summarized in Equation 3.1[22,23], where ΔF_{net} is the net change in free energy, σ_{ps} is the interface energy between the particle and the solid, and σ_{pl} is the interface energy between the particle and the liquid:

$$\Delta F_{net} = \sigma_{ps} - \sigma_{pl} \qquad (3.1)$$

If $\Delta F_{net} < 0$, then particle engulfment will occur and if $\Delta F_{net} > 0$, then particle rejection will occur at the interface.

The kinetic approach is based on the assumption that if there is always a layer of liquid of finite thickness between the particle and the solid, then the particle will not be trapped[23]. It is assumed that there is what is effectively a repulsive force between the solid and the particle, which prevents the particle from being engulfed. Several of the postulations for the source of this force include: an increase in surface free energy, that particles may be electrically charged relative to the solid, that Van der Waals forces exist when the particle breaks the liquid film and touches the solid/liquid interface. The presence of a "gap" was observed as early as 1967 by Hoekstra[18] who demonstrated that water migrates to a transition layer between the interface and glass beads under the influence of electrical and temperature gradients.

Both the thermodynamic and kinetic approaches assume that the solid/liquid interface is planar, which is not a very realistic assumption. Most recent experimentation and theory have shown that solid/liquid interface shape is affected by the thermal conductivity difference between the matrix and the particle[19,24,25,26,27,28,29]. Many researchers have observed and modeled the gap which forms between the interface and the particle[24,30,31,32]. The thermal conductivity difference is used in the calculations which summarize the shape and size of the gap. Kim calculated the curvature of the solid liquid interface, Equation 3.2.

$$k = \frac{Ga}{\Gamma}\left[\frac{\alpha - 1}{3}\right] \qquad (3.2)$$

where: $\Gamma = \frac{\sigma_{SL}\, T_m}{\rho H}$

= the curvature of the interface

Where: ρ = density of the solid phase

H = heat of fusion

σ_{SL} = surface energy of the interface

T_m = The temperature of the interface

In this, the curvature of the interface (k) is a function of surface tension of the interface, and also the thermal gradient imposed on the interface far away from the particle (G). The equation also shows that when α, the ratio of the thermal conductivity of the particle to the thermal conductivity of the liquid, is unity, then the interface is planar. If $\alpha > 1$ then the interface is concave, and convex if $\alpha < 1$. It was demonstrated by Zubko[24] that in systems where $\alpha < 1$ the particles were repelled and when the surface was concave the particles were captured. It was postulated that once a particle was surrounded to more than half of it's diameter then the interface would capture it.

It was originally proposed by Uhlmann that a particle would become incorporated into the solid if the liquid could not diffuse behind the particle quickly enough[17]. Shortly after,

Smith and co-workers demonstrated with transparent analogues and metals that relative movement, both rolling or gliding, between the inclusion and the advancing solid/liquid interface could maintain the liquid bridge between the particle and the interface and so permit pushing at velocities far in excess of V_c[33,34,35]. Whether the particle was trapped or pushed as it moved in the liquid streaming past the interface depended on whether it was small or large relative to the "stagnant" boundary layer at the interface. As a result of these studies, Smith proposed that forced fluid flow could be used to control the capture of inclusions by an advancing crystal interface.

More recently, Han[31] has revisited the concept of the importance of relative movement between the particle and the interface. Han confirms the earlier claims of Smith and co-workers that if there is significant fluid flow into the gap between the particle and the solid/liquid interface then the particle will not be incorporated into the solid. As shown by Smith et. al. when the liquid flow rate is high, the boundary layer will be smaller and the resulting unbalanced viscous drag will cause the particle to be put into motion, and tend to spin as it gets closer to the solid/liquid interface. As it spins it will bring it's own liquid boundary layer with it and so avoid entrapment and hence be pushed. This motion will keep the particle moving with the interface through the solidifying melt, however if the liquid flow is limited such that the thickness of the boundary layer becomes larger, then the particle will be more easily engulfed. Han and Hunt showed the effect of clustered particles in the melt. It was seen that a cluster will have a much higher critical flow rate than a single particle. This means that the clusters will be more easily incorporated into the solid. This further confirms the earlier observations of Smith and co-workers since for a given particle or aggregate diameter, the chance of being engulfed will increase as the local melt velocity falls with consequent increase in the thickness of the stagnant boundary layer. (Figure 3.1)

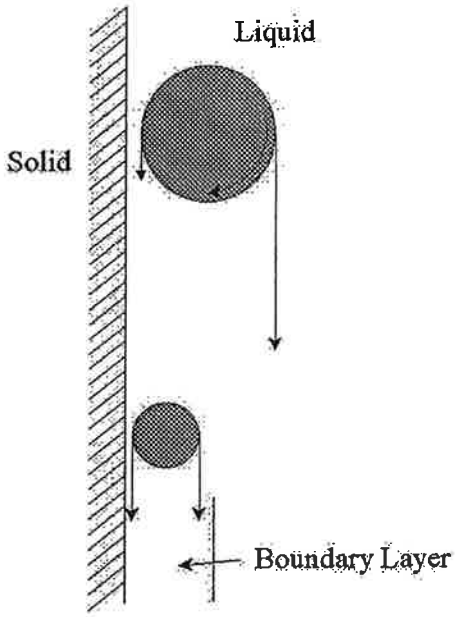

Figure 3.1 Forces Acting on Large and Small Particles Near an Interface[33]

The specific characteristics of the particles also play an important role in determining the ease of pushing or capture into the solid. Uhlmann et. al.[17] concluded that below 15μm diameter, V_c was independent of particle size, and that for large facetted particles, with the facet parallel to the planar solid/liquid interface, V_c increased with increasing diameter. This was rationalized on the basis that making contact with asperities on the surface permitted the liquid to flow/diffuse into the particle/interface gap more easily and so permit pushing. However, above a limiting size, V_c must decrease as particle size increases due to the increasing viscous drag. The surface roughness was also examined by Bolling and Cissé[19] who concluded that a well defined bump on a particle would act as the particle radius in determining whether incorporation into the solid would occur. Three sets of equations were developed, depending on how the bump radius compared to the actual particle radius[19]. In an experiment with inert particles in water, Cissé and Bolling[19] developed an inverse power law between the size of the particle and the critical velocity for smooth particles. However, more recently, in a theoretical analysis, Pötschke et. al.[32] deduced that $V_c \sim G^{0.5} R^{-1}$ (where G is the temperature gradient in the liquid and R is the radius of the particle.) An earlier, less rigorous analysis by Chernov et. al.[36] showed that a relationship of $V_c \sim R^{-2}$ appeared to fit experimental data.

Although there has been extensive research performed and many analyses developed to summarize the behavior of particles interacting with a solid-liquid interface, each approach and set of equations is specific to some particular metal and particle systems. This was demonstrated by both Gallerneault[37] and Kim[27] who applied a series of models to one PMMMC system and calculated the Vc as predicted by each. Both Gallerneault and Kim calculated Vc values for aluminum with SiC particles, Table 3.1, however Gallerneault assumed a particle diameter of 10 μm, while Kim assumed one of 20 μm. This difference accounts for the discrepancies in critical velocity values obtained for each model. Both researchers observed that there is a large difference between the predicted value of each model when the models are all applied to the same PRMMC system. The values in the table make it very clear that further refinement is needed to find a model which is valid for industrial PRMMC systems and which can be transferred from one material to another.

Mortensen and Jin published a review paper 1992.[38] They were able to summarize the vast range of reported results in three simple categories. While the experimental data which exists is very difficult to compare directly because each author used different experimental materials, Mortensen and Jin noted that certain matrix – particle combinations always behaved in a closely similar manner. There are some combinations in which the particles are always engulfed, regardless of the growth conditions. This was attributed to the negative net free energy change required to transfer the particles from liquid to solid, (implying that the particle /solid interfacial energy is lower than the particle/liquid interfacial energy). The particular materials which appear to exhibit this characteristic include graphite or SiC particles in eutectic or hypereutectic Al-Si alloys. Other non-MMC examples include silicone glass in biphenyl, polystyrene in naphthalene, and "Teflon" in biphenyl.

Table 3-1 – A Comparison of Critical Velocity Values Calculated from Various Models by Kim[27] and Gallerneault[37], for an Aluminum / SiC PRMMC System

Author	Governing Equations	V_C Calculated by Kim (μm/s)	V_C Calculated by Gallerneault (μm/s)
Uhlmann et al. 1964	$V_c = \frac{(n+1)}{2}\frac{(La_0V_0D_1)}{(kTR_1^2)}$	0.187	0.43
Hoekstra et al. 1967	$V_c = \frac{2D\Delta H_f K}{RT^2\Delta V\alpha}(\frac{d}{r})[\frac{dT}{dl}]$		3.78×10^{-4}
Chernov et al. 1976	$V_c = \frac{0.14B_3}{\eta R_1}(\frac{\sigma_{s1}}{B_3R_1})$; $\frac{\lambda^2}{1} > R_1$	1.959	0.7
	$V_c = \frac{0.14B_3}{\eta R_1}$; $\frac{\lambda^2}{1} < R_1$	2.38	
Bolling and Cissé 1971	$V_c = [\frac{4\Psi(\alpha)KT\sigma_{s1}A_0}{9\pi\eta^2R_1^3}]^{0.5}$; $R_1 < R_B$	4.24	3.9
Stefanescu et al. 1988	$V_c = \frac{\Delta\sigma a_0}{6(n-1)\eta R_1}[2-\frac{k_p}{k_1}]$	3120	
Potschke et al. 1989	$V_c = \frac{1.3\Delta\sigma}{\eta}[16(\frac{R^2}{a_0})^2\mu(15\mu+x)+x^2]^{-0.5}$		5.0
Stefanescu et al. 1990	$V_c = \frac{1}{6\eta_f R}[\frac{\Delta\sigma_0 d_0}{2}[2-\frac{k_p}{k_L}]-\frac{4R^3}{3}g\Delta\rho]$		3700
Shangguan et al. 1992	$V_c = \frac{\Delta\sigma a_0}{6(n-1)\eta\alpha R_1}[\frac{n-1}{n}]^n$	986	
Kim et al. 1998	$V_c = \frac{\Delta\sigma a_0(kR_1+1)}{18\eta R_1}$	5800	

They go on to report that there are some systems for which a critical velocity (Vc) does exist. They report that the velocity, Vc, below which pushing occurs and above which the particles are captured, is known to be dependent on many different experimental variables including particle size, melt viscosity, temperature gradient, thermal conductivity differences, and matrix solute content, amongst others. Examples of systems known to exhibit a critical velocity for the transition between pushing and engulfment include Ni in salol, graphite in thymol, silicon dioxide in water, latex in water and nylon in naphthalene. Equation 3.3 is a generalization of the critical velocity relations which have been developed in the literature.

$$V_c = Cd^n \qquad (3.3)$$

Where: C is a constant,
d is the particle diameter
$0.5 < n < 3$

Finally they conclude that there are some particle-matrix combinations in which the particles are always pushed regardless of the processing conditions. There are many examples of these systems including SiC in Al-2%Mg, SiC in Al-7%Si, ZrB_2 in Al-3%Mg, but most importantly, most hypoeutectic aluminum alloy matrix composite systems with a non-planar interface fall into this category.

It should be noted that the MMC systems selected for this study fall into the category of hypoeutectic aluminum alloy matrix composites and so entirely pushing behavior might be expected. However the particulate phases used differed considerably from one another with respect to particle size, shape and thermal conductivity.

b) Experimental Design Considerations

Any attempt to correlate the experimental values observed for V_C with theoretical predictions is risky unless close attention is paid to the actual interaction conditions between the inclusion and the advancing solid/liquid interface. In this regard there are a number of important considerations. Some of these are:

i. Buoyancy – Clearly, gravitation forces can produce marked effects in particle distribution in PRMMCs.
ii. Viscous Inertia – The forces required to "push" a particle by an advancing solid/liquid interface will be markedly influenced by the contact that a particle is likely to have with others in the neighboring liquid, their size and densities, the viscosity of the liquid and the normal velocity of the interface.
iii. Particle Volume Fraction V_F – As V_F increases, and pushed particles begin to accumulate at the solid/liquid interface, "viscous inertia" will increase.
iv. Particle Shape / Irregularity – Following Cissé and Bolling, particle radius at the point of interface contact and what we describe as "Viscous Inertia" in (ii.) above are likely to be

intimately connected. Angular single particles would be expected to be trapped more easily than the same mass of particle when spherical.

v. Liquid Shear - Following Smith et. al., liquid shear at an advancing solid/liquid interface can cause particle rotation and so reduce the possibility of capture.

These considerations prompted the selection of the materials for the QUELD II particle pushing experiments on MIR. The volume fractions of the reinforcement was varied over a wide range so that the various considerations outlined above could be quantitatively explored in the absence of buoyancy effects. In addition, since the QUELD II facility was mounted on MIM, it was also possible to provide forced oscillation of the QUELD II samples in order to induce relative movement between the particles and any local solid/liquid interfaces. With this facility, it was hoped to be able to examine the likelihood of being able to use controlled liquid shear to produce inclusion-free solids, or trap particles in desirable regions of a freezing body, and examine further why Mortensen and Jin concluded[38] that eutectics and faceting proeutectic-phase interfaces (for example primarily Si in hypereutectic Al-Si) never push particles, but engulf them.

c) Experimental

Experiments were performed to examine particle pushing in three different PRMMC systems, namely Duralcan, (A356 + SiC particles), Comral (6061 + particles which are primarily Al_2O_3), and Duralcan (6061 + Al_2O_3). [Note: A356 is Al - 6.5-7.5% Si, <0.2% Cu, 0.25-0.45% Mg and 6061 is Al – 0.4-0.8% Si, 0.15-0.4% Cu, 0.8-1.2% Mg, 0.04-0.35% Cr.] The Comral MMC contains microspheres manufactured by Comalco, called Micral – 20 reinforcement. It is a unique material because the particles are manufactured to be as close to spherical as possible. The average particle size of the spheres is 20 μm. This differs from the 6061 + Al_2O_3 material because the particles in this MMC are very angular. The commercial metal matrix composites received contain 15 or 20 vol. % particles. These materials were diluted with pure aluminum to reduce the vol. % particles to 2%. The reason for this dilution was to be able to perform experiments where the interface at any point was interacting with single particles as opposed to large clusters.

The dilutions were performed by melting the MMC with the pure aluminum and stirring the mixture to combine and blend the material. The diluted MMC was cast into a heated steel mould to produce 8mm diameter rods. These rods were then swaged to reduce them to the required 4mm diameter.

The experimental facility used was again QUELD II, as used for the liquid diffusion samples described earlier, and again using the MIM as a services and support platform. The facility was used on MIR for particle pushing experiments with the above three PRMMC systems. The experimental work outlined in this section also includes samples processed in a Ground Based Unit (GBU) of QUELD II, and for the samples processed on MIR. With use of QUELD II in a gradient-freeze mode, a sample can be directionally solidified at specific rates. The rates used were 1, 2, 5, 10, and 100μm/sec. The 1g samples processed in the GBU furnace

were held with their major axis horizontal and with the macroscopic solid-liquid interface vertical and moving perpendicular to the gravity vector.

The forced vibrations used for these gradient-freeze experiments on MIR again consisted of an induced frequency of 0.1Hz at 45° to the sample's major axis and at a amplitude of 4mg.

The sample encapsulation used for the QUELD II samples is described in Appendix III.

After processing, the space-based samples were returned to earth via the Space Shuttle. When the samples were removed from their capsules, the processing direction was noted. For metallographic examination, the samples were cut lengthways using Electro-Discharge Machining (EDM). One side of the sample was reserved for further longitudinal analysis, while the other side was cut into three equal sized pieces along the sample length also using the EDM. The sample sectioning is shown in Figure 3.2.

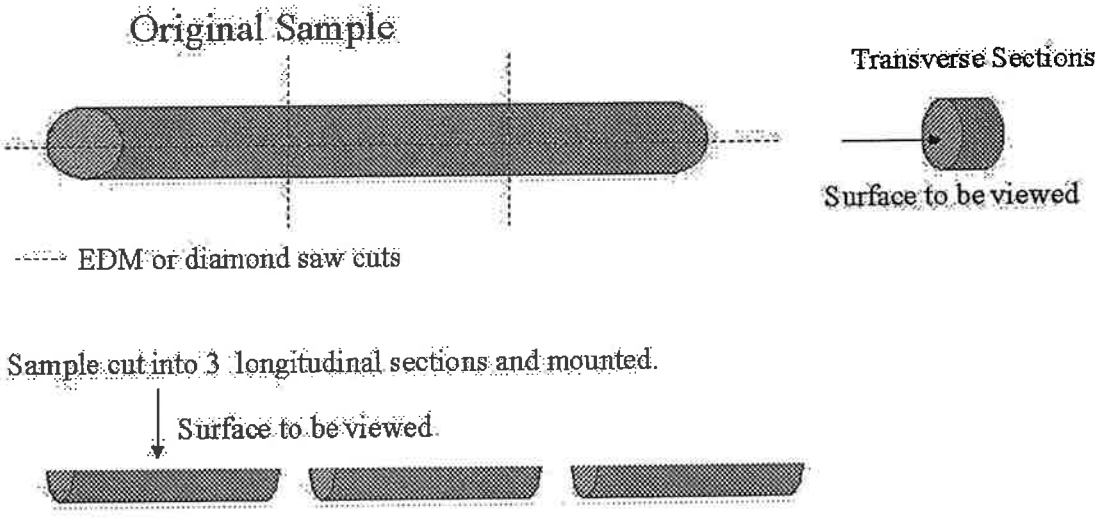

Figure 3.2 The Sectioning of a QUELD II Sample for Microscopy

After mounting, the samples were initially ground using Grid-Abrade discs (68 μm, 30 μm, 12 μm, and 6 μm) which were found to be very effective at cutting through both the particles and the matrix to ensure that the initial surface was as flat as possible. The samples were then polished for 5 minutes on a Pan W cloth with each of 6 and 1 μm diamond air sprays to cut the particles, followed by 30 seconds on a high nap cloth with colloidal silica to polish the matrix. This method resulted in an even surface with equal removal of both particles and matrix. Etching was used to help identify solute-rich phases in the samples. The two etches used were Barker's Colour Etch and Weck's reagent. Etched surfaces were examined using an optical microscope and micrographs were taken.

A summary of the samples and processing conditions is given in Table 3.2, and Table 3.3.

Table 3-2 – A Summary of the Comral Samples Processed on MIR

Sample number	Material	Processing rate (μm/sec)	MIM Mode	Observations: Metalographic Structure	Particle Behavior
403	Comral	1	isolating	Cells develop towards end of sample	Entrapped particles at cell boundaries and within cells
407	Comral	1	0.1 Hz	Cells develop towards end of sample	Entrapped particles at cell boundaries
405	Comral	2	isolating	Striations seen towards end of sample	Unclustered Random pattern
409	Comral	2	0.1 Hz	No structure observed	Unclustered Random pattern
404	Comral	5	isolating	Little structure observed	Unclustered Random pattern
408	Comral	5	0.1 Hz	Little structure observed	Unclustered Random pattern
406	Comral	10	isolating	Iron phase present Striations indicating cellular structure	Particles in solute bands due to cellular growth
410	Comral	10	0.1 Hz	Striations indicating cellular structure	Particles in cell grooves
417	Comral	100	No Data (0.1 Hz)	Strong cellular grown Iron phase present	Entrapment of particles and iron rich phase

Table 3-3 – A Summary of the Duralcan Samples Processed on MIR

Sample number	Material	Processing rate (μm/sec)	MIM Mode	Observations: Metalographic Structure	Particle Behavior
411	2% SiC	1	No Data (isolating)	Dendritic with eutectic filling interdendritic space - some porosity	Entrapment Pushing into interdendritic spaces
418	2% SiC	1	No Data (0.1 Hz)	Dendritic with eutectic filling interdendritic space	Entrapment Pushing into interdendritic spaces
412	2% SiC	10	No Data (isolating)	Dendritic throughout sample Entrapment	large eutectic phases Uniform particle distribution throughout sample
416	2% SiC	10	Highly Latched	Dendritic throughout sample large eutectic phases - some porosity	Entrapment Sample uniform and of mottled appearance
415	15%SiC	1	Highly Latched	Cellular hypoeutectic dendrites	Entrapment - Heavy loading of particulate between columns of hypoeutectic phase
413	Al2O3	1	Highly Latched	Columnar dendrites	Entrapment Gross pushing laterally and along length of sample
414	Al2O3	10	Highly Latched	Columnar dendrites	Entrapment No evidence of gross pushing along sample length

d) Results and Discussion

In order to interpret the interaction of the particulate with the solid/liquid (s/l) interface, it was necessary to establish the probable interface morphology during the freezing of each space sample.

It is now well understood that when a dilute alloy freezes, it generally does so in a cellular or cellular/dendritic fashion, as shown in Figure 3.3

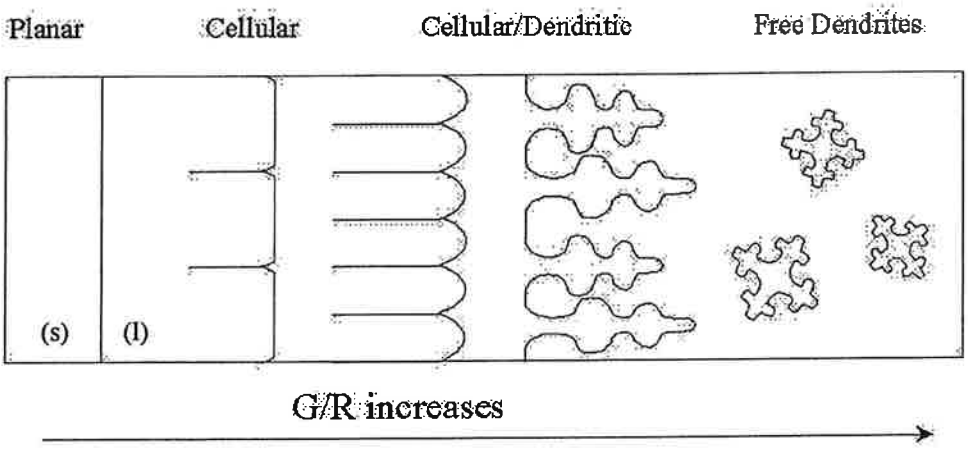

Figure 3.3 Interface Morphology Transition from Planar to Free Dendritic

The type of interface present depends on the solute concentration and the growth conditions for a given alloy system. As the quotient G/R decreases, where G is the temperature gradient in the liquid and R is the macroscopic rate of crystal growth, then constitutional undercooling at the solid/liquid interface will arise[39] when then inequality in Equation 3.4 becomes true; then, a planar interface becomes unstable and cellular projections form on the solid/liquid interface.

$$\frac{G}{R} < \frac{mC_O\,(1-k_O)}{(k_O)} \qquad (3.4)$$

Where: m = liquidus gradient
C_o = alloy concentration
K_o = partition coefficient for the alloy system

As the value of G/R falls, the cell size continues to decrease and the cellular shape becomes much more pronounced. Eventually side branches form on each projection and the interface becomes cellular/dendritic. A further decrease in G/R will cause free dendrites to appear in the liquid ahead of the macroscopic solid/liquid interface.

Normally, cellular growth can be detected by etching a polished cross section of the unidirectionally frozen sample. However if the sample has been frozen very slowly, the cellular solute segregation will have had a chance to "anneal out" since, once formed, the solid just past the solid/liquid interface will be subjected to an extended period at a high temperature, thus permitting the cellular segregation to be removed.[40] As the solute diffuses to homogenize the sample, any accommodating dislocations, which had been incorporated in the solid to accommodate ill-fitting solute atoms, will be free to move into low angle arrays (striations), to annihilate each other or diffuse to the surface in order to reduce the free energy of the sample.

Most of the samples processed in space were grown slowly and so they were homogenized, thus reducing, or removing all traces of cellular growth. In view of this it was necessary to freeze samples of the matrix alloys at the rates of crystal growth used in the MIR space program. Since the presence of particulate compromises the sensitivity of the metallographic study, only diluted matrix alloys were used for this study.

The aim was to freeze samples of the diluted matrix alloys at the rates used in space, and when approximately half of the sample has frozen, to quench the sample[41] As the result of this operation, the microstructure on either side of the interface should be revealed by etching since the solute laid down in the crystal near the quenched solid/liquid interface will not have had time to diffuse away.

e) Quenched Interface Studies of Dilute 6061 Particle-Free Ground-Based Samples

The particle-free diluted 6061 aluminum alloy samples were processed to examine the residual microstructure and solute segregation pattern at each growth rate without the influence of the particles. The samples were first grown using the QUELD II program corresponding to each matching sample profile. The second run of samples was conducted by arresting the growth by quenching when the sample was only 50% processed. It was found that all samples had grown in a cellular or cellular/dendritic manner.

For each quenched sample, the cell size was measured just behind the interface. The results are plotted below in Figure 3.4 and show that cell size decreases with an increase in growth rate, as expected, confirming the conclusion that all samples processed in the Ground Based Unit (GBU) grew in a cellular fashion.

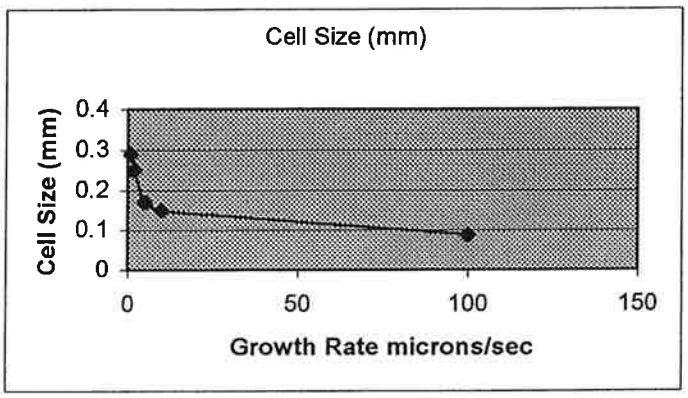

Figure 3.4 Decrease in Cell Size for 6061 Aluminum Quenched Interface Samples

However, when attempting to transfer this information into the analysis of the space-grown samples, we should note that with the GBU used with the sample axis horizontal during processing there would be some opportunity for convection in the samples. The net result of this would be to reduce the value of "G" in Equation 3.4 and so increase the severity of constitutional supercooling in the ground based samples as compared with those grown using the same QUELD II program in space.

f) Ground Based Processing of PRMMCs

The main result seen from the QUELD II ground-based samples is that particle settling is a major complication for samples exposed to gravity. Figure 3.5 shows a transverse section of a sample. This figure shows clearly that the particles were not buoyant during the processing. It can also be clearly seen from Figure 3.5 that the particles are clustered between primary aluminum dendrite arms. This resulted in a uneven distribution of particles throughout the material which, in a commercial engineering component, would lead to poor mechanical properties.

No Etch 1mm

Figure 3.5 1μm/sec Grown Comral Ground-based Sample Showing Particle Settling

g) Interpretation of Unidirectional Solidification Results

The manner in which a particle existing in the liquid ahead of an advancing solid/liquid interface will behave will depend on:

i. the morphology of that interface ,
ii. the velocity of that liquid relative to that of the interface , and
iii. the characteristics of the particle.

The effects of (ii.) have already been summarized in section 2(a) (Background).

With respect to (i.), Juretzko et. al.[42] have summarized the situation as shown in Figure 3.6.

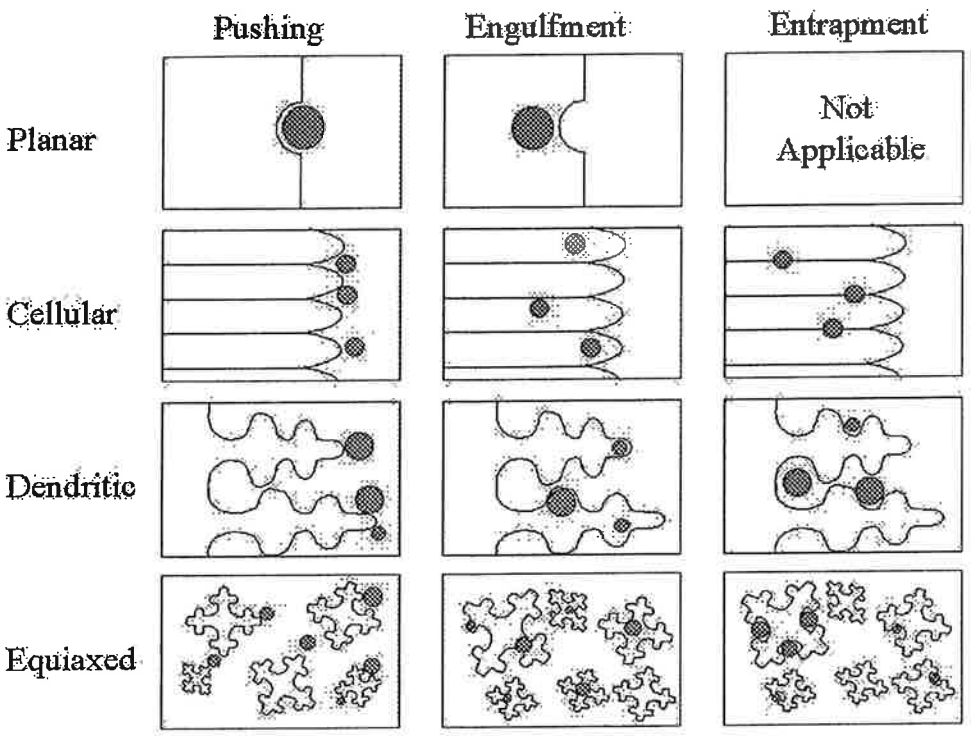

Figure 3.6 Particle Interface Interactions[42]

For the particle sizes encountered in these PRMMCs, Figure 3.6 represents an oversimplification since the particles concerned tend to be small with respect to cell or dendrite arm diameters. The situation is better represented by Figure 3.7 in which it is shown that the component of the velocity perpendicular to the solid surface of the projection at the point at which the particle comes up to it is important. This distinction is used in the following discussion of the flight sample results.

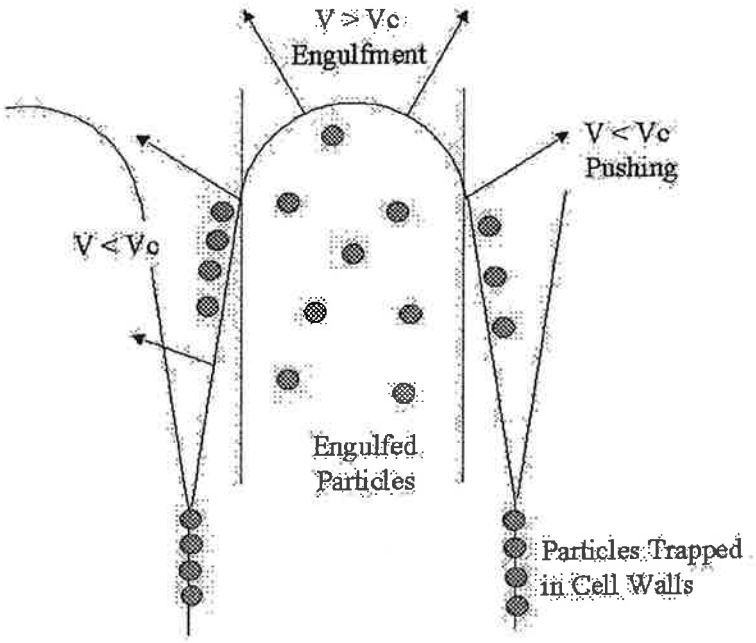

Figure 3.7 The Velocity Difference Around a Cell Affects the Particle Behaviour

h) Comral Reinforced Space–Based Samples

The results from these samples have been collected in Table 3.2. The longitudinal sections from sample 403 are shown in Figure 3.8. The premature quenching of this sample before unidirectional freezing had been completed resulting in a quenched interface being captured; Figure 3.8. It is noted that the sample must have been freezing in a cellular fashion up to the point at which quenching took place. Virtually all Comral particles are entrapped between what had been cellular projections; Figure 3.9, and Figure 3.10. However, close examination of the longitudinal sections of Figure 3.8 showed that some Comral particles had been engulfed within the cellular projections as shown in Figure 3.11, and Figure 3.12, presumably following the sequence of events shown in Figure 3.7. However most of them had been pushed laterally into the cellular grooves to form string-like clusters, Figure 3.14.

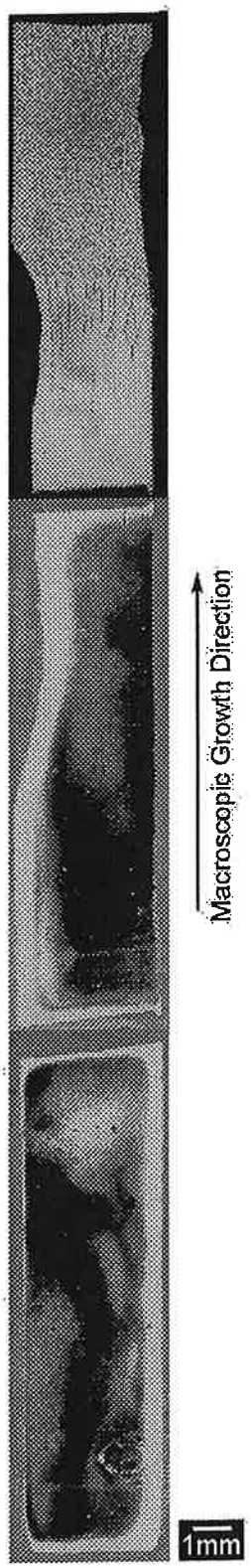

Etch: Weck's Reagent

Figure 3.8 The Longitudinal Sections of Sample 403

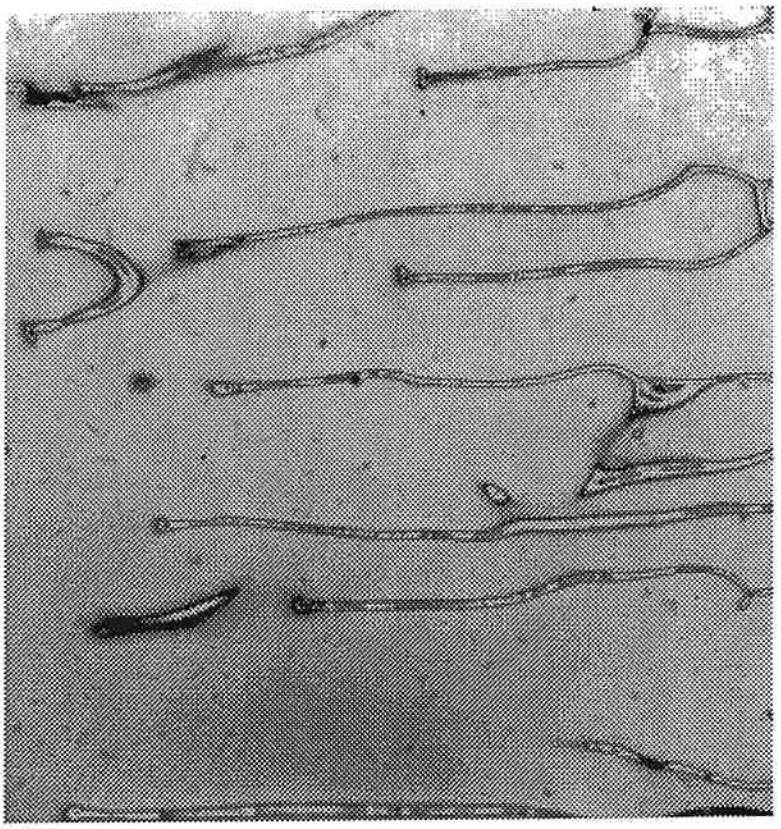

macroscopic growth direction → Etch: Weck's Reagent $\overline{100}$ μm

Figure 3.9 Space-based Comral Sample 403 Grown at 1μm/sec with MIM in Isolating Mode

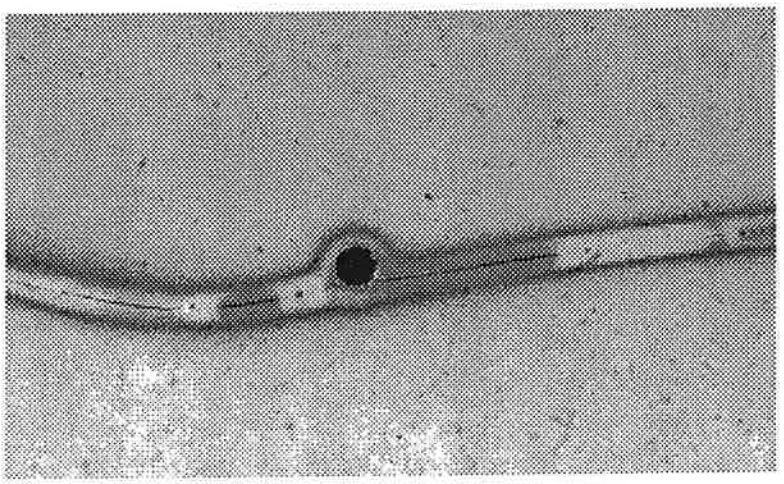

macroscopic growth direction → Etch: Weck's Reagent $\overline{10}$ μm

Figure 3.10 Space-based Comral Sample 403 Grown at 1μm/sec with MIM in Isolating Mode, Enlargement of a Cell in Figure 3.9

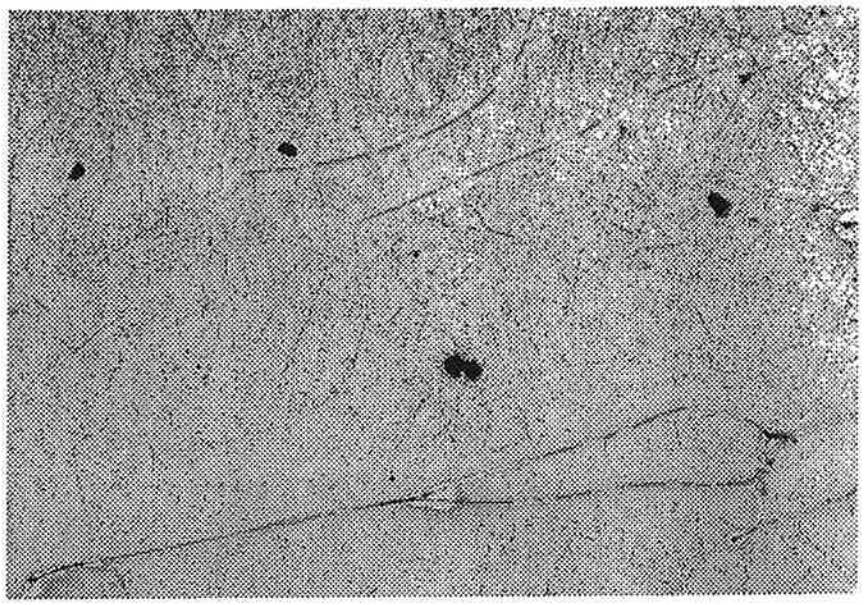

macroscopic growth direction → Etch: Weck's Reagent 100 μm

Figure 3.11 Sample 403, Space-based Comral Sample Grown at 1μm/sec with MIM in Isolating Mode Showing Comral Particles Trapped in the Body of a Cell

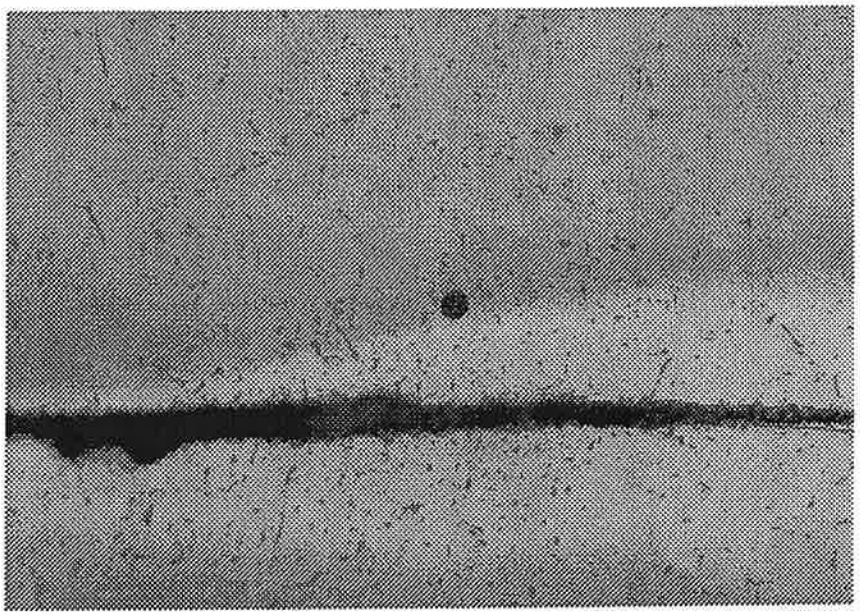

macroscopic growth direction → Etch: Weck's Reagent 10 μm

Figure 3.12 Sample 403 Showing a Comral Particle in the Body of a Cell

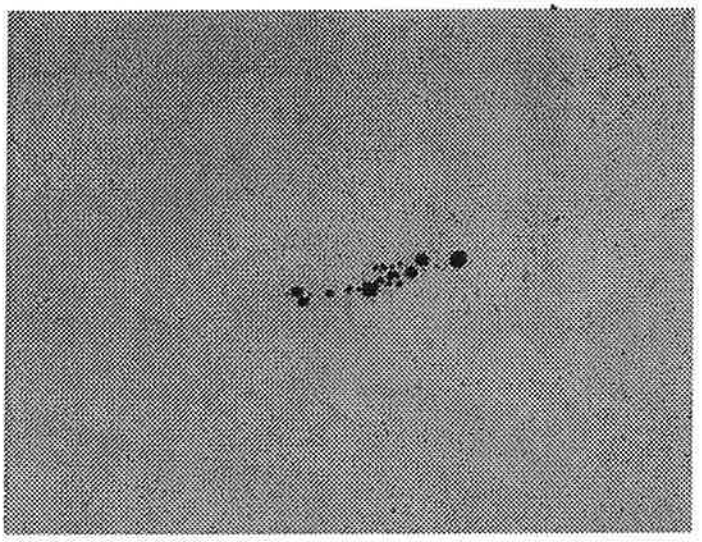

macroscopic growth direction → No Etch 100 μm

Figure 3.13 A Comral Cluster in the Body of Sample 403

The micrographs obtained from longitudinal sections of sample 407, which had been processed in an identical fashion to that of sample 403, except that an oscillation of 0.1 Hz at 4 mg amplitude (at 45° to the long axis of the sample) had been superimposed on the isolating condition, are shown in Figure 3.14. Here we see a Comral sphere entrapped in an earlier cellular groove, much as was seen in sample 403, Figure 3.9. However in marked contrast to sample 403, no spheres were found to have been engulfed within the cellular projections themselves (Figure 3.15).

This suggests that the forced g-jitter was able to provide sufficient liquid shear at the local solid/liquid interface around the cellular projections to prevent engulfment of the Comral sphere by the advancing cellular projection. The net result was that the particles all moved down into the intercellular grooves where they were finally entrapped as the groove walls enclosed in on them from all directions.

This observation suggests that if the crystal growth conditions are such that constitutional supercooling can be avoided and a planar solid/liquid interface maintained, an inclusion free crystal may be grown in microgravity using the MIM in forcing mode. All of the inclusions would be pushed normally to the solid/liquid interface and finally frozen in the terminal liquid. Quite clearly this could also be done at 1g, if a planar interface can be established and sufficient liquid shear is maintained between the particles and the advancing solid/liquid interface, as proposed by Smith in 1971.[33,34]

Since there was particle engulfment by the cellular projections at 1 μm/sec growth rate i.e. $V_c < 1$ μm/sec for the isolating condition, similar engulfment would be expected at the higher growth rate. (Table 3.2) However, with MIM in a Forcing Mode (0.1 Hz at 4 mg) then it appears that 1 μm/sec $< V_c < 2$ μm/sec since there appeared to be trapping in sample 409 and all those of higher growth rates. Such an increase in Vc is to be expected, with the increase being commensurate with the amplitude of the forcing acceleration.

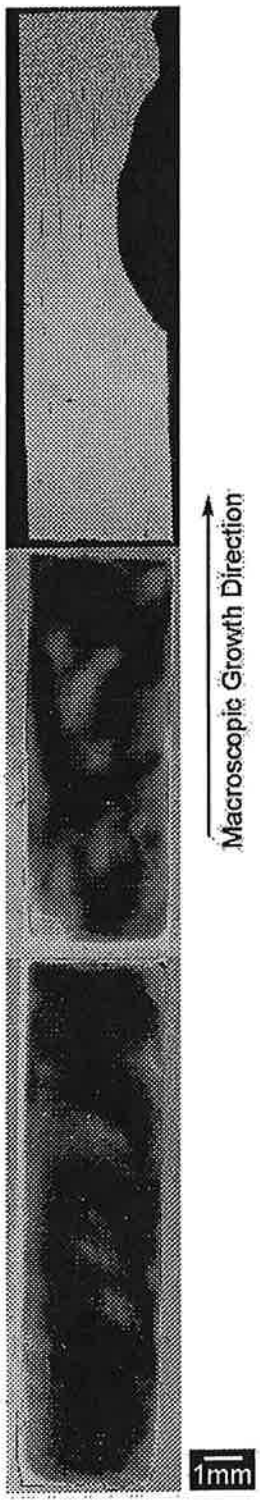

Etch: Weck's Reagent

Figure 3.14 The Longitudinal Sections of Sample 407

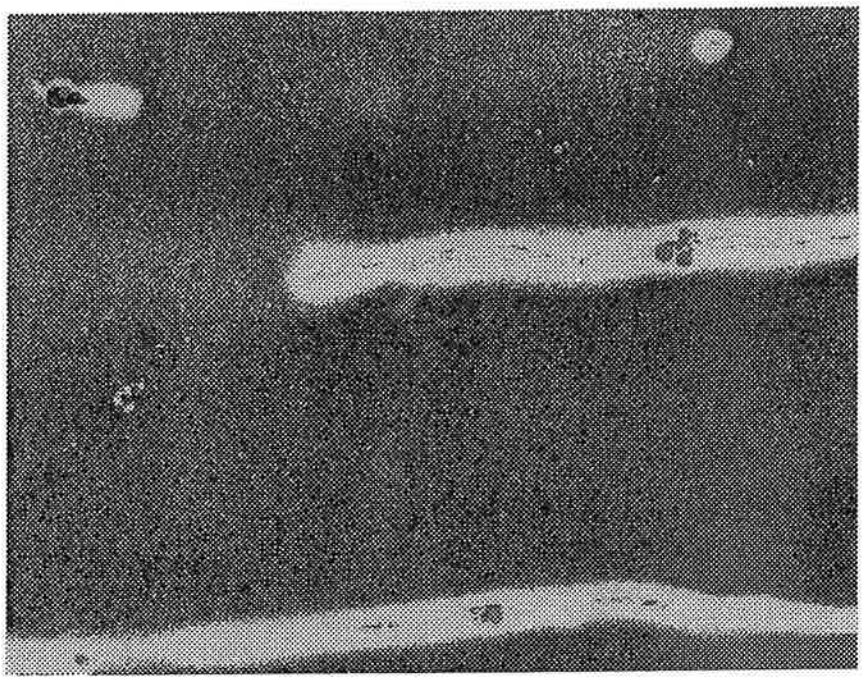

macroscopic growth direction → Etch: Weck's Reagent 100 μm

Figure 3.15 Space-based Comral Sample 407 Grown at 1μm/sec with MIM in 0.1 Hz Forced Oscillation Mode, Particle are on the Cell Boundaries

i) Silicon Carbide Reinforced A356 Aluminum Space-Based Samples

A summary of the SiC reinforced samples is located in Table 3.3. As with sample 403, the silicon carbide reinforcement appears clustered, together with Al-Si eutectic, in primary Al-rich phase interdendritic spaces, with few particles in dendrite stems (see Figure 3.16, and Figure 3.17). This suggests that for SiC as a reinforcement in this Al-Si matrix, and for these unspecified MIM conditions, V_c must be similar to the overall growth rate of 1μm/sec.

Similar results were obtained with MIM "highly latched", so that considerable g-jitter was experienced by the sample. However, it is noted that the dendritic primary phase is clear of SiC particles, meaning all SiC has been pushed into the interdendritic spaces, Figure 3.18. Even with 15% SiC, sample 415 grown at 1μm/sec shows SiC-free dendrite stems. Also, it is noted that most of the interdendritic SiC particles are surrounded by eutectic silicon, confirming the claims by Mortensen and Jin that while primary aluminum phases may 'push' particles of SiC, eutectic and hypereutectic silicon does not, see Figure 3.19.

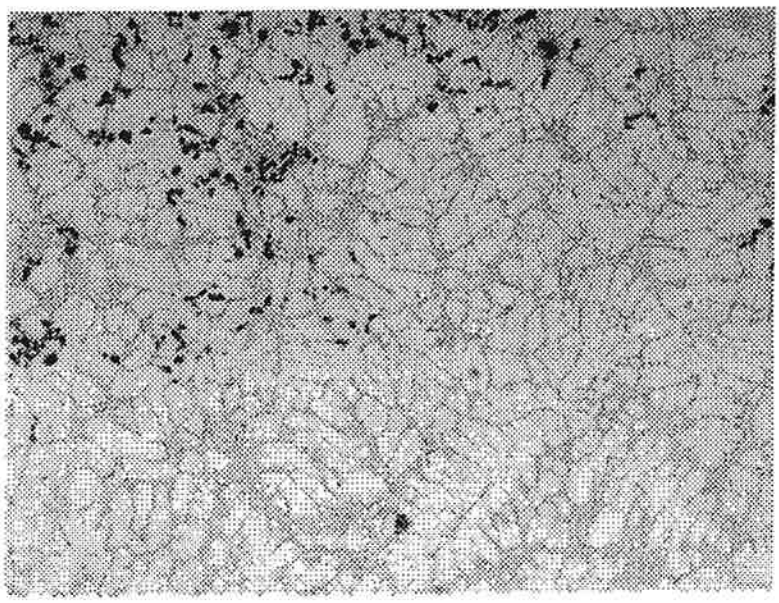

macroscopic growth direction → No Etch 100 μm

Figure 3.16 Particle Entrapment in a Space-based 2% SiC Reinforced Sample, Grown at 1μm/sec, Enlargement of Figure 3.17, Near Start End on Left Side

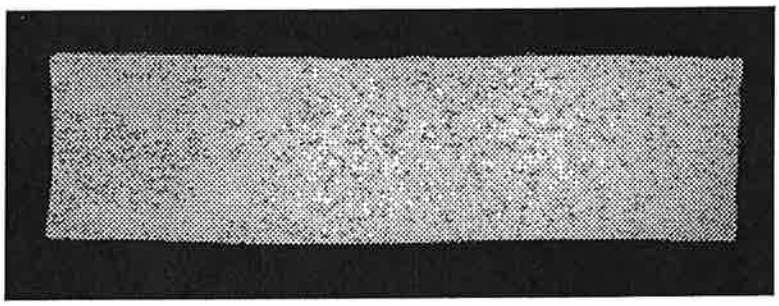

macroscopic growth direction → No Etch 1mm

Figure 3.17 Particle Entrapment and Vertical Bands in a Longitudinal Section of Space-based 2% SiC Reinforced Sample Grown at 1μm/sec

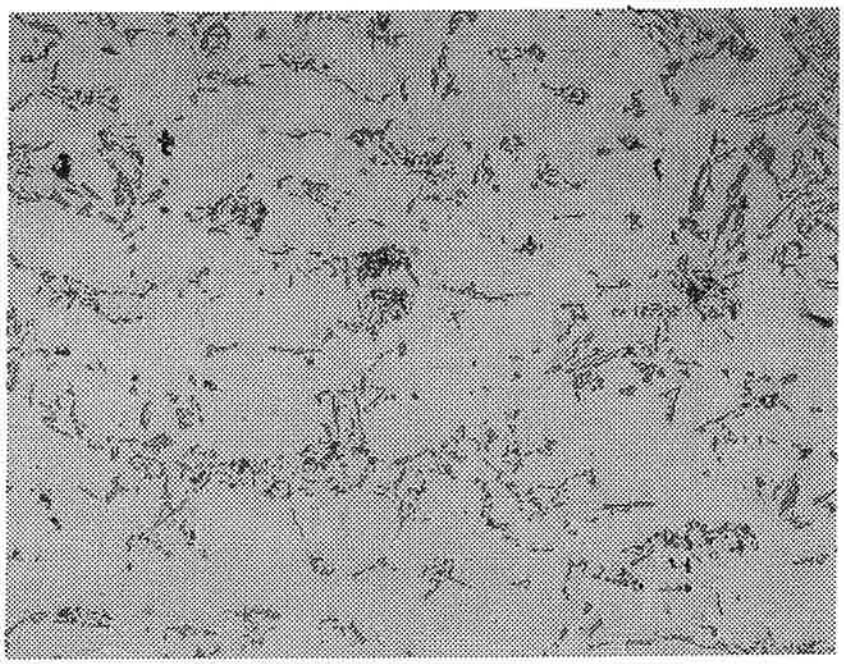

macroscopic growth direction → No Etch 100 μm

Figure 3.18 Sample 416, 2% SiC Grown at 10 μm/sec with MIM in "Highly Latched" Condition

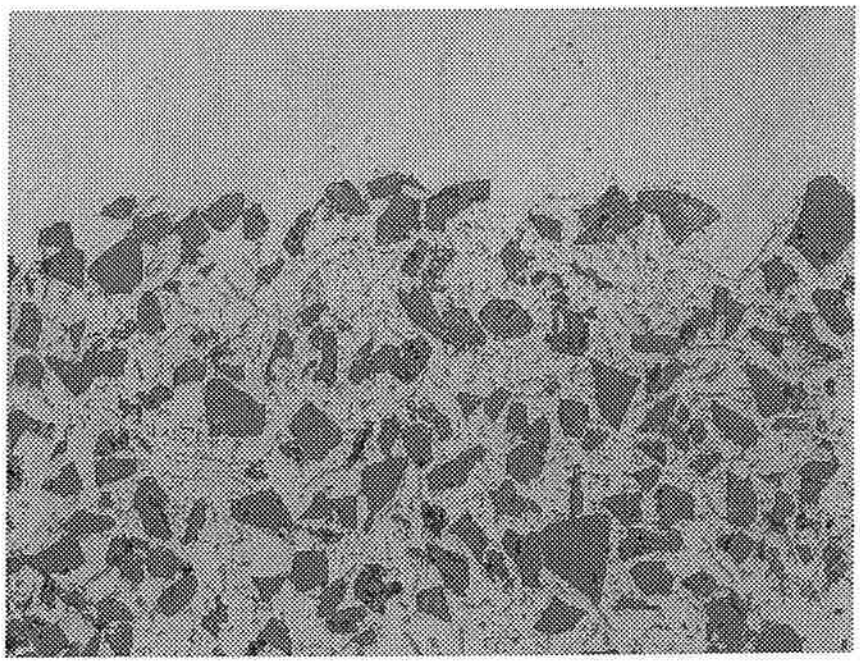

macroscopic growth direction → No Etch 10 μm

Figure 3.19 15% SiC Reinforced Aluminum Sample Grown at 1μm/sec

j) Alumina Reinforced 6061 Aluminum Space-Based Samples

A summary of the processing for the Al_2O_3 reinforced samples is located in Table 3.3. Unfortunately, the entire set of samples of this alloy were processed without MIM giving the desired isolation, so that all samples experienced some degree of g-jitter. In general, the angular particulate appeared primarily in intercellular regions, Figure 3.20, together with the eutectic phases.

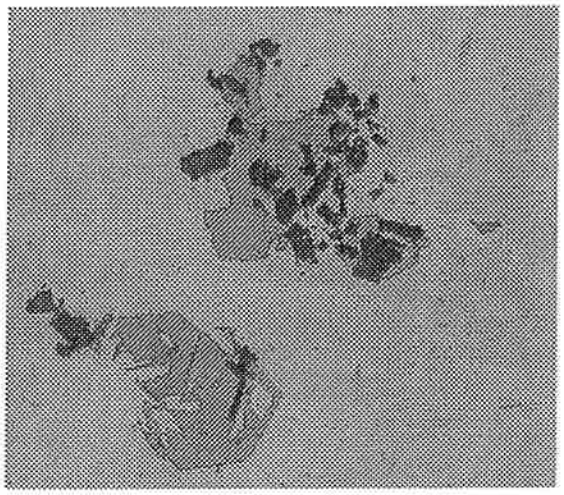

macroscopic growth direction → No Etch $\overline{10}$ μm

Figure 3.20 Particle Entrapment in a Space-based Al_2O_3 Reinforced Sample with Angular Particles, Grown at 1μm/sec

k) Conclusions

These may be simply stated:

1) If particle reinforced metal matrix composites (PRMMCs) are frozen unidirectionally in microgravity and are isolated from g-jitter, then the critical velocity above which an advancing solid/liquid interface will capture an incident particle is less than 1μm/sec and this appears to be independent of particle shape for the particle sizes tested (less than 20 μm diameter).
2) If forced oscillation is superimposed on the isolating state, then the critical velocity is increased.
3) The engulfment of particles by an advancing solid/liquid interface can be prevented if sufficient liquid shear is maintained at the solid liquid interface. In microgravity and with g-jitter isolation, a 0.1 Hz oscillation of 4 mg amplitude is sufficient to prevent overgrowth at a growth rate of 1μm/sec. This suggests a method of using microgravity to prepare highly perfect crystals.

4 Overview of the Effectiveness of the Queen's University Activities in the MIR/MIM/QUELD II Research Program

The entire QUELD II programme involved the Queen's University Microgravity Group in a variety of interactive modes. These were:

a) the design and construction of the five QUELD II units and two flight units (with strong collaboration from Millenium Biologix Inc.);
b) the design, construction, testing and certification of all samples sent to MIR for processing, and to provide an effective interface with the toxicology staff of NASA;
c) to instruct all users in the capabilities and operation of QUELD II;
d) to assist all users in the design and manufacture of flight specimens and ground-based-test specimens, including the development of ground-based sample manufacturing kits for all users;
e) to provide a full-time referral centre for all sample information of interest to users, CSA staff and NASA officials; and
f) to host periodic meetings in Kingston of all research and administrative personnel involved in the programme.

These various activities were pursued vigorously in addition to the development of the research programme into liquid diffusion and particle pushing discussed in detail in sections 2 and 3, respectively, of this report.

This is probably the most complex multi-user, multi-national agency single research programme attempted to-date without a huge NASA management team assigned full-time to its prosecution. Remarkably, with only a very small management group in addition to the Queen's staff, the CSA was able to bring a diverse research programme to fruition.

The success of the individual programmes may be judged from the Proceedings of the QUELD Review Meeting of August 27, 28 1998. At that time, the Queen's Group presented an interim report since their analysis was still in progress. However, all samples have now been analyzed and their results point clearly to well defined conclusions. These are:

1) Liquid Diffusion: all alloy systems examined are consistent in indicating that:
   (i) $D \alpha T$ over the temperature range examined;
   (ii) g-jitter may significantly increase the measure D value at any temperature; and
   (iii) MIM operating in forcing mode may be used to increase D.

2) Particle Pushing: for the diluted commercial PRMMC systems examined:
   (i) the value of V_C above which particles suspended in the melt are occluded (engulfed) is approximately 1 μm/sec and is independent of particle type, size and shape up to 20 μm diameter;
   (ii) V_C increases when g-jitter is present.

It was found that some of the samples were processed under unplanned MIM operating conditions. The CSA staff described these as "strongly latched" and the accelerometer "logs" showed the samples so processed experienced large transient accelerations. The samples were found to have anomalous results which could not be fitted into the body of consistent results.

The occurrence of "strongly latched" MIM behaviour is regrettable but apparently arose because of faulty programming of MIM operation by the MIR staff and resulted in the MIM flotor movement exceeding that of the "rattle space" provided and hitting the stator movement restrictors. This could have been avoided had the MIM control system been able to receive instructions from QUELD II via the RS 232 port provided in QUELD II.

During the design phase of QUELD II, the Queen's-MBI team had requested and had been told that the ROM card built into QUELD II and containing all the processing data for each sample could call up a prepackaged programme on the MIM Hard Disk in order to drive MIM into a mode of operation appropriate to each sample. Unfortunately, to the great dismay of the QUELD II design team, the engineering model of MIM was found to possess no available RS 232 port to receive instructions from QUELD II. Instead, MIM had been designed with 8 analogue entry ports and could receive only four temperature indications and four system voltages which were to be used to monitor QUELD II performance. Distressingly, it was only at the end of the experimental programme that the Queen's-MBI team learned that it would have been possible to change the operational mode of MIM for the processing of the second sample during any two-sample run even though the QUELD II design team had requested this and provided an acceptable electrical signal to MIM via one of the analogue ports.

Hopefully, any MIM variant to be used on the International Space Station will permit pre-programmed operation to be called-up by the microprocessor controlling sample processing since this will permit changes in operating mode to be made during the processing of any single specimen. This would be of considerable value when the materials processing facility is operating in gradient freeze mode for crystal growth.

5 Continuing studies

The Queen's University QUELD II Science Programme has involved parts (i) and (ii) of an integrated three part activity:

(i) reduced gravity experiments,
(ii) terrestrial experiments, and
(iii) the development of a theoretical framework which would permit (a) the prediction of diffusion coefficients for liquid metals and metalloid alloys, and (b) the processing conditions to produce inclusion-free crystals or a uniform dispersion of particles throughout the crystallising medium.

It should be noted that in pursuing (i) and (ii), the successful flight samples have been analysed and the results are reported in sections 2 and 3. These show a clear and consistent

behaviour which may be used in the future to develop improved theoretical models for both liquid diffusion and particle pushing. The data have been reported in various scientific media, in particular, the proceedings of recent TMS Experimental Methods in Microgravity Materials Science and the Journal of Microgravity Science and Technology.

With respect to the terrestrial (ground-based) experiments there is still much to be done. In particular, for liquid diffusion studies, a detailed examination of the "wall effect" needs to be carried-out since some of the reported data shows no more of a reduction in D when using a capillary diameter of approximately 0.8mm than when going from 1g to microgravity or microgravity to g-jitter-less operation. It is possible that the reduced capillary size used by earlier workers did in fact provide sufficient viscous damping to provide convection-free conditions for solute transport. This needs to be verified or rejected by careful experimentation in order to better understand the liquid diffusion process. Also, careful ground-based experiments need to be done in order to get a 1g characterization of diffusion in the various alloy systems examined in microgravity in order to provide the qualifying factors to deduce the intrinsic value of D at a given temperature for any particular alloy system. Work reported at the 1999 Gordon Conference on materials microgravity effects suggests that intense magnetic fields can be used to reduce convective transport.

In addition to the 1g experimental diffusion work, there is much to be done to develop the theoretical framework to embrace and explain the universal $D \propto T$ relationship which has been observed.

The primary ground-based studies needing to be completed with respect to the particle pushing experiments are to examine particle occlusion/pushing at rates less than 1μm/sec and without constitutional supercooling since the latter complicates the analysis of the pushing process. In addition, detailed electron metallography needs to be done on serial sections of particle clusters to determine the cementation phase(s) causing the particles to stick together. As noted earlier, this leads to non-uniform particle distributions and degraded mechanical properties.

6 Acknowledgements

The efforts of many people have gone into the preparation of samples, certification of flight samples, isothermal annealing, chemical analysis and the theoretical review of the results of these experiments. They include Drs. X. Zhu, M. Kaya, W.G.M. Gallerneault, M.C. Tunnicliffe, Mr. Jikai Chen, Ms Josée Robert, Carolyn Russell and various individuals from Alcan International Limited. However, none of this work would have been possible without the direct financial assistance of the Canadian Space Agency, the National Science and Engineering Research Council and Queen's University and the access to the STS and MIR space platforms made available to the CSA through NASA and the Russian Space Agency; all this assistance is most gratefully acknowledged.

7 Bibliography

1 Malmejac, Y., Frohberg, G., "Mass Transport by Diffusion", Chapt. V, Fluid Sciences and Materials Science in Space, ed. Walter, H.U., Springer-Verlag, Berlin, p. 159 (1986).

2 Frohberg, G., Kraatz, K.H., Wever, H., "Microgravity Experiments on Liquid Self- and Inter-diffusion", Symposium Norderney, p. 27 Aug. (1986).

3 Zhu, X., Smith, R.W., "Diffusion in Liquid Pb-Au Binary System", Materials Science Forum, Vols. 215-216, 113, (1996).

4 Zhu, X., "Diffusion in Liquid Binary Alloys", Ph.D. thesis, Queen's University, Canada, (1997).

5 Zhu, X., Smith, R.W., "Impurity Diffusion of Gold in Liquid Lead", Adv. Space Res., Vol. 22, No. 8, 1253, (1998).

6 Glasstone, S.K., Laidler, K.J., Eyring, H., "Theory of Rate Processes", New York, McGraw-Hill (1941).

7 Cohen, M.H., Turnbull, D., "Molecular Transport in Liquids and Glasses", J. Chem. Phys. 31, 5, 1164, (1959).

8 Frohberg, G., Kraatz, K.H., Wever, H. "Diffusion and Transport Phenomena in Liquids Under Microgravity", Proc. 6th European Symposium Under Microgravity Conditions, Bordeaux, France, 2-5 Dec. 1986 (ESA, 1987), SP-256, p. 585.

9 Swalin, R.A., "Self-Diffusion of Liquid Metals", Acta Met., 7, p. 736 (1959).

10 Reynik, R.J., "A Semiempirical Small Fluctuation Theory of Diffusion in Liquids"" Trans. Met. Soc. AIME, 245, 73 (1969).

11 Bruson, A., Gerl, M., "Diffusion Coefficient of ^{113}Sn, ^{124}Sb, ^{110m}Ag and ^{195}Au in Liquid Sn" Phys. Rev., B 21, 12, p. 5447, (1980).

12 Shimoji, M. and Itami, T., "Atomic Transport in Liquid Metals", Trans Tech. Publ. Ltd., Switzerland (1986).

13 Griesche A., Kraatz K. H., Frohberg G., "A Modified Shear Cell for Mass Transport Measurements in Melts", Rev. Sci. Instrum., American Institute of Physics, vol. 69, 1, January 1998, 315.

14 Hildebrand, J.L., "Viscosity and Diffusivity", Chapt. 1, New York, John Wiley, (1977).

15 Foiles, S.M., Baskes, M.I., Daw, M.S., "Embedded-atom-method Functions for the F-CC Metals Cu, Ag, Au, Ni, Pd, Pt and Their Alloys", Phys Rev., B33, 7983, (1986).

16 Murphy, A.M., Howard, S.J., Clyne, T.W., "Characterization of the Severity of Particle Clustering and its Effect on the Fracture of Particulate MMCs", submitted to Mat. Sci. & Tech., Jan. 1998.

17 Uhlmann, D.R., Chalmers, B., Jackson, K.A., "Interaction Between Particles and a Solid-Liquid Interface", Journal of Applied Physics, Vol. 35, No. 10, 1964, 2986-2993.

18 Hoekstra, P., Miller, R.D., "On the Mobility of Water Molecules in the Transition Layer Between Ice and a Solid Surface", Journal of Colloid and Interface Science, Vol. 25, 1967, 166-173.

19 Bolling, G.F., Cissé, J., "A Theory for the Interaction of Particles with a Solidifying Front", Journal of Crystal Growth, Vol. 10, 1971, 56-66.

20 Cissé, J., Bolling, G.F., "A Study of the Trapping and Rejection of Insoluble Particles During the Freezing of Water", Journal of Crystal Growth, Vol. 10, 1971, 67-76.

21 Cissé, J., Bolling, G.F., "The Steady State Rejection of Insoluble Particles by Salol Grown from the Melt", Journal of Crystal Growth, Vol. 11, 1971, 25-28.

22 Omenyi, S.N., Neumann, A.W., "Thermodynamic Aspects of Particle Engulfment by Solidifying Melts", Journal of Applied Physics, Vol. 47, No. 9, September 1976, 3956-3962.

23 Stefanescu, D.M., Dhindaw, B.K., "Behavior of Insoluble Particles at the Solid/Liquid Interface", Metals Handbook, 9th Edition, Vol. 15, ASM International, 1988, 142-146.

24 Zubko, A.M., Lobanov, V.G., Nikonova, V.V., "Reaction of Foreign Particles with a crystalline Front", Sov. Phys. Crystallogr., Vol. 18, No. 2, Sept.-Oct. 1973, 239-241.

25 Sasikumar, R., Ramamohan, T.R., "Distortion of the Temperature and Solute Concentration Fields due to Presence of Particles at the Solidification Front-Effects on Particle Pushing", Acta Metall. Mater., Vol. 39, No. 4, 1991, 517-522.

26 Sasikumar, R., Ramamohan, T.R., Pai, B.C., "Critical Velocities for Particle Pushing by Moving Solidification Fronts", Acta Metall., Vol. 37, No. 7, 1989, 2085-2091.

27 Kim, J.K., Rohatgi, P.K., "An Analytical Solution of the Critical Interface Velocity for the Entrapping of Insoluble Particles by a Moving Solid/Liquid Interface", Metallurgical and Materials Transactions A, Vol. 29A, January 1991, 351-358.

28 Stefanescu, D.M., Dhindaw, B.K., Kacar, S.A., Moitra, A., "Behavior of Ceramic Particles at the Solid-Liquid Metal Interface in Metal Matrix Composites", Metallurgical Transactions A, Vol. 19A, November 1998, 2847-2855.

29 Shangguan, D., Ahuja, S., Stefanescu, D.M., "An Analytical Model for the Interaction Between an Insoluble Particle and an Advancing Solid/Liquid Interface", Metallurgical Transactions A, Vol. 23A, February 1992, 669-680.

30 Chernov, A.A., Temkin, D.E., Mel'nikova, A.M., "Theory of the Capture of Solid Inclusions during the Growth of Crystals from the Melt", Sov. Phys. Crystallogr., Vol. 21, No. 4, July-August 1976, 369-374.

31 Han, Q., Hunt, J.D., "Particle Pushing: Critical Flow Rate Required to Put Particles into Motion", Journal of Crystal Growth, Vol. 152, 1995, 221-227.

32 Pötschke, J., Rogge, V., "On the Behavior of Foreign Particles at an Advancing Solid-Liquid Interface", Journal of Crystal Growth, Vol. 94, 1989, 726-738.

33 Delamore, G.W., Smith, R.W., "Controlled Dispersion of Inclusions, I", A.F.S. Trans., Vol. 79, 1971, 560.

34 Smith, R.W., Delamore, G.W., Mackay, W.B.F., "Controlled Dispersion of Inclusions, II", A.F.S. Trans., Vol. 80, 1972, 299.

35 Mehra, N.K., "Effect of Induced Fluid Flow on the Distributions of Inclusions in Cast Metals", M.Sc. Thesis, Queen's University, 1973.

36 Chernov, A.A., Temkin, D.E., Mel'nikova, A.M., Soviet Phys. Cryst., Vol. 23, 1977, p. 13

37 Gallerneault, W.M.T., "Particle Reinforcement Distributions and Solidification Structures in Directionally Solidified Metal Matrix Composites", Ph.D. Thesis, Queen's University, 1991.

38 Mortensen, A., Jin, I., Solidification Processing of Metal Matrix Composites, International Materials Reviews, Vol. 37, No. 3, 1992, p. 101-128.

39 Chalmers, B., The Principals of Solidification, John Wiley and Sons, 1964.

40 Spittle, J.A., Hunt, M.D., Smith, R.W., Journal of International Metals, Vol. 93, 1965, p. 234.

41 Hunt, M.D., Crystal Growth, Ph.D. Thesis, University of Birmingham, 1965.

42 Juretzko, F.R., Dhindaw, B.K., Stefanescu, D.M., Sen, S., Curreri, P.A., Particle Engulfment and Pushing by Solidifying Interfaces: Part 1. Ground Experiments, Metallurgical and Materials Transactions A, Volume 29A, June 1998, p. 1691-1696.

APPENDIX I

DESCRIPTION OF THE MICROGRAVITY VIBRATION ISOLATION MOUNT

The Microgravity Vibration Isolation Mount (MIM) is a six degree of freedom (6DOF) magnetic levitation (MAGLEV) system designed to isolate experiments from the vibratory accelerations (>0.01 Hz) on the space shuttle, MIR and ISS, while passing the quasi-static accelerations (<0.01 Hz) to the experiment. Given the typical 2 micro-g steady state acceleration in low earth orbit, the system is capable of isolating an experiment of practically unlimited mass, providing attenuation of the acceleration levels of up to 60 dB, thereby providing the desired clean acceleration environment to experiments. The performance limit depends primarily on the character of the umbilical required between the MIM base and the MIM flotor on which an experiment is mounted. The emphasis with the MIM design is to isolate at the experiment level, ideally isolating only the sensitive elements of an experiment. This limits the need for a heavy umbilical. In the current implementation the umbilical provides power to the experiments mounted on the flotor, and provides data acquisition and control services to the experiments. With the wire umbilical the MIM has demonstrated good isolation performance in operations on the MIR space station.

The MIM may be viewed as consisting of two major components: the fixed stator and the free flotor. The MIM achieves isolation in six degrees of freedom (6 DOF) using eight Lorenz actuators. These actuators consist of permanent magnets on the flotor interacting with coils mounted on the stator. The control system tracks the flotor motion in 6 DOF and the flotor and stator accelerations in the three linear DOF, and determines the currents required in each of the coils such that full 6 DOF control of the flotor is achieved. For tracking the position and attitude of the flotor with respect to the stator, three light emitting diodes (LED) mounted on the flotor are imaged onto three 2-D Position Sensing Devices (PSD) mounted on the stator. This provides position tracking of the flotor with respect to the stator with a resolution of the order of 10 micrometres linearly and of the order of 10^{-4} radians rotationally. The MIM provides for a range of motion of approximately 9mm in the three linear DOF and 3.5 degrees in the three rotational DOF about its nominal home position. The MIM operating parameters are given on the next page.

MIM OPERATING PARAMETERS

MIM Operating Parameters

Volume:	1 MLE (Mid-deck Locker Equivalent)
Total System Mass	54 lb. (Estimate)
Power Requirements (Excluding experiments, PGSC and MOD):	
Nominal power	106 Watts
Peak power in driven mode	120 Watts
Maximum touch temperature	Less than 40 C

Experiment Support

Mounting Surface Dimensions	36.2 cm x 36.2 cm (14.25 in. x 14.25 in.)
(Experiment hardware can overhang this where space is available)	
Volume available on STS-85	Approx. 1 MLE
Isolated Mass	Volume limited only
Experiment Power	10A @ 28 VDC derated per NSTS-21000-IDD-MDK
Analog data channels	9
Channel Input Gains	1
Input range	+/- 10 Volts
Resolution	16 bit
Data Sampling Rates	500 to 1500 samples/sec/channel
Anti-Aliasing Filters	Fourth order Butterworth analog filters set at 100 Hz
Digital filtering/Decimation	Available from 1.0 Hz to 100 Hz range with storage rate from 5 s/s to 1000 s/s
Data Storage	2 Gbytes on MIM hard drive with SCSI port for transfer to external storage medium
Experiment control lines	8 analog output, 16 bit resolution, +/- 10 V 100 Hz response
Data Down-link	Data transfer via the OCA

System Performance

Experiment Support Continued

Isolation Frequency Range	0.01 Hz to 100 Hz
Frequency Response	Second order and fourth order roll off achieved above cutoff frequency depending on control algorithm
Maximum attenuation	60 dB at 0.5 Hz and above limited by noise floor
Noise Floor	1 $(\text{micro-g})^2$/Hz above 0.5 Hz
Acceleration Range	17 mg depending on frequency and rattle space constraints
Acceleration Accuracy	10 micro-g
Acceleration Resolution	1 micro-g
Programmable g inputs	
Frequency Range	DC to 50 Hz
Motion Range	+/- 8 mm (+/- 0.3 in)
Maximum Force	5N (1.1 lb. wt) in vertical direction and 2.5N (0.55 lb. wt) in the horizontal directions

APPENDIX II

THE QUELD II FURNACE FACILITY, CALIBRATION AND USE

1 The QUELD II Facility

The following is a paper appearing in the proceedings of the 10th International Symposium on Experimental Methods for Microgravity Materials Science, given at the 127th TMS Annual Meeting, San Antonio, Texas, USA, 1997.

I INTRODUCTION

In October 1992, the Shuttle Columbia carried Astronaut Steve MacLean into orbit to perform the package of experiments code-named CANEX-2. One of these was "**Q**ueen's **U**niversity **E**xperiment in **L**iquid **D**iffusion". Some thirty samples were processed successfully in a manually-operated equipment designed and built at Queen's - (QUELD I). This consisted of two isothermal furnaces, sample-loading/quenching gear and furnace controls, all packed into a 15 cm cube!

This experiment had been conceived in 1983 when one of us (RWS) won the National Research Council of Canada competition to fill a Get-Away-Special (GAS-can) for a microgravity "Payload of Opportunity" flight on a NASA Shuttle. Unfortunately, the STS Challenger disaster delayed this flight but in September 1992, QUESTS I, the automated GETAWAY SPECIAL with 12 diffusion samples (and three eutectic experiments) finally flew into low earth orbit (LEO) on STS Endeavor. QUELD I used a somewhat simpler manually operated furnace and quenching system derived from the QUESTS I project. This permitted many more samples to processed using an experimental facility which weighed only 9 lb. QUESTS and QUELD facilities provided high quality liquid diffusion data.

When the opportunity to fly the Canadian Microgravity Isolation Mount (MIM) on the Russian Space Platform MIR arose, the CSA invited Queen's to consider a reflight of QUELD I, but used in conjunction with MIM. This was welcomed but further review suggested an automated minimum crew facility, QUELD II, might better exploit the flight opportunity. Thereupon, the Queen's Group invited Millenium Biologix (MBI), a principal (TS) of which had contributed to the Group's design activities since 1982, to collaborate in preparing a conceptual design of QUELD II which would incorporate the essential elements of the successful QUESTS I and QUELD I units into a more user-friendly automated facility. For this, MBI was able to tap into its considerable past experience of the design and production of high-reliability, miniaturized microprocessor-controlled biomedical devices and so help to produce a number of ground-based units (GBUs) for individual experimenters to use and also two flight articles (F.A.s) to go up to MIR. The essential features of the QUELD II facility will now be described.

II QUELD II FACILITY

As noted earlier, in order to attempt to ensure a trouble-free extended lifetime for QUELD II in space, the conceptual design drew heavily on the most relevant aspects of the space-qualified and flight-proven QUESTS I and QUELD I units. QUELD I had been used solely for isothermal processing and since the operating astronauts had to select the operating temperatures manually and change the temperature setting immediately after inserting the furnaces, two single zone furnaces were used. However, QUESTS I was an automated facility with three-zone furnaces, and sample-quench facilities; as a result, it could be used for isothermal and gradient-freeze sample processing. The QUESTS furnaces and quench system had also been used in a rocket-born materials processing facility which contained 14 of the furnace units. In all cases the furnaces and quench block systems had performed as required and so give confidence that they could be used with some high level of confidence for extended use on MIR in order to process various types of samples. To do this, the astronaut/cosmonaut would have to select the sample from a storage magazine, insert it in the sample carrier, enter the sample identity number and presses the start button. Following this, they would be processed automatically in one of the three modes:

1) isothermal
2) temperature-gradient
3) gradient-freeze

The scientific programme carried-out to date has exploited capabilities of QUELD II in all of these three modes.

The QUELD II system processes samples via the automatic insertion of the sample into a preheated furnace. The furnace temperature is controlled via a programmed temperature controller. Following the required thermal exposure, the samples are automatically withdrawn and are subsequently quenched by the automatic closure of paired spring-loaded quench blocks. Once the samples are at a safe handling temperature, the samples are released by the quench mechanism and await manual removal from the hardware.

All sample processing routines are contained within a removable memory module. A single module contains the information necessary to process approximately 50 different samples. The specific sample routine is defined using two digit selector switches on the front panel of the QUELD II hardware.

The capacity of the QUELD II system is enhanced by the use of two fully independent sample processing channels. Due to power limitations on MIR, only one channel is in operation at any given time, however, it is possible to load both channels at the same time and make use of a preprogrammed time offset to sequence the processing routines for each sample and so reduce demands on astronaut/cosmonaut time by only requiring their attention for reloading samples after every second sample has been processed.

III THE SAMPLE

A. Specifications

The QUELD II system has as its focus the accurate thermal processing of a wide series of specimen-types. Each type of specimen must be encased in a protective metallic container to permit processing without hazard for the operator or the equipment. The whole assembly is referred to as a "sample". A schematic drawing of a typical sample is shown in Figure II-1. Its specifications are shown in Table II-1.

Table II-1 Listing of the Primary Specifications for the QUELD II Experimental Samples

Parameter	Description
Nominal Sample Diameter	6.4 mm
Nominal Sample Length (Including Mounting)	157 mm
Nominal Crucible Diameter	5.4 mm
Maximum Crucible Length Including Cap	60 mm
Nominal Crucible Wall Thickness	0.6 mm
Nominal Specimen Diameter	4 mm
Sheathing Material	321 Stainless Steel or 601 Inconel
Crucible Material	Pyrolitic Carbon or Boron Nitride

B. Chemical Containment

The requirements for containment are that the specimen, when liquid, does not reach beyond its immediate environment and that none of the specimen constituents are permitted to leak into the QUELD II flight unit or elsewhere. This requires that the specimen be contained in a suitably inert crucible, closed with a spring loaded plug to ensure that no free surface exists during microgravity processing to avoid any potential Marangoni convection.

The selection of the crucible and sheathing materials was based on meeting the requirement that the specimen materials, when in the liquid state, do not seriously affect the crucible or sheathing materials' integrity when exposed in direct contact for a period of at least twice the duration of the planned experiment.

C. Structural Containment

The materials and assembly techniques selected for the sample must be able to withstand the internal loading likely to arise within the capsule in the unlikely event of a furnace run-away condition. For the QUELD II, this required that the entire sample must be able to withstand a temperature of 950^0C for 10 hr. As a result, duplicates of all sample types are routinely tested in this manner. In practice, in order to be accepted for microgravity processing, all specimens must be enclosed in two impervious sealed shells. Metallic diffusion couples are best placed first in a graphite or boron nitride crucible and then sealed by laser welding in two vacuum-tight layers of

stainless steel. Springs are included not only to prevent Marangoni convection within the crucible but also to gently force the crucible to make good thermal contact at its base with the central steel plug of the stainless steel envelope. (Figure II-1) This permits the user to place a thermocouple through a hole drilled in the plug to within 1 mm of the inner crucible in order to obtain confirmation that the processing temperature at that point is closely similar to that obtained during the ground-based testing. Whilst it is recognized that the temperature measured in the plug by the external thermocouple will be below the value of that existing at the actual base of the specimen, ground-based testing with thermocouples mounted in the actual specimen permit a close reproducible correlation of the two temperatures.

Should the nature of the specimen permit sealing in quartz, then only one level of protective stainless steel needs to be used, thus permitting a larger specimen size.

Following laser welding, the samples are subjected to a series of tests. The first of these involves taking a duplicate sample of each type and exposing it in a furnace at 950^0C, in air, for 10 hours. If the protective metallic container is still fully protective after this exposure, the containment technique is deemed adequate from a toxicological point of view.

Then the intended flight samples are examined by X-radiography to ensure the required specimen and sample components are in place. Finally, each flight sample is subjected to a "leak-detection" test in which the welded sample is first placed into a vessel under alcohol at a pressure of 50 p.s.i. in order to force a volatile fluid into any micro cavities existing in the stainless steel case. Following this, the sample is surface-dried and placed in vacuum system, which is then sealed. The time taken for the pressure in the vacuum system to fall to a given value is then measured. If the steel case is perforated due to incomplete welds or other manufacturing defects, the rate of reduction of pressure is much reduced and so the sample condition can be identified to be "leaking" or "suspicious" and returned for re-manufacture. Following the successful passing of the leak test, the sample is ready for flight testing.

IV QUELD II FEATURES AND SPECIFICATIONS

The key features of the QUELD II system are:

- Maximum operating temperature of 900^0C
- Maximum temperature gradient of 70^0C/cm
- Isothermal and temperature gradient exposure profiles
- Twin independent channels for increased processing capacity
- Three-zone furnace windings for control of thermal gradients
- Required astronaut crew time of only 5 minutes per double sample selection and exchange
- Automatic sample insertion into a preheated furnace to more rapidly bring the sample to the desired operating temperature
- Automatic sample quench
- Complete sample process information set by a two digit code on front panel
- All sample processing codes present on replaceable memory modules

In addition to the above, there are several advantages to the combination of the QUELD II system with the MIM platform. It is noted that the MIM may be used in three modes:

1. "Latched": In this condition, the MIM g-jitter of the platform on which MIM is mounted is passed directly to QUELD II.

2. "Isolating": Here, the ability of the MIM to improve the quality of the microgravity environment to a quiescent level of 10^{-6} g permits, for example, the collection of high fidelity thermophysical data.

3. "Forcing": In this mode, the MIM continues to isolate the QUELD unit from local g-jitter but then forces the platform to vibrate in desired manner.

This ability of the MIM to generate controlled microgravity fluctuations not only permits the study of the effects of gravity on physical processes, particularly the triggering of interface instabilities, but also allows the operator to conduct experiments designed to refine the theoretical understanding of the effects of gravitationally-induced convection. For example, it may be reasoned that when a given sample is subjected to a particular vibration pattern, then certain convection should result, leading to a particular solute redistribution in a growing crystal. The experiment can be carried-out and the resulting solute distribution determined. This is then compared with that predicted and, if these do not correspond, then the theoretical prediction is modified to better reflect the fact. The final advantage of the MIM/QUELD combination is that the available data transfer ports on the MIM permit the recording of experimental parameters important in the post-mission analysis of sample properties. The capacity to do this is large since the MIM uses an optical disk storage system. Figure II-2 is an illustration of the QUELD II system installed above the MIM unit.

V SCIENCE SUPPORT CAPABILITIES

As noted earlier, samples may be processed isothermally, in a fixed temperature gradient, or in the falling temperature gradient characteristic of the gradient-freeze crystal growth process. This permits a wide range of science objectives to be achieved. The following is a summary of the science activities carried-out this far.

A) Liquid Diffusion

A series of dilute binary and ternary diffusion couples have been processed to determine the diffusion coefficients for particular temperatures and examine how these change with the processing temperature. The former is of direct use in the mathematical modelling of industrial processes involving liquid metals whilst the latter provides fundamental knowledge with respect to the structure of liquids.

These experiments are best done in a microgravity environment since buoyancy convection is much reduced and so more accurate data may be obtained. When these are done, using the Microgravity Isolation Mount (MIM) in "Isolating Mode", then even better data has

been obtained. In work carried-out to date, g-jitter has been shown to increase the measured diffusion coefficient of gold in liquid lead by a factor of two.

B) Ostwald Ripening in a Molten Salt Medium

When a fine dispersion of a given medium contained within another is exposed at high temperature, it is usually found that the larger particles coarsen (or ripen) at the expense of the smaller ones such that, over time, the fine dispersion becomes completely replaced by one of larger particles. This phenomenon, examined by Ostwald at the turn of the last century, is of critical importance in many technological areas and so much work has been done to try to obtain a better understanding of the associated kinetics. If such experiments are performed in space, buoyancy effects are removed and so liquid/solid and liquid/liquid systems may be studied.

In the present MIR/MIM/QUELD II campaign, both the ripening of a liquid/solid and a liquid/liquid system have been studied in the presence and absence of g-jitter.

C) Processing of Heavy Metal Fluoride Glasses

The overall objective of this work is to realize the predicted ultra-low losses for infra-red radiation transmission in heavy metal fluoride (HMF) glass fibres by processing in microgravity. Empirical studies have shown that glasses cooled in microgravity are less susceptible to devitrification. Hence various glasses will be processed using the MIM to help towards obtaining a better understanding of why this occurs. Such glasses, when drawn to fibres, achieve a very high value-added status and have many applications, particularly for military use.

D) Solute Partitioning in InSb and GaSb

In the growing of semiconductor crystals with controlled doping it is essential that the manner in which solute partitions between the solid and the contiguous liquid be known precisely. However, the accurate determination of such partition coefficients in a terrestrial laboratory is plagued with error due to buoyancy effects. Hence the QUELD II facility has been used in a gradient freeze mode to permit crystal growth under diffusion-controlled conditions of binary and tertiary compound semiconductors. The MIM is being used to determine the influence of g-jitter on such solute transport processes.

VI DESCRIPTION OF QUELD II MICROGRAVITY FURNACE

Physical Layout

The design of the QUELD II system is based on the use of the original QUESTS I furnace core design with three-zone temperature control, in combination with standard industrial subassemblies appropriately rated or upgraded for space flight qualification.

The essential features of the flight hardware are:

- Aluminum enclosure
- Modular CPU/process controller
- Interface backplane for I/O modules
- Replaceable memory module containing sample processing profiles
- Aluminum enclosure "plug-in modules" to contain furnaces
- DC drive linear actuators for sample insertion
- Paired quench blocks operated via linear actuators
- Mounting plates to interface with MIM

The internal layout of the hardware is shown in Figure II-3 The CPU/process controller and complementary I/O modules plug directly into a rigid backplane designed specifically for use with the process control units. This backplane contains all the necessary communication hardware and wiring between the units. The backplane is in turn securely mounted to the structural rails of the enclosure. The furnace plug-in module which contains the two furnace cores is inserted to one side of the enclosure and is secured in place using standard mounting hardware. The linear drives and quench block assemblies are mounted to a subframe that is fastened to the structural rails of the enclosure. Sample insertion and removal is performed by extensions from twin linear drives mounted below the furnace module. The front panel of the enclosure contains all the user interface components required for operation by the astronaut, plus access to the sample mounting locations.

VII IN ORBIT OPERATING EXPERIENCE TO-DATE

The MIR/MIM/QUELD II programme has been a learning exercise in generating the necessary understanding and tolerance to permit space organizations and individuals with initially very different scientific and operational backgrounds to work together for a common purpose. The result has been of significant scientific success since, for the first time ever, the effects of existing and forced g-jitter on a number of physical processes has been measured. In addition, the difficulties experienced have been analyzed and documented so that the optimum path for the equipping and manning of the International Space Station Alpha (ISSA) may be defined. To this end, taking note of the enormous premium likely to be placed on operator time on the ISSA, the QUELD II design group is now working to define the operational envelope of a fully automated QUELD III, where larger samples may be processed over a wider range of experimental conditions on a MIM III, all space-qualified for the ISSA.

In passing, it is noted that the MIM/QUELD package has been selected by the Russians for a further two years of operation on MIR, thus permitting the possibility of further international collaborative studies.

VIII CONCLUSIONS

The Canadian experience of what it takes to carry-out successful science in a microgravity environment is typified by the QUELD II programme, namely, plan for minimum

exposure to risk. This involves using components and designs which have had extended success in terrestrial applications and where possible extensive pre-testing in space. In addition, electronic components are best selected from industrial production .... where the production volumes permits good statistical methods to be in place, if trouble free operation over extended period is to be obtained.

IX ACKNOWLEDGEMENTS

This has been truly a most satisfying (though at times frustrating) international collaboration and we at Queen's University and Millenium Biologix Inc. are deeply indebted to our NASA and Russian colleagues for their patience and understanding in assisting us to overcome early teething problems and to the Canadian Space Agency for financial support. In particularly, the help of Mr. Duncan Burnside and John Marrone is much appreciated.

Lists of Figures

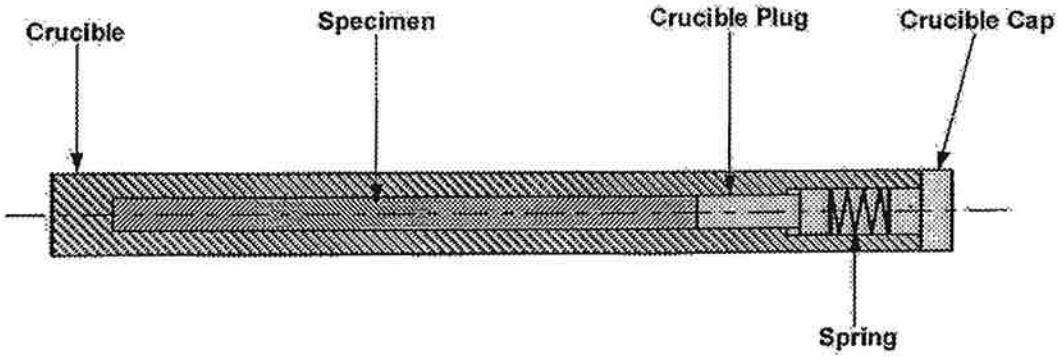

Figure II-1 Schematic of a Typical Sample

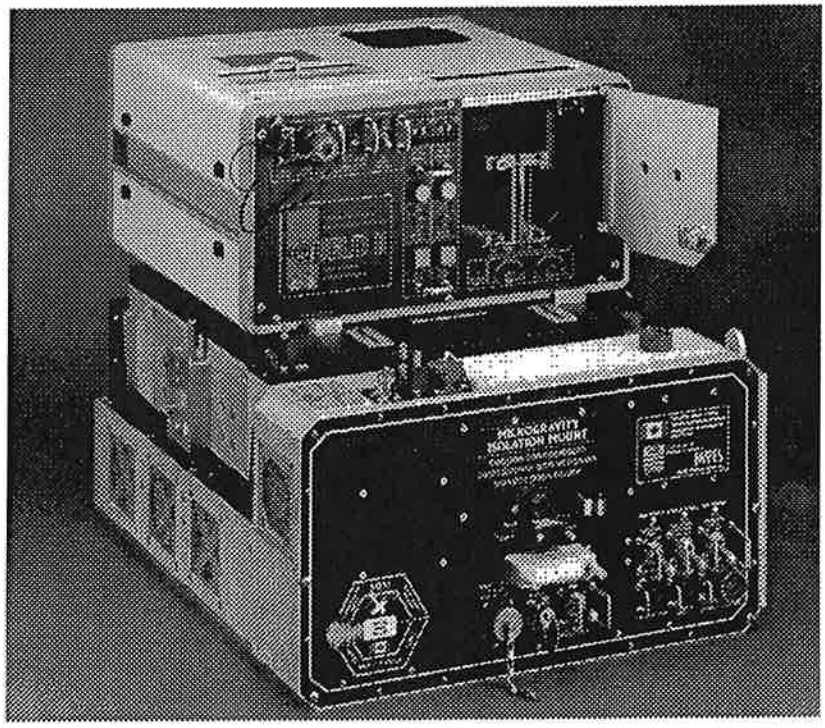

Figure II-2 QUELD II System Installed on MIM

QUELD II

Top View — Cover Removed

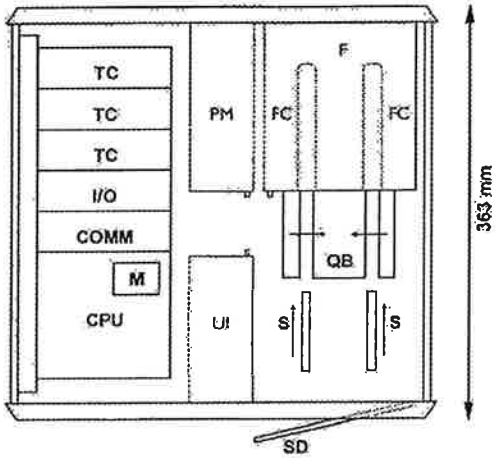

Legend

C	-Controls
CPU	-Central Processing Unit
COMM	-Communication Module
EM	-Electric Motor
F	-Furnace
FC	-Furnace Core
I/O	-Input/Output Module
LS	-Linear Slide Mechanism
M	-Memory Module
PM	-Power Control Module
QB	-Quench Blocks
S	-Sample
SD	-Sample Door
SS	-Sample Selector
TC	-Temperature Control Module
UI	-User Interface Module
⟶	-Motion of Component

Note: Access to Memory Module via top panel

Front View

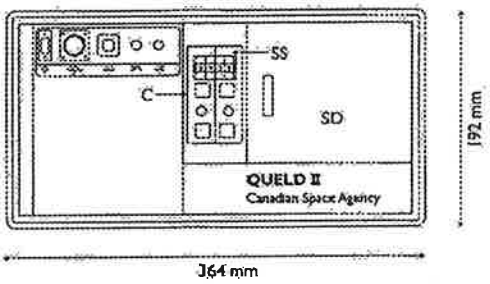

Layout of Sample and Furnace

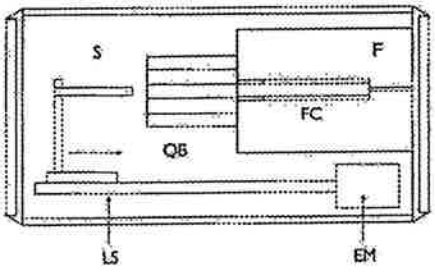

Features

- Automated Sample Processing
- Minimal Operator Time
- Process Parameters on Memory Card
- Robust Modular Design

Canadian Space Agency
Queen's University
Millenium Biologix Inc.

Figure II-3 Internal Layout of QUELD II

2 Calibration and Use of QUELD II

At the "Review of QUELD II – Facilities and Science" held at Queen's University on July 17, 1995, R.W.S. presented the QUELD SCIENCE P.I.'s with a description of the operation of the facility and the manner in which any PI must first use a ground-based unit to derive calibration data for their particular experiments. In particular, attention was directed to the physics of using a three-zone furnace to achieve the near-isothermal or temperature-gradient processing of QUELD II samples.

R.W.S. noted that for isothermal processing, as was required for the liquid diffusion couples of this project, the use of three individually controlled zones permitted the operator to compensate for small variations in heat losses along the length of the electrical heating elements. However, note must also be taken of the free end losses of the outer zones. This is usually done by differentially winding the end-zones to provide a large heat ouptput at the free ends of the zones to compensate for the higher losses in these areas. However, these end losses are proportionately higher at higher furnace temperatures. As a result, if adequate end loss compensation is made in the upper part of the temperature range being used for experiments, there will be over compensation at lower temperatures. This effect is shown in Figure II-4, where the temperature rises slightly as the end of the furnace is approached for a nominal temperature of 500°C. The stability of the temperature in each zone is shown in the temperature/time plots of Figure II-5.

To determine the actual temperatures experienced by a diffusion couple specimen, a 0.5 mm diameter sheathed thermocouple was past through the sample end-cap into the crucible containing the specimen in order to measure the temperatures at the points A, B, and C, see Figure II-6. The temperatures obtained are shown in Table II-3 and are plotted in Figure II-7 for a lead specimen; the equivalent for tin is shown in Figure II-8.

Two features are of note in Figures II-7 and II-8, namely:

a) there is a small temperature gradient across the specimen's length; and
b) the actual sample temperature is lower than the nominal temperature at which the furnace is controlled.

However, as is described in Appendix III, the small temperature gradient is a necessary component to obtain sound specimens using the quenching method employed in QUELD II, and the departure of specimen temperature from furnace setting (nominal) temperature will be known to the experimenter from prior ground-based testing.

Table II-2 Temperature Measurements in Cross-section of the Furnace

Distance (mm)	Temperature (°C)	Distance (mm)	Temperature (°C)
0	328	55	502
5	385	60	504
10	433	65	504
15	462	70	496
20	488	75	481
25	500	80	455
30	505	85	418
35	504	90	383
40	503	95	349
45	502	100	303
50	502		

Note:

- Distance is from the front end of the furnace.
- The length of the furnace is 100 mm.
- The temperature is 502~505 °C for the segment (30-65 mm) where a specimen will be located.
- The temperature measurement was carried out by locating a thermocouple in a small cylinder of aluminum (5 mm dia. x 5 mm length) for 2.5 minutes at each point.

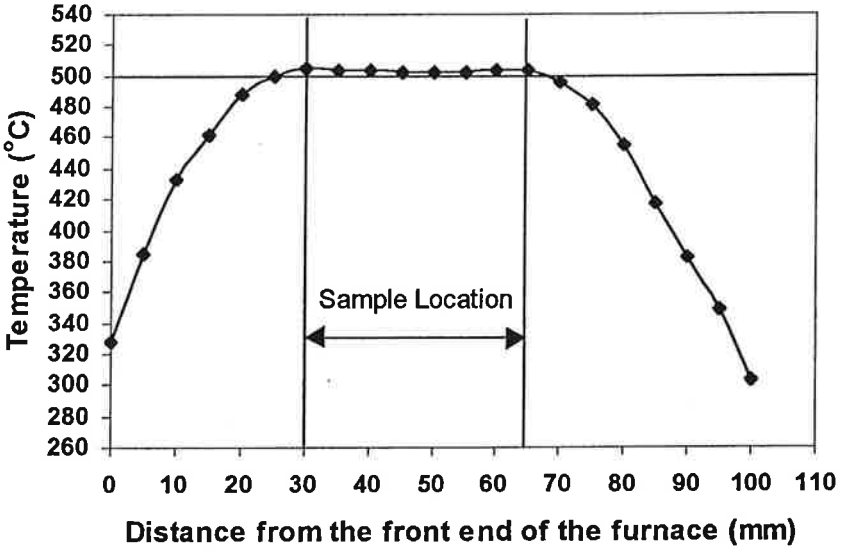

Figure II-4 Temperature Measurements in Cross-section of the Furnace

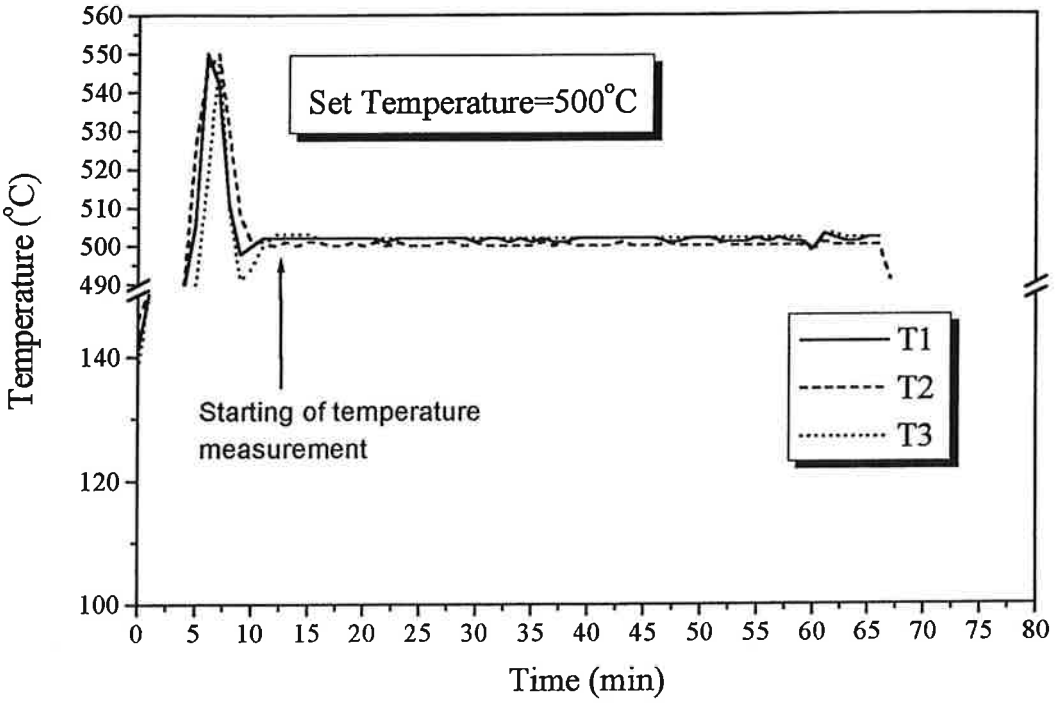

Figure II-5 Temperature Stability of the Three Heating Zones (T1, T2 and T3)

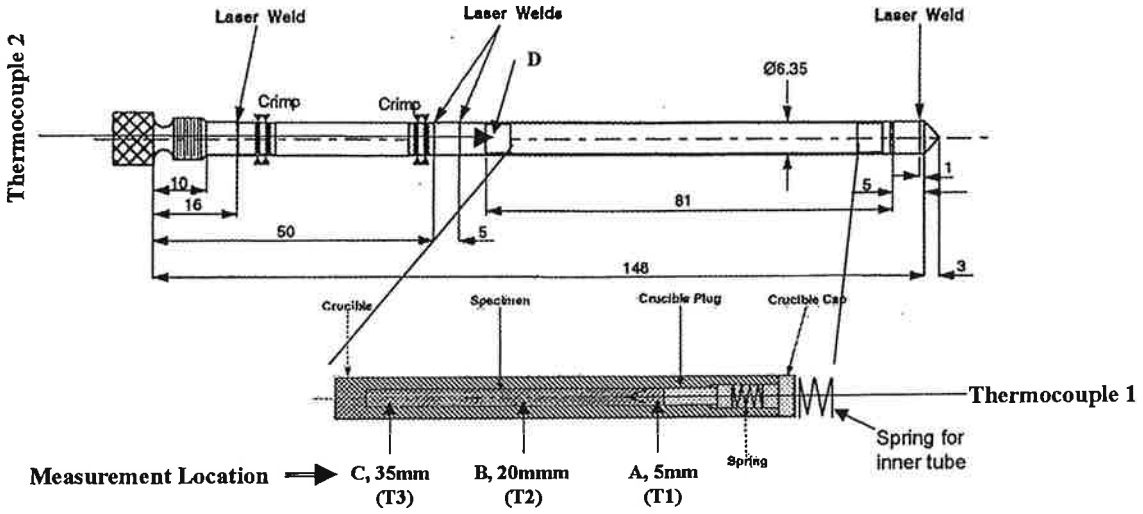

Figure II-6 Schematic of the Location for Temperature Measurements in QUELD II

Table II-3 Temperature Verification of QUELD II for Lead Sample

Set Value (°C)			Process Value of Furnace (Tf)			Sample Temperature (Ts)			Outside Sample	Δ T = Tf – Ts			Max $\Delta T(Ts^A - Ts^C)$ inside Sample
T1	T2	T3	T1	T2	T3	A	B	C	D	T1-A	T2-B	T3-C	
400	400	400	402	400	401	392	390	384	335	10	10	17	8
500	500	500	498	499	498	494	492	484	419	4	7	14	10
600	600	600	598	598	598	594	592	574	486	4	6	24	20
700	700	700	702	700	702	691	684	671	472	11	16	31	20
800	800	800	800	798	798	792	785	773	649	8	13	25	19

Note:

- The temperature measurements were made by inserting a thermocouple of 0.02" into the sample from the backplate of the QUELD II. A and C points are located 5 mm away from both ends of the sample; point C is located in the middle of the sample. Point A is closer to the backplate of the furnace than B and C.
- Another thermocouple was inserted from the front of the unit to measure the temperature outside the graphite crucible (point D).
- Sample length = 40 mm and sample diameter = 2 mm.
- Metal is pure lead.
- ΔT = Tf - Ts is the temperature difference between the furnace and the sample for the three heating zones.

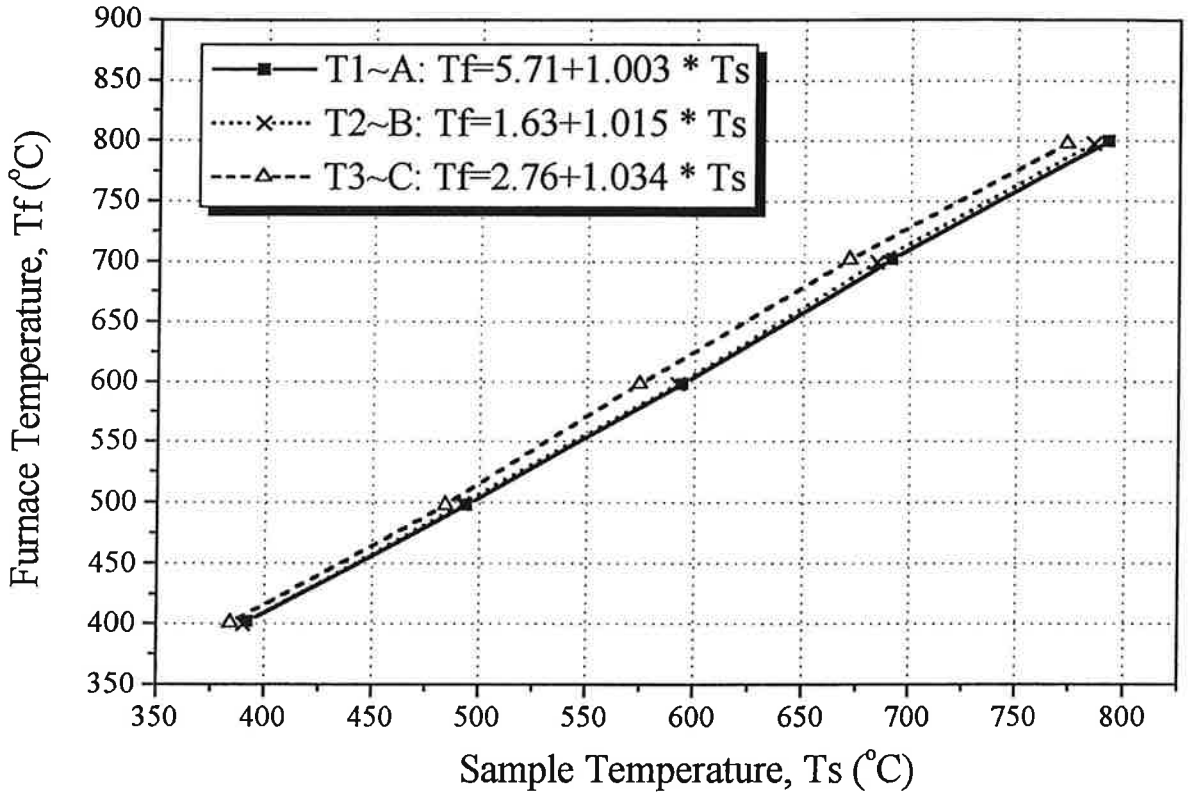

Figure II-7 Temperature Relationship between the Furnace and the Sample for the Three Heating Zones (T1-A, T2-B and T3-C) for a 2 mm dia. Pb Sample

Table II-4 Temperature Verification of QUELD II for Tin Sample

Set Value (°C)			Process Value of Furnace (Tf)			Sample Temperature (Ts)			Outside Sample	Δ T = Tf - Ts			Max $\Delta T(Ts^A - Ts^C)$ inside Sample
T1	T2	T3	T1	T2	T3	A	B	C	D	T1-A	T2-B	T3-C	
400	400	400	399	400	399	394	391	386	344	5	9	13	8
500	500	500	501	500	501	488	482	472	424	3	8	9	16
600	600	600	602	601	602	590	585	574	515	12	6	28	16
700	700	700	702	701	702	690	684	671	597	12	18	31	19
800	800	800	801	801	800	793	785	779	646	8	16	21	14
500	500	500	501	500	500	500	500	490		1	0	10	Without sample

Note:

- The temperature measurements were made by inserting a thermocouple of 0.02" into the sample from the backplate of the QUELD II. A and C points are located 5 mm away from both ends of the sample; point C is located in the middle of the sample. Point A is closer to the backplate of the furnace than B and C.
- Another thermocouple was inserted from the front of the unit to measure the temperature outside the graphite crucible (point D).
- Sample length = 40 mm and sample diameter = 3 mm.
- Metal is pure tin.
- $\Delta T = Tf - Ts$ is the temperature difference between the furnace and the sample for the three heating zones.

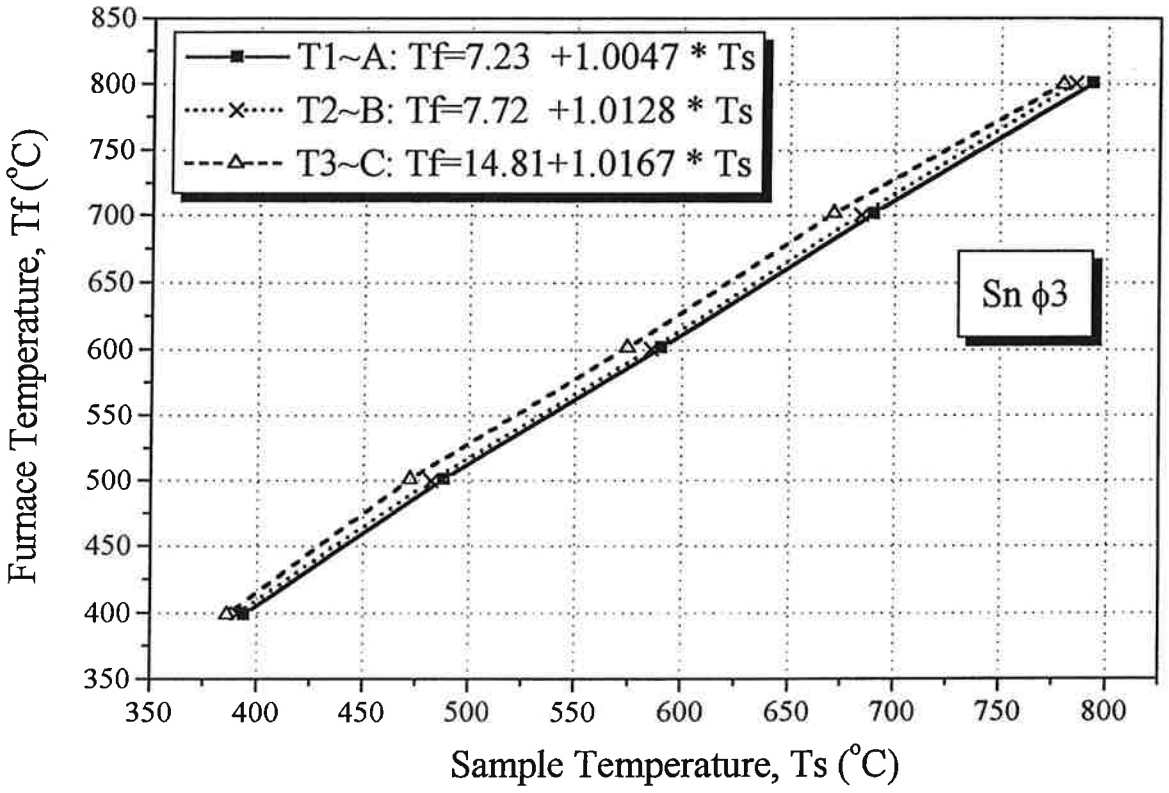

Figure II-8 Temperature Relationship between the Furnace and the Sample for the Three Heating Zones (T1-A, T2-B and T3-C) for a 3 mm dia. Sn Sample

APPENDIX III

SAMPLE QUENCHING

The method of quenching used in this work was evaluated earlier and is described in detail in references 3 and 4. In this, following the diffusion anneal, spring-loaded aluminum quench blocks are brought into contact with the sample along that part of the sample surface covering the specimen in order to induce the radial removal of heat from the specimen. This results in the rapid solidification of the specimen. Since the freezing front moves from the outer surface rapidly to the centre-line of the specimen, dendritic growth takes place. This results primarily in lateral interdendritic segregation with a little solute being pushed towards the centre-line of the sample.

However, since the scale of the dendritic growth is much finer than that of the sample width used for determining the composition/distance plot of the specimen, local segregation does not influence the final composition determination. It is noted that this method has worked efficiently with alloy systems which contract on freezing (metals) and also those which expand (metalloids and semiconductors) when using graphite crucibles to contain the specimens and with a small temperature gradient applied to the sample so that the macro-solid-liquid interface proceeds as a narrow V from the closed end of the crucible to the other end where a spring-loaded piston is used to ensure no free-volume will have contact with the specimen when liquid. Prior to the use of the quench block system for QUELD II on MIR, extensive modelling and physical testing had been completed at Queen's University, and on KC135 flights, QUESTS I and II and QUELD I space flights.

APPENDIX IV

THE QUELD II SAMPLE CONFIGURATION

The design, testing and certification of QUELD II samples was the subject of Contract N° 9F007-5-6329/01-ST. In brief, the sample encapsulation used for the QUELD II samples was designed to provide safe operation on MIR in microgravity and was based on NASA requirements. The same encapsulation was used for the ground-based samples as for the space-based samples to ensure, as far as possible, the reproducibility of thermal exposure of samples and permit close comparison of results between the ground- and space-based samples. Each specimen was first placed in a graphite (or boron nitride) crucible, which was then encapsulated in two stainless steel tubes. Springs were used between the plug and end caps of the graphite crucible to ensure no free space existed above the sample surface when molten and to press the crucible against the end of the sample tube containing the thermocouple. The QUELD II sample capsule is shown in Figure IV-1.

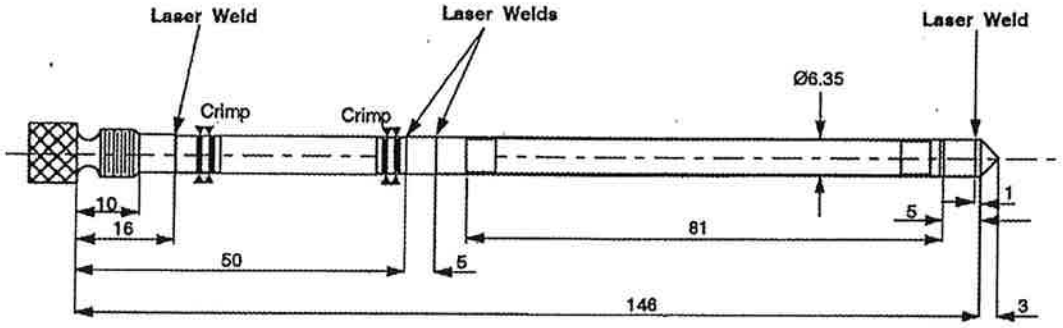

Figure IV-1 QUELD II Sample Configuration (the dimensions are in mm)

APPENDIX V

SUMMARY OF QUELD II SAMPLES ASSEMBLED AND TESTED BY QUEEN'S UNIVERSITY

Table V-1 Summary of QUELD Samples Assembled and Tested By Queen's University

Date of Delivery to NASA	Sample Number	ROM Card	P.I.	Material	MIM Mode	Diff. Coeff. $(mm^2/s)10^{-3}$	Comments
95/12/20	1	A	Queen's	Pb-Au	isol.	-	not melted
95/12/20	2	A	Queen's	Pb-Au	isol.	1.93	satisfactory
95/12/20	3	A	Queen's	Pb-Au	isol.	2.51	satisfactory
95/12/20	4	A	Queen's	Pb-Au	isol.	3.07	satisfactory
95/12/20	5	A	Queen's	Pb-Au	isol.	3.58	satisfactory
95/12/20	6	A	Queen's	Pb-Ag	isol.	2.46	satisfactory
95/12/20	7	A	Queen's	Pb-Ag	isol.	2.26	unsatisfactory
95/12/20	8	A	Queen's	Pb-Ag	isol.	3.89	satisfactory
95/12/20	9	A	Queen's	Pb-Ag	isol.	2.17	unsatisfactory
95/12/20	10	A	Queen's	Pb-Ag	isol.	2.83	unsatisfactory
95/12/20	11	B	Queen's	Sn-Au	isol.	3.51	satisfactory
95/12/20	12	B	Queen's	Sn-Au	isol.	4.54	satisfactory
95/12/20	13	B	Queen's	Sn-Au	isol.	-	not processed
95/12/20	14	B	Queen's	Sn-Au	isol.	-	not processed
95/12/20	15	B	Queen's	Sn-Au	isol.	4.17	unsatisfactory
95/12/20	16	B	Queen's	Sn-Au	isol.	-	not processed
95/12/20	17	B	Queen's	Sn-Ag	isol.	3.88	satisfactory
95/12/20	18	B	Queen's	Sn-Ag	isol.	4.48	unsatisfactory
95/12/20	19	B	Queen's	Sn-Ag	isol.	4.13	unsatisfactory
95/12/20	20	B	Queen's	Sn-Ag	isol.	7.91	unsatisfactory
95/12/20	21	B	Queen's	Pb-Au	isol.	3.04	satisfactory
95/12/20	22	B	Queen's	Pb-Au	isol.	4.16	unsatisfactory
95/12/20	23	B	Queen's	Sn-Au	isol.	3.42	satisfactory
95/12/20	24	B	Queen's	Sn-Au	isol.	10.07	satisfactory
95/12/20	25	B	Queen's	Al-Cu	isol.	-	unsatisfactory
95/12/20	26	B	Queen's	Al-Cu	isol.	6.82	satisfactory
95/12/20	27	B	Queen's	Al-Cu	isol.	-	unsatisfactory
95/12/20	29	B	Queen's	Al-Ni	isol.	-	unsatisfactory
95/12/20	30	B	Queen's	Al-Si	isol.	-	unsatisfactory
95/12/20	45	A	Queen's	Pb-Au	latch.	2.30	satisfactory
95/12/20	46	A	Queen's	Pb-Au	latch.	3.94	satisfactory
95/12/20	47	A	Queen's	Pb-Au	latch.	3.09	unsatisfactory
95/12/20	48	A	Queen's	Pb-Au	latch.	2.00	unsatisfactory
95/12/20	49	A	Queen's	Pb-Au	latch.	-	not processed
95/12/20	50	A	Queen's	Pb-Au	latch.	4.32	satisfactory
95/12/20	53	A	Queen's	Sn-Ag	isol.	5.54	satisfactory
95/12/20	54	A	Queen's	Sn-Ag	isol.	5.41	unsatisfactory
95/12/20	141	A	Amistar	Not Applicable			
95/12/20	142	A	Amistar	Not Applicable			
95/12/20	143	A	Amistar	Not Applicable			

38 +17

Table V-1 Summary of QUELD Samples Assembled and Tested By Queen's University (Continued)

Date of Delivery to NASA	Sample Number	ROM Card	P.I.	Material	MIM Mode	Diff. Coeff. $(mm^2/s)10^{-3}$	Comments
95/12/20	144	B	Amistar	Not Applicable			
95/12/20	145	B	Amistar	Not Applicable			
95/12/20	146	B	Amistar	Not Applicable			
95/12/20	121	A	Manitoba	Not Applicable			
95/12/20	122	A	Manitoba	Not Applicable			
95/12/20	123	A	Manitoba	Not Applicable			
95/12/20	124	A	Manitoba	Not Applicable			
95/12/20	125	A	Manitoba	Not Applicable			
95/12/20	126	A	Manitoba	Not Applicable			
95/12/20	127	B	Manitoba	Not Applicable			
95/12/20	128	B	Manitoba	Not Applicable			
95/12/20	129	B	Manitoba	Not Applicable			
95/12/20	130	B	Manitoba	Not Applicable			
95/12/20	131	B	Manitoba	Not Applicable			
95/12/20	132	B	Manitoba	Not Applicable			
96/4/30	233	D	Queen's	Sb-Ga	isol.	0.45	
96/4/30	234	F	Queen's	Sb-Ga	isol.	4.27	
96/4/30	235	D	Queen's	Sb-Ga	isol.	8.12	
96/4/30	236	D	Queen's	Sb-Ga	isol.	-	Note 4
96/4/30	237	D	Queen's	Sb-Ga	isol.	5.93	
96/4/30	238	D	Queen's	In-Sb	isol.	3.85	
96/4/30	239	F	Queen's	In-Sb	isol.	-	not processed
96/4/30	240	D	Queen's	In-Sb	isol.	6.53	
96/4/30	241	F	Queen's	In-Sb	isol.	8.03	
96/4/30	242	D	Queen's	In-Sb	isol.	9.29	
96/4/30	243	D	Queen's	In-Sb	isol.	8.84	
96/4/30	244	D	Queen's	In-Sb	isol.	8.09	
96/4/30	245	D	Queen's	Sb-In	isol.	-	not melted
96/4/30	246	F	Queen's	Sb-In	isol.	5.67	
96/4/30	247	D	Queen's	Sb-In	isol.	7.10	
96/4/30	248	D	Queen's	Sb-In	isol.	8.02	
96/4/30	249	D	Queen's	Sb-In	isol.	6.21	
96/4/30	250	D	Queen's	$Ga_{0.4}Sb_{0.6}$-	isol.	-	Note 5
96/4/30	251	E	Queen's	$Ga_{0.6}Sb_{0.4}$	isol.	-	Note 5
96/4/30	252	D	Queen's	"	isol.	-	Note 5
96/4/30	253	D	Queen's	$In_{0.4}Sb_{0.6}$	isol.	-	Note 5
96/4/30	254	E	Queen's	$In_{0.6}Sb_{0.4}$	isol.	-	Note 5
96/4/30	255	E	Queen's	"	isol.	-	Note 5
96/4/30	28	C	Queen's	Al-Fe	isol.	-	not melted

62 31

Table V-1 Summary of QUELD Samples Assembled and Tested By Queen's University (Continued)

Date of Delivery to NASA	Sample Number	ROM Card	P.I.	Material	MIM Mode	Diff. Coeff. $(mm^2/s)10^{-3}$	Comments
96/4/30	55	C	Queen's	Al-Fe	isol.	3.26	
96/4/30	56	C	Queen's	Al-Fe	isol.	5.28	
96/4/30	57	C	Queen's	Al-Si	isol.	12.37	
96/4/30	58	C	Queen's	Al-Si	isol.	-	not processed
96/4/30	59	C	Queen's	Al-Ni	isol.	3.43	
96/4/30	60	C	Queen's	Al-Ni	isol.	4.83	
96/4/30	61	F	Queen's	Pb-Ag	isol.	3.80	
96/4/30	62	F	Queen's	Pb-Ag	isol.	4.97	
96/4/30	63	F	Queen's	Pb-Ag	isol.	5.88	
96/4/30	64	F	Queen's	Pb-Ag	isol.	7.04	
96/4/30	65	F	Queen's	Pb-Ag	isol.	8.10	
96/4/30	67	C	Queen's	Pb-Au	isol.	5.10	
96/4/30	68	C	Queen's	Sn-Au	isol.	7.78	
96/4/30	69	E	Queen's	Bi-Au	isol.	4.27	Note 6
96/4/30	70	F	Queen's	Bi-Au	isol.	6.10	Note 6
96/4/30	71	E	Queen's	Bi-Au	isol.	14.68	
96/4/30	72	E	Queen's	Bi-Sb	isol.	5.00	Note 6
96/4/30	73	E	Queen's	Bi-Sb	isol.	8.36	Note 6
96/4/30	74	E	Queen's	Bi-Sb	isol.	11.82	
96/4/30	75	E	Queen's	Bi-Ag	isol.	-	Note 7
96/4/30	76	E	Queen's	Bi-Ag	isol.	7.20	
96/4/30	77	E	Queen's	Bi-Ag	isol.	11.38	
96/4/30	78	E	Queen's	Sn-Sb	isol.	3.62	
96/4/30	79	E	Queen's	Sn-Sb	isol.	5.98	
96/4/30	80	E	Queen's	Sn-Sb	isol.	8.32	
96/4/30	81	E	Queen's	Sn-Sb	isol.	8.94	
96/4/30	82	E	Queen's	Pb-Sb	isol.	2.74	
96/4/30	83	E	Queen's	Pb-Sb	isol.	4.21	
96/4/30	84	E	Queen's	Pb-Sb	isol.	5.91	
96/4/30	85	E	Queen's	Pb-Sb	isol.	6.75	
96/4/30	201	C	Queen's	Ga-Sb, Au	isol.	-	Note 5
96/4/30	202	C	Queen's	Ga-Sb, Au	isol.	-	Note 5
96/4/30	203	F	Queen's	Ga-Sb, Au	isol.	-	Note 5
96/4/30	204	F	Queen's	Ga-Sb, Au	isol.	-	Note 5
96/4/30	205	C	Queen's	Ga-Sb, Au	isol.	-	Note 5
96/4/30	206	C	Queen's	Ga-Sb, Pb	isol.	-	Note 5
96/4/30	207	E	Queen's	In-Sb, Au	isol.	-	Note 5
96/4/30	208	F	Queen's	Ga-Sb, Pb	isol.	-	Note 5
96/4/30	209	F	Queen's	Ga-Sb, Pb	isol.	-	Note 5

55

101

Table V-1 Summary of QUELD Samples Assembled and Tested By Queen's University (Continued)

Date of Delivery to NASA	Sample Number	ROM Card	P.I.	Material	MIM Mode	Diff. Coeff. $(mm^2/s)10^{-3}$	Comments
96/4/30	210	C	Queen's	Ga-Sb, Pb	isol.	-	Note 5
96/4/30	211	C	Queen's	In-Sb, Au	isol.	-	Note 5
96/4/30	212	C	Queen's	In-Sb, Au	isol.	-	Note 5
96/4/30	213	F	Queen's	In-Sb, Au	isol.	-	Note 5
96/4/30	214	C	Queen's	In-Sb, Au	isol.	-	Note 5
96/4/30	215	F	Queen's	In-Sb, Au	isol.	-	Note 5
96/4/30	216	C	Queen's	In-Sb, Au	isol.	-	Note 5
96/4/30	217	D	Queen's	In-Sb, Au	isol.	-	Note 5
96/4/30	218	D	Queen's	In-Sb, Pb	isol.	-	Note 5
96/4/30	219	D	Queen's	In-Sb, Pb	isol.	-	Note 5
96/4/30	220	F	Queen's	In-Sb, Pb	isol.	-	Note 5
96/4/30	221	D	Queen's	In-Sb, Pb	isol.	-	Note 5
96/4/30	222	F	Queen's	In-Sb, Pb	isol.	-	Note 5
96/4/30	223	D	Queen's	In-Sb, Pb	isol.	-	Note 5
96/4/30	224	D	Queen's	In-Sb, Pb	isol.	-	Note 5
96/4/30	225	D	Queen's	In-Sb, Ga	isol.	-	Note 5
96/4/30	226	D	Queen's	In-Sb, Ga	isol.	-	Note 5
96/4/30	101	E	U. of T.	Not Applicable			
96/4/30	102	C	U. of T.	Not Applicable			
96/4/30	103	F	U. of T.	Not Applicable			
96/4/30	104	C	U. of T.	Not Applicable			
96/4/30	105	E	U. of T.	Not Applicable			
96/4/30	106	E	U. of T.	Not Applicable			
96/4/30	107	C	U. of T.	Not Applicable			
96/4/30	108	E	U. of T.	Not Applicable			
96/4/30	109	C	U. of T.	Not Applicable			
96/4/30	110	F	U. of T.	Not Applicable			
96/4/30	111	E	U. of T.	Not Applicable			
96/4/30	112	C	U. of T.	Not Applicable			
96/4/30	113	F	U. of T.	Not Applicable			
96/4/30	114	C	U. of T.	Not Applicable			
96/4/30	115	E	U. of T.	Not Applicable			
96/4/30	116	F	U. of T.	Not Applicable			
96/4/30	117	C	U. of T.	Not Applicable			
96/4/30	118	F	U. of T.	Not Applicable			
96/4/30	119	C	U. of T.	Not Applicable			
96/4/30	120	F	U. of T.	Not Applicable			
96/8/15	401	G	Queen's	Pb-Au	0.1Hz	5.89	
96/8/15	402	G	Queen's	Pb-Ag	0.1Hz	3.38	

120 (61)

Table V-1 Summary of QUELD Samples Assembled and Tested By Queen's University (Continued)

Date of Delivery to NASA	Sample Number	ROM Card	P.I.	Material	MIM Mode	Diff. Coeff. $(mm^2/s)10^{-3}$	Comments
96/8/15	403	G	Queen's	Comral	-	-	Particle Pushing
96/8/15	404	G	Queen's	Comral	-	-	Particle Pushing
96/8/15	421	G	U. of T.	Not Applicable			
96/8/15	422	G	U. of T.	Not Applicable			
96/8/15	431	G	Amistar	Not Applicable			
96/8/15	434	G	B.M.HiTech	Not Applicable			
96/8/15	435	G	B.M.HiTech	Not Applicable			
96/8/15	405	G	Queen's	Comral	-	-	Particle Pushing
96/8/15	406	G	Queen's	Comral	-	-	Particle Pushing
96/8/15	407	G	Queen's	Comral	-	-	Particle Pushing
96/8/15	408	G	Queen's	Comral	-	-	Particle Pushing
96/8/15	423	G	U. of T.	Not Applicable			
96/8/15	424	G	U. of T.	Not Applicable			
96/8/15	432	G	Amistar	Not Applicable			
96/8/15	436	G	B.M.HiTech	Not Applicable			
96/8/15	437	G	B.M.HiTech	Not Applicable			
96/8/15	409	G	Queen's	Comral	-	-	Particle Pushing
96/8/15	410	G	Queen's	Comral	-	-	Particle Pushing
96/8/15	411	G	Queen's	2% SiC	-	-	Particle Pushing
96/8/15	412	G	Queen's	2% SiC	-	-	Particle Pushing
96/8/15	425	H	U. of T.	Not Applicable			
96/8/15	426	H	U. of T.	Not Applicable			
96/8/15	433	H	Amistar	Not Applicable			
96/8/15	438	H	B.M.HiTech	Not Applicable			
96/8/15	439	H	B.M.HiTech	Not Applicable			
96/8/15	413	H	Queen's	Al_2O_3	-	-	Particle Pushing
96/8/15	414	H	Queen's	Al_2O_3	-	-	Particle Pushing
96/8/15	415	H	Queen's	15% SiC	-	-	Particle Pushing
96/8/15	416	H	Queen's	2% SiC	-	-	Particle Pushing
96/8/15	427	H	U. of T.	Not Applicable			
96/8/15	428	H	U. of T.	Not Applicable			
96/8/15	440	H	B.M.HiTech	Not Applicable			
96/8/15	441	H	B.M.HiTech	Not Applicable			
96/8/15	417	H	Queen's	Comral	-	-	Particle Pushing
96/8/15	418	H	Queen's	2% SiC	-	-	Particle Pushing
96/8/15	419	H	Queen's	Pb-Au	isol.	5.94	
96/8/15	420	H	Queen's	Pb-Ag	isol.	2.92	
96/8/15	429	H	U. of T.	Not Applicable			

+18 138

Table V-1 Summary of QUELD Samples Assembled and Tested By Queen's University (Continued)

Date of Delivery to NASA	Sample Number	ROM Card	P.I.	Material	MIM Mode	Diff. Coeff. $(mm^2/s)10^{-3}$	Comments
96/8/15	430	H	U. of T.	Not Applicable			
96/8/15	442	H	B.M.HiTech	Not Applicable			
96/8/15	443	H	B.M.HiTech	Not Applicable			
96/8/15	444	H	B.M.HiTech	Not Applicable			
96/8/15	445	H	B.M.HiTech	Not Applicable			

Note: 1- This listing does not include samples prepared for Acceptance Test purposes.
2- Material given as Solvent-Solute for impurity diffusion and Alloy/Solvent, Solute for ternary-impurity diffusion. Samples 250-255 are interdiffusion specimens.
3- For further details of samples 1-27, 29, 30, 45-50, 53 and 54 (the first 37 samples of the above table), see Appendix VI.
4- Chemical analysis of Gallium was below the detection limit of the AAS method due to the diffusion at high temperature to obtain an accurate and reliable diffusion coefficient.
5- Diffusion did not take place because the alloy segment of the specimen was not fused to the solvent segment due to the great difficulty of casting semiconductors and since metalloids contract upon melting, they remained as distinct segments.
6- Upon melting, specimen contracted and split in two. However, the first half (the one with the alloy at one end) was long enough, i.e., the solute did not diffuse to the end, to apply the conditions of the semi-infinite model calculations.
7- Upon melting, specimen contracted and split in two. The first half was not long enough to apply the conditions of the semi-infinite model calculations.
8- The particle pushing samples are discussed in details in this report in Tables 3.2 and 3.3.

APPENDIX VI Part (a)

QUELD-II INCREMENT-2 EXPERIMENT ANALYSIS

(Conducted and Reported in November 1996)

1. Concern about the Sample Processing

There is some information which shows that some of the Increment-2 samples were not processed as required. It has been recently found with GBU tests in Queen's University that the problem is most likely due to the partial insertion of a sample rather than full insertion as designed. Since the processing parameters (temperature and time) are critical for the generation of successful results, a series of tests were conducted in Queen's University.

2. Ground-Base Examination

Vacuum test, colour identification test and temperature calibration test have been designed to examine the flight sample conditions and to identify the processing temperature and time.

Using a vacuum test, no leakage has been found in all post-flight samples.
Some fundamental colour identification test results will be coming shortly.
The temperature calibration tests were finished and are reported here in detail.

Two kinds of tests were designed in order to trace the actual temperature of specimen. In one of these tests, the sample was fully inserted into the furnace when the processing temperature was reached. Without moving the sample, the sample temperature was recorded as the thermocouple was withdrawn a certain distance away from its original position. In another kind of test, the sample thermocouple was fixed at its original position while the sample temperature was recorded as the whole sample was pulled out a certain distance from its full insertion position in the furnace.

3. Results and Discussion

The results of the temperature calibration of the GBU are shown in Table VI-1 and Table VI-2. Two calibration profiles were generated with the data in Table VI-2, as shown in Figure VI-1. The sample position could be estimated from these diagrams with sample temperature data. This procedure has applied to the available experiment records. The comments about the flight experiments based upon above analysis are given in Table VI-3.

The extent of the influence of partial insertion on the diffusion experiments depends upon how far the sample was away from the designed position. The whole length of the diffusion specimen is 40 mm. The alloy part of the specimen, which is 2 mm long, was placed in the front of the sample. In order to meet the boundary conditions, the processing parameters (temperature and time) were designed so that the alloying element should not reach the other end of the specimen. This implies that it may not have significant influence on diffusion experiment if the

whole sample was just a short distance away from its designed position, or the whole specimen was still in the isothermal zone.

Table VI-1 Sample Temperature with Thermocouple at Different Positions

Processing Temperature (°C)	Sample Temp. (°C) as thermocouple at distance (mm) away from its original position				
	0	1	5	10	20
450 grad	300	296	279	260	149
300 isol	256	-	238	229	-
600 isol	517	508	491	465	326
700 isol	590	585	563	537	379

Table VI-2 Sample Temperature with Sample at Different Positions

Processing Temperature (°C)	Sample Temp. (°C) as sample at different positions (mm)						
	0	20	25	30	35	40	45
600	517	406	377	343	308	280	-
700	590	458	425	395	355	319	285

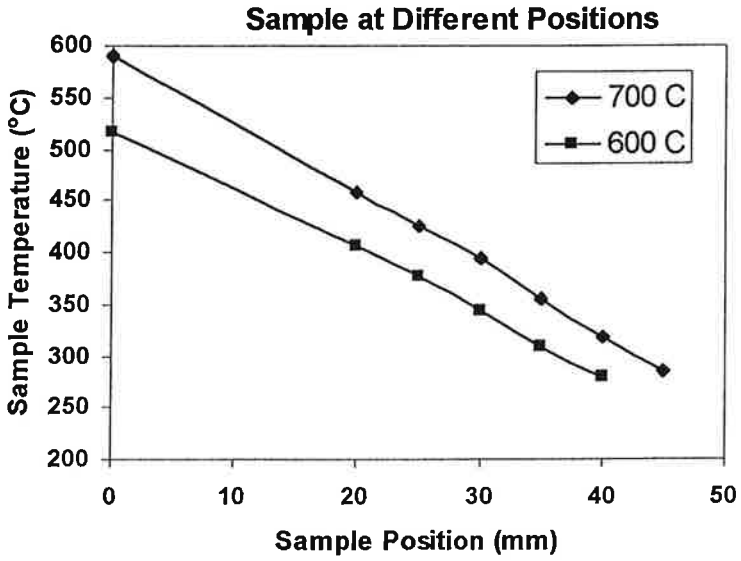

Figure VI-1 Sample at Different Positions (from Table VI-2)

Table VI-3 QUELD-II Increment-2: Status Report for February 1997

1	2	3	4	5	6	7	8	9
Sample No	Sample Composition	Programmed Processing Temperature °C	Probable Processing Temperature °C	Degree of Sample Insertion	Chemically Analysed	Results	Sample Reflight requested	New Sample required
1	Pb-Au	400	400	P	X	U	X	X
2	"	500	500	P	X	S		
3	"	600	600	P	X	S		
4	"	700	700	P	X	S		
5	Pb-Au	800	800	P	X	S		
6	Pb-Ag	400	400	F	X	S		
7	"	500	500	P	X	U	X	X
8	"	600	600	F	X	S		
9	"	700	700	P	X	U	X	X
10	Pb-Ag	800	700	P	X	U	XX	X
11	Sn-Au	300	300	F	X	S		
12	"	400	400	F	X	S		
13	"	500		U			X	
14	"	600		U			X	
15	"	700	700	P	X	U	X	X
16	Sn-Au	800		U			XX	
17	Sn-Ag	300	300	F	X	S		
18	"	500	500	P	X	U	X	X
19	"	600	600	P	X	U	X	X
20	Sn-Ag	800	730	P	X	U	X	X
21	Pb-Au[3]	400	400	P	X	S		
22	"	800	730	P	X	U	XX	X
23	Sn-Au[3]	300	300	F	X	S		
24	"	800	730	P	X	S		
25	Al-Cu	670		P	-	U	X	
26	"	730	730	F	X	S		
27	"	800		P	-	U	X	
29	Al-Ni	670		P	-	U	X	
30	Al-Si	670		P	-	U	X	
45	Pb-Au	400	400	F	X	S		
46	"	500	500	F	X	S		
47	"	600	600	P	X	U	X	X
48	"	700	700	P	X	U	X	X
49	Pb-Au	800		U			XX	
50	Pb-Au[3]	400	400	F	X	S		
53	Sn-Ag	400	400	F	X	S		
54	Sn-Ag	700	700	P	X	U	XX	X
Note:								
Column 5: P = partial insertion; U = unprocessed; F = full insertion.								
Column 6: N/A= not available as of 28/2/97								
Column 7: S = satisfactory; U = unsatisfactory								
Column 8: XX = first priority for reflight; X = second priority for reflight								

(38)

54

APPENDIX VI Part (b)

(Conducted and Reported in December 1996)

Confirmation of QUELD Increment 2 spaceflight processing by an analysis of specimen tube oxidation

Submitted by

Professor Reginald W. Smith

Department of Materials and Metallurgical Engineering

Queen's University, Kingston, Ontario

to

The Canadian Space Agency

Table of Contents

Abstract

Concern about possible non-isothermal conditions during the processing of QUELD II diffusion couples on the MIR space station required an analysis to determine whether the specimens were fully inserted into the furnace.

The thickness of the oxide generated on the stainless steel sheathing may be estimated from its colour. An extensive discussion of high-temperature oxidation theories is provided to verify that the oxide thickness is dependent on temperature.

The furnace temperature was confirmed from the oxide colour on the endcap of the sample tube, and the degree of insertion was estimated by comparison of the endcap oxidation to a region at the other end of the specimen.

Introduction

The Queen's University Experiment in Liquid Diffusion, QUELD, is one of a series of investigations of liquid diffusion in microgravity, conducted by the Queen's University Department of Materials and Metallurgical Engineering in conjunction with the Canadian Space Agency and NASA.

The intent of these experiments was to further the understanding of the behaviour of liquid metals, as diffusion coefficients determined in terrestrial experiments have proven to be irreproducible. By determining the diffusion coefficient of a binary alloy in microgravity and comparing it to data from ground-based tests, it is possible to detect the degree to which convection causes deviation of experimental results from theoretical predictions.

The first QUELD experiments, CANEX II, were conducted in September 1992 aboard the U.S. Space Shuttle Columbia. In these, four binary alloy systems were analysed: Pb-Au, Pb-Ag, Bi-Ag and Bi-Mn. QUELD Increment 2 sent 37 diffusion couples in Pb-Au, Pb-Ag, Sn-Au, Sn-Ag, Al-Cu, Al-Ni, and Al-Si to the Russian Space Station MIR. Corresponding terrestrial runs were also performed. In all cases, the prepared diffusion couples were contained in graphite crucibles within sealed metallic tubes, and were processed in an apparatus developed by Queen's University specifically for these experiments. The design of both the sample tubes and the QUELD furnace are discussed more extensively later in this paper, but it should be noted now that isothermal conditions must be maintained at all times along the length of the diffusion couple in order for the results obtained from it to be meaningful.

Unfortunately, it would seem that some difficulties encountered during processing on MIR may have led to a non-isothermal condition in several sample tubes. The astronaut performing the experiments noted that several of the tubes were not fully inserted into the furnace while they were being heated. There is concern that some work performed on the furnace apparently bent one of the arms which hold the sample tubes and move them within the device. Therefore, tubes were entering the furnace itself at an angle, and were catching on the walls before full insertion was achieved. In addition, there was a great deal of interest about a number of questionable thermocouple readings which might indicate a temperature gradient or other processing problems.

It was therefore determined that an analysis of evidence on the protective tubes would be beneficial, as it could help confirm whether a sample was processed under the desired conditions. More specifically, it was hoped that the oxide film on the tubes would provide specific information about the furnace temperature, the treatment time, and the degree of container insertion into the furnace.

An understanding of appropriate high-temperature oxidation theories provides a link between processing and oxide thickness. Simple physics – the principle of visible light interference tints -- may then be used to form the basis of an analysis, since oxide colour can be shown to be a function of its thickness.

Apparatus

The basis of the design of the QUELD furnaces is the importance of ensuring that the diffusion couple are processed isothermally. As any temperature gradient along the liquid metal would affect the observed diffusion coefficient, the length of time required to bring the sample tube up to the holding temperature and the time to quench it back to room temperature must be minimised, in addition to maintaining a constant temperature along the entire length of the sample at all times.

The QUELD devices consist of two independent isothermal furnaces and two aluminum quench block assemblies. A sample tube is inserted into a preheated furnace, where it is quickly heated to the processing temperature and held for a specified period. Upon removal, it is clamped between the quench blocks which bring it rapidly to room temperature.

The QUELD II furnace is very similar to the original QUELD device, but it incorporates a number of design improvements. Operations which were previously performed manually, including moving the sample into the furnace, and thence to the quench blocks, are handled by a computer-controlled motor system in the QUELD II design. The astronaut needs only designate a ROM card program, screw the sample into the holding arm, and insert a thermocouple into the tube. The computer preheats the furnace, mechanically advances the arm to insert the sample into the furnace, holds it at temperature for the programmed length of time, removes it, and quenches it.

The sample tubes used in the QUELD Increment 2 space diffusion tests were cylinders with dimensions in mm, as illustrated below in Figure VI-2,

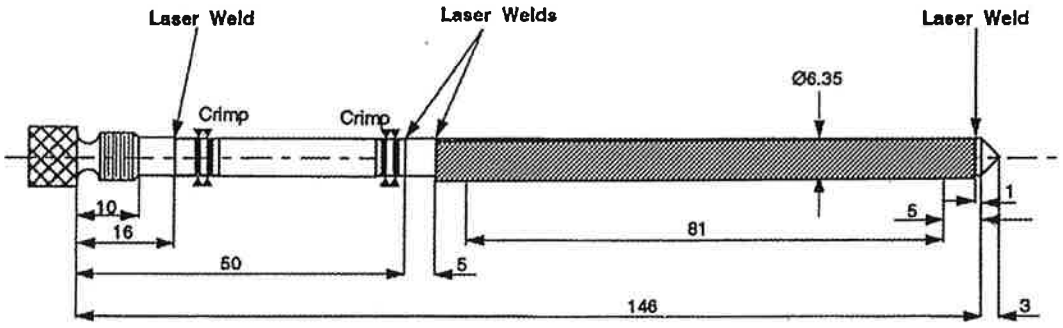

Figure VI-2 QUELD Increment 2 Sample Tubes

constructed from several lengths of "321" stainless steel tubing that had been laser-welded together. The section of the tube (shaded) which contained the diffusion couple was dipped in a zirconia-based sol-gel to protect it from liquid metal attack. The diffusion couples themselves were contained in graphite crucibles, with graphite caps held in place with springs to prevent liquid metal leakage due to thermal expansion. All components were polished to 600 grit, assembled, and cleaned with acetone prior to assembly and laser welding.

Theoretical Considerations

Since the only evidence of the manner in which the samples were processed existed in the oxides on the outside of the tubes, it was hoped that some information could be deduced from the characteristics of this oxide layer.

Upon visually inspecting an oxide thin film, one notes that it has a characteristic colour. This is due to the interference of light waves reflected from the upper and lower surfaces of the oxide layer. The observed colour comes from the visible wavelength of maximum intensity, which is produced by constructive interference. The condition for constructive interference is $2d = \lambda, 2\lambda, 3\lambda, \ldots$ (Ohanian, 1989) Therefore an oxide which appears straw-coloured (5800 Å) would be 2900 Å thick, and a 4000 Å blue oxide generated at a higher temperature would be about 4000 Å thick. Because of these interference tints, optical measurement – whether by eye or by photometer – of the observed (i.e., the strongest) wavelength allows one to estimate the thickness of the oxide layer.

Initial consideration of this problem posed an obvious question: since it is the temperature gradient in the region of the diffusion couple that are of interest, is it possible to deduce either of these from the oxide on the zirconia-coated tubes? A visual inspection revealed that these oxides are highly variegated in appearance, with many bands of different breadth and colour giving them the appearance of a rainbow. Variation between tubes indicated that slight anomalies in the coating procedure had a significantly greater effect on the oxide than the actual processing did. Furthermore, literature (Cox, 1990) notes that recent work which suggests that oxidation of zirconium-based alloys in the 300-350 °C region is not controlled entirely by solid state processes, such as oxygen diffusion along crystallite boundaries, has made it clear that the process of zirconium oxidation are not as well understood as previously believed.

When most metals are oxidised under relatively low-temperature conditions such as those encountered in the processing being considered here, the initial oxide formation up to thicknesses in the region of 0.1 μm is characterised by an initially rapid reaction whose progress is quickly reduced to a very small rate. This rate behaviour has been shown to conform to logarithmic laws of the form:

$$x = k_{log} \log(t + t_0) + A \qquad \text{(log function)}$$

$$\frac{1}{x} = B - k_{ilog} \log t \qquad \text{(inverse log function)}$$

where A, B, t_0, k_{log}, and k_{ilog} are constant at constant temperature (Birks and Meier, 1983).

Several theories have been developed to account for the logarithmic kinetics of low-temperature oxidation. They suggest a broad variety of rate-determining processes, from adsorption, to ion transport through a thin film, to coupled and low-resistance diffusion (Kofstad, 1966).

Anderson and Gallagher (1961) note that logarithmic behaviour is not limited to surfaces, but is also observed in internal processes in solids. They suggest that the overall oxidation process comprises a series of independent steps, and discuss the possible effects of nonisothermal conditions on this reaction.

The concept of oxidation as a set of independent steps which have a distribution of activation energies is similar to that in the Elovich equation for chemisorption kinetics. It also forms the basis for Kofstad's (1962-63) derivation of a logarithmic rate equation from a distribution of the energies of oxide nucleation and growth, which are dependent on surface orientation, defects, grain boundaries, etc...

Halsey (1951) and Landsberg (1955) have also developed logarithmic rate equations based on the assumption that chemisorption is rate-determining.

Adsorption-controlled kinetics are observed during the initial reaction of a clean metal surface, where chemisorption is the mechanism and the "sticking coefficient" is close to 1. The formation of a monolayer (in some cases only a partial monolayer) causes an abrupt reduction in this sticking coefficient, which falls to a very low level as the surface becomes covered in an oxide film (Kofstad, 1966). The oxidation rate decreases at a correspondingly rapid rate; the resultant state is the one to which most oxidation theories apply.

Once a thin film of oxide is established, it is generally assumed that the transport of electrons or reacting ions through this film is the rate determining step. The mechanism by which this diffusion occurs is a point of some contention.

Mott (1939 and 1940) initially proposed a direct logarithmic law from a model in which electron tunnelling was the rate-determining step. Hauffe and Ilschner have elaborated on this model, and Evans developed an alternate derivation (1960).

The basis of most models in which the inverse logarithmic rate limited by ion transport is the mechanism developed by Mott and Cabrera. It includes the adsorption theory just mentioned, but elaborates on how electrons pass through the thin oxide film by tunnelling to establish an equilibrium between the metal and the adsorbed oxygen atoms. This movement develops an electric field within the oxide which facilitates ion transport across it, and is valid for films up to 20 Å in thickness, at which point the electron tunnelling becomes insufficient to maintain the field (Cabrera, 1957).

However, the Mott-Cabrera theory does contain a rather significant flaw – it assumes that the defect concentration is constant throughout the oxide – Hauffe has demonstrated that the same result may be obtained without this assumption, and that an inverse logarithmic equation may also come from ion, rather than electron, transport.

Grimley and Trapnell (1956) have also elaborated on Mott and Cabrera's work, but using a constant field intensity within the film, rather than a constant potential difference across it. If they assume that the transport of metal occurs via vacancies rather than interstitial positions, a direct logarithmic equation is obtained.

It has been suggested by Evans (1960) and Davies *et al.* (1954) that the transport of atoms or ions during the oxidation process occurs preferentially along low-resistance paths such as pores, grain boundaries, and dislocations. Logarithmic rate equations are obtained if it is assumed that the formation of fresh oxide blocks nearby pathways be exerting compressional stress on them (Davies *et al.*, 1954; Harrison, 1965), or if the film thickening is not uniform, continuously shrinking the area available for transport (Evans, 1960). A good example of the latter is when metal vacancies are responsible for transport, if they collect at the metal/oxide interface, they tend to form cavities which block solid-state diffusion.

While all of the above theories pertain to most metals, there are some additional factors which specifically affect the oxidation of alloys, such as differences in the oxygen affinities, mobilities, or diffusivities of the metallic constituents, the formation of higher oxides, the mutual solid solubility of the oxides, and sub-surface oxide precipitation (Birks and Meier, 1983).

The stainless steel considered in this experiment is type 321, an austenitic steel containing 0.08% C, 17.0-19.0% Cr, 9.0-12.0% Ni, 2.0% Mn, 1.00% Si, 0.045% P, 0.03% S, and 0.4% Ti (min) (Davis, 1996). Therefore, it is the processes of the oxidation of Fe-Cr-Ni that are of greatest interest.

In Fe-Cr-Ni alloys, both iron and chromium have a much greater affinity for oxygen than nickel does. Therefore, Ni acts as a noble element, and because Ni diffuses more readily in ferrite and austenite and does not build up at the metal/oxide interface, essentially no nickel oxidation occurs (Rawers, 1986).

Chromium alloyed in iron forms stable Cr_2O_3 upon oxidation. When this occurs below 700°C, the minimum concentration required to form this oxide is 16 wt%. Below this concentration, the sesquioxide $(Cr,Fe)_2O_3$ forms (Lloyd *et al.*, 1977). Only below 10 wt% Cr does an iron oxide form, generally an inner spinel layer of magnetite (Fe_3O_4) (Taylor *et al.*, 1980). It should be noted, however, that the composition of the oxides do not significantly affect the kinetics of their formation, especially during the very rapid initial formation that is pertinent to the problem under consideration.

While it is certainly possible to discuss to a greater extent the theoretical basis of low range high-temperature oxidation in stainless steel, one must bear in mind that the details of such interpretations have little bearing on the scale at which the oxide films are being considered. All that is required for the purposes of this discussion is to recall that initial oxide formation is extremely rapid and quickly arrested; therefore, the thickness of the oxide film on a sample that has been heated for a few hours is characteristic of the temperature of the process, not of its duration nor the composition of the oxide layer.

Procedure

The primary task of these experiments was to determine whether or not the sample tubes from MIR were fully inserted into the furnace during their processing. As it was not possible to glean any information from the coated length of tube, the only direct way to identify any temperature gradient is by comparing the oxides on the endcap and the "neck" of the sample. An additional benefit of this method is that identifying the temperature at the endcap of the sample – which was definitely in the furnace – confirms the processing temperature.

The review of research into the high-temperature oxidation of metals summarised above indicated that a characterization of the thickness of the oxide thin film on the uncoated stainless components of the sample tube would be the best way to proceed.

This determination could be more accurately performed by microscopic methods, either using scanning Auger electron spectroscopy to sputter away the oxide until metal is detected, or by using scanning electron microscopy on a heavily deformed sample to measure the thickness of the oxide at a crack.

Because of the large number of tubes to be considered, it was decided to use the faster, cheaper photometric method made possible by the interference tints discussed above. It was initially hoped that the photometer at the Alcan Research Laboratories in Kingston could be used to analyse the reflected wavelengths, but it has an incident beam about 3 cm in diameter – much too large for the small areas on the sample tube.

A series of small 321 stainless steel rods had one end machined to match the morphology of the flight specimen endcaps. These were then polished to 600 grit and cleaned with acetone to ensure that the surface conditions – so vital to the short-term formation of oxides – were as similar to those on the actual sample tubes as possible. These slugs were heated to a variety of temperatures for several different lengths of time, as follows:
First, they were processed for 30, 60 and 90 minutes at each of 300, 450, 550, and 700°C. It was noted from these runs that there is no variation in the interference tints with time for a given processing temperature. Therefore, just one 60 minute run was performed at each of 250, 350, 400, 500, 600, and 650°C, giving a spectrum of oxide samples from 250 to 700 °C at 50° intervals.

Since it was not possible to use a photometer to quantitatively determine the wavelengths that the oxide reflects, the only method which remained was visual comparison to the oxide colour/temperature standards discussed above. In order to minimise the effect that a narrow range of incident wavelength might have, the comparisons were made under conditions of indirect sunlight.

Two comparisons to the standards were performed on each sample tube: the endcap, and the hollow "neck" of the tube, just above the short plug section. While it was generally not possible to identify an oxide colour corresponding to an exact temperature, it was not difficult to "bracket" the flight sample in a 50° range between two standards.

If the range for the endcap contained the program temperature assigned for that sample, the processing temperature was designated as "okay". It was rather more difficult to designate the minimum standard for the neck temperature, as it is not intended to be inserted into the furnace and hence is heated only by conduction from further down the tube. One would therefore expect the neck to indicate a slightly lower temperature, but the permissible difference is yet to be determined. For example, none of the sample tubes had neck oxides that indicated temperatures greater than 550°C, which may suggest that none of the 700°C samples were fully inserted into the furnace, but may just be due to insufficient conduction.

It was hoped that the tubes from ground-based QUELD II experiments would yield some examples of the oxide patterns one should expect if the sample is fully inserted, but re-use of the neck portion of the tube rendered this impossible.

Instead, an empty sample tube was assembled. While it did not contain the inner sheath or crucible, it was similar in most respects to the spaceflight samples and was constructed entirely of 321 stainless steel, Indeed, all of the components except the endcap were from the original stock. The long "body" tube section used was designated #361, and the threaded piece was stamped 287. The endcap was machined to have the same external appearance as those of the flight samples, and the whole assembly was crimped together. While it is possible that the absence of laser welds may have affected the conductivity between the "body" and the "neck" tubes, it is believed that its effect is negligible relative to the contact area between the tubes and the piece which connects them.

This sample tube was processed in a ground-based unit for 60 minutes at 700°C. It was ensured that the tube was fully inserted into the furnace by manually advancing the holding arm completely along its travel. The resulting "neck" oxide colour provided an indication of what should be expected from higher-temperature processing.

As the first flight specimens were removed from the sample tubes and analysed by atomic absorption spectroscopy, it was noted that in at least one case, insertion was insufficient to allow full melting of both alloys.

Results

Comparison of sample processed in the ground-based unit at 700°C to the oxide colour standards revealed that the "neck" temperature was almost exactly 450°C. The following criteria are based on this knowledge and are used in Table VI-4:

Designations for endcap and processing temperature comparison:

"Yes" -- ranges are the same or adjacent

"No" -- ranges > 50°C different

Designations for endcap and neck temperature comparison (insertion estimation):

"Yes" -- ranges up to 50°C apart

"No" -- ranges > 100°C for <650°C endcap temperature

ranges > 200°C for >650°C endcap temperature

Table VI-4 Summary of Temperature and Insertion Estimations

Sample Number	Temperature OK?	Insertion OK?
1	Yes	No
2	Yes	No
3	Yes	No
4	Yes	No
6	Yes	Yes
7	Yes	Yes
8	Yes	Yes
9	Yes	Yes
10	Yes	No
11	Yes	Yes
12	Yes	Yes
13	Not Processed	Not Processed
14	Not Processed	Not Processed
15	Yes	Yes
16	Not Processed	Not Processed
17	Yes	Yes
18	No	Yes
19	Yes	Yes
20	Yes	Yes
23	Yes	Yes
24	Yes	No
26	Yes	Yes
27	Yes	Yes
29	Yes	Yes
30	Yes	Yes
45	Yes	Yes
46	Yes	Yes
47	Yes	Yes
48	Yes	No
49	Not Processed	Not Processed
53	Yes	Yes
54	Yes	Yes

Conclusions

Most of the samples seem to have been processed at the designated temperatures and fully inserted into the furnace, indicating that it is unlikely that there was a temperature gradient along the diffusion couple while it was molten. However, the following tubes had differences between their endcap and neck oxide colours which exceeded the set criteria: 1, 2, 3, 4, 10, 24, and 48; the experimental results from the diffusion couples they contained should be of particular concern. Sample 18 was processed at full insertion but 150-200°C below the program temperature, and samples 13, 14, 16, and 49 do not appear to have been processed at all.

Suggestions for Further Work

If it is determined that a quantitative and significantly more accurate measurement of the oxide thickness should be made in order to validate the results that will obtained from these methods, it will be necessary to physically measure the depth of this thin film. While the use of a scanning Auger electron microscope is the ideal method for such a determination, there is no apparent reason why sufficient accuracy could not be obtained by deforming the tubes and observing the oxide layer in the scanning electron microscope available through the Queen's University Department of Materials and Metallurgical Engineering. The only drawback to this method is that it requires destruction of the tubes, which would negate the possibility of conducting any further tests on them.

Bibliography

Anderson, J. S., and K. J. Gallagher, "Reactivity of Solids", in Proc. 4th International Symp. on the Reactivity of Solids, J. H. de Boer, Ed. Elsevier, Amsterdam, 1961, p. 222.

Birks, N., and G. Meier, *Introduction to High Temperature Oxidation of Metals*, Edward Arnold (Publishers) Ltd., London, 1983.

Cabrera, N., Semiconductor Surface Physics, R. H. Kingston, Ed. University of Pennsylvania Press, Philadelphia, 1957.

Cox, B., "Zirconium alloy oxidation – why do we still understand so little about it?" in Proceedings of the International Symposium on High-Temperature Oxidation and Sulphidation Processes, J. D. Embury, Ed. Permagon Press, Toronto, 1990, pp. 170-181.

Davies, D. E., *et al.*, Proc. Roy. Soc. (London), A225, 1954, p. 443.

Davis, J. R., Ed., ASM Specialty Handbook – Stainless Steels, ASM International, Materials Park, OH, 1996, p. 10.

Evans, U. R., The Corrosion and Oxidation of Metals, Edward Arnold Ltd., London, 1960.

Grimley, T. B., and B. M. W. Trapnell, Proc. Roy. Soc. (London), A234, 1956, p. 405.

Halsey, G. D., J. Phys. Colloid Chem., 55, 1951, p. 21.

Harrison, P.L., J. Electrochem. Soc., 112, 1965, p. 235.

Kofstad, P., High-Temperature Oxidation of Metals, John Wiley & Sons, 1966.

Kofstad, P., J. Inst. Metals., 91, 1962-63, p. 209.

Lloyd, G., O., *et al.*, "Breakaway Oxidation of Fe-10wt% Cr and Fe-20wt% Cr at Temperatures up to 600°C", Corrosion Science, 17, 1977, pp. 269-299.

Mott, N. F., Trans. Faraday Soc., 35, 1939, p. 1175.

Mott, N. F., Trans. Faraday Soc., 36, 1940, p. 472.

Ohanian, H. C., Physics, 2nd Ed., Expanded, W. W. Norton & Company Inc., New York, 1989.

Rawers, J., "Understanding the Oxidation Protection of Fe-Cr-Si Alloys", Norman L. Peterson Memorial Symposium – Oxidation of Metals and Associated Mass Transport, M. A. Dayananda *et al.*, Eds. The Metallurgical Society Inc., Warrendale PA, 1986.

Taylor, M. R., *et al.*, "The Mechanism of Corrosion of Fe-9% Cr Alloys in CO_2", Oxidation of Metals, 14, 6, 1980, p. 499.

Uhlig, H. H., Acta Met., 4, 1956, p. 541.